Photovoltaic Effects in Cadmium Telluride-Mercury Telluride Heterostructures

by

GEORGE STANLEY ALMASI

CENTER FOR SPACE RESEARCH

and

ENERGY CONVERSION AND SEMICONDUCTOR LABORATORY
DEPARTMENT OF ELECTRICAL ENGINEERING
MASSACHUSETTS INSTITUTE OF TECHNOLOGY
CAMBRIDGE 39, MASSACHUSETTS

SCIENTIFIC REPORT NO. 2

on

November 1, 1966

PHOTOVOLTAIC EFFECTS IN CADMIUM
TELLURIDE-MERCURY TELLURIDE HETEROSTRUCTURES

by

George Stanley Almasi

CENTER FOR SPACE RESEARCH

and

ENERGY CONVERSION AND SEMICONDUCTOR LABORATORY
Department of Electrical Engineering
MASSACHUSETTS INSTITUTE OF TECHNOLOGY
Cambridge 39, Massachusetts

SCIENTIFIC REPORT NO. 2

on

November 1, 1966

PHOTOVOLTAIC EFFECTS IN CADMIUM TELLURIDE-MERCURY TELLURIDE HETEROSTRUCTURES

by

George Stanley Almasi

ABSTRACT

This paper reports the results of measurements on photovoltaic devices made by the interdiffusion of CdTe and HgTe. It is found that the devices display rectification and possess a spectral response which decreases exponentially with decreasing energy from a maximum at the energy corresponding to the CdTe bandgap (1.5 eV). The theoretical model developed to account for this behavior involves a sandwich of constant energy gap material and graded gap material, with a p-n junction in the constant-gap material immediately adjacent to the graded region. The exponent of the spectral response is then found to reflect the band-edge variation of the carrier species being collected by the junction. The devices may be useful as detectors in applications where long wavelength response and a short response time (theoretically below 10^{-8} sec) are more important than sensitivity (10^{-3} $\mu V/\mu W$ at most). They are also fairly sensitive in a narrow spectral region (1.4 eV-1.5 eV) just below the CdTe bandgap energy (noise-equivalent-powers down to 2 x 10^{-9} watts/cps). However, because the spectral bandwidth is so narrow, the devices in their present form offer no improvement over present photovoltaic energy converters. To improve their performance as photodetectors, a more precise control of the equilibrium carrier concentrations must be developed.

ACKNOWLEDGEMENTS

The author would like to express his appreciation to both Professor John Blair, who suggested this problem and was the original supervisor, and Professor Arthur Smith, who guided it to its successful completion. He would also like to thank the two other members of his thesis committee, Professors Paul Gray and David C. White, for both technical advice and moral support.

The able assistance of Mr. William Brennan and Mr. Rusvi Wong in the preparation of samples is gratefully acknowledged. Dr. John Halpern of the National Magnet Laboratory graciously made his equipment available, and the help of Mr. Joseph Stella in making measurements there was invaluable. Professors Yizhak Yacoby, R. B. Adler, and R. H. Rediker, Mr. Lawrence Rubin of the National Magnet Laboratory and Dr. Alan Strauss of the Lincoln Laboratories all gave of their time in helpful discussions.

The cooperation with Dr. J. W. Conley in the growth of CdTe was both pleasant and profitable, as was the help of Dr. Lavine of Raytheon in the CO_2 laser experiments. The author hopes that the countless number of people in the Electrical Engineering Department, in the Materials Science Center, in the National Magnet Laboratory, and at Lincoln Laboratories who gave help when it was needed know that their help was appreciated.

The smooth production of the manuscript was the result of the talents of both Miss Barbara Smith and Mrs. Donna Spencer. The drawings are from the fine shops of Mr. John Mara and Mr. Harold Tonsing.

The author would like to thank his wife Carol for her truly unfailing encouragement and support.

Finally the author would like to thank the National Aeronautics and Space Administration for its financial support. This research was carried out under contract: NASA Grant NsG 496 (part).

TABLE OF CONTENTS

LIST OF TABLES

LIST OF FIGURES

LIST OF SYMBOLS

A = junction area

B = magnetic field strength

C_o = zero-bias junction capacitance

D_n = electron diffusion constant

D_p = hole diffusion constant

$D*$ = ambipolar diffusion constant

E_c = conduction band edge

E_f = equilibrium Fermi level

E_g = energy gap

E_v = valence band edge

$\underline{\mathcal{E}}$ = $d\delta_o/dx$ = $1/kT[d(E_c-E_f)/dx]$ = normalized conduction band edge gradient

$\vec{\mathcal{E}}$ = electric field strength

g = rate of generation of excess carriers

h = $h/2\pi$ = Planck's constant

I = current

J_n = electron current density

J_p = hole current density

k = Boltzmann constant

L_n = diffusion length of electrons

L_{dr} = drift length

n = total electron concentration

n_o = equilibrium electron concentration

Δn = excess electron concentration

N_c = $2(2\pi m_e kT/h^2)^{3/2}$ = effective conduction band edge density

N_v = $2(2\pi m_h kT/h^2)^{3/2}$ = effective valence band edge density

N_a = acceptor concentration

N_d = donor concentration

p = total hole concentration

P_o = equilibrium hole concentration

Δp = excess hole concentration

q_o = incident photon flux

s = surface recombination velocity

t = width of graded region (except in Section 3.1, where
t = duration of diffusion)

T = temperature

V_{14}, V_{24} = front-to-back voltages

V_{34} = PEM voltage

x = spatial coordinate

α = optical absorption coefficient

β = mole fraction Cd

γ = $- \ln p/N_v$

δ = $- \ln n/N_c$

ϵ = dielectric constant

λ = wavelength

μ_n = electron mobility

μ_p = hole mobility

μ^* = ambipolar mobility

ν = photon frequency

σ = conductivity

τ = excess carrier lifetime

ϕ_o = equilibrium electrostatic potential

$\phi - \phi_o$ = photopotential

CHAPTER 1

INTRODUCTION

The research described here started out as an effort to improve the performance of semiconductor photovoltaic energy converters by eliminating several of the factors which limit the efficiency of such devices. As described by Wolf[1] in discussing p-n junction photovoltaic solar cells, one of the major losses in such devices is due to the fact that the maximum voltage it is possible to obtain from them is smaller than the potential difference between the top of the valence band and the bottom of the conduction band, independent of the photon energy $h\nu$. This comes about because the portion of the photon energy which is utilized is just the energy necessary to transfer an electron from the top of the valence band across the energy gap E_g to the bottom of the conduction band. For high energy photons ($h\nu > E_g$), the energy in excess of E_g is lost to the semiconductor lattice in the form of heat, while the energy of photons with $h\nu < E_g$ is lost completely because they are not absorbed. Wolf shows that for the solar energy spectrum, these two loss mechanisms alone reduce the maximum conversion efficiency to 46%, obtained for an energy gap of 0.9 electron-volts (eV).

This loss of efficiency can be alleviated somewhat by cascading a number of cells with different energy gaps. However, the approach taken here goes beyond this, and proposes the use of a material in which the energy gap varies continuously from a relatively high value on the illuminated (front) side to a low value on the dark (back) side. The idea then is to absorb the high energy photons in the large energy gap region and the low energy photons in the small gap region, thus (hopefully) permitting a larger fraction of the incident solar energy to be retrieved. As will be explained later,

there is also the possibility that such a device would make a
high-speed photodetector which would be sensitive to a wide
range of photon energies. However, as pointed out by Segall
and Pell[2], in order to appraise either of these possibilities,
it is necessary to investigate the mechanism for getting
power out of such a device.

In 1957, Kroemer[3] showed on the basis of quantum-
mechanical considerations that in such a graded energy gap
region, the conduction and valence band edge gradients act
upon the electron and hole movement as through they were
electric fields; however, since the two slopes are different,
these "quasi-electric" fields are not the same for electrons
and holes.

In the same year, Tauc[4] used arguments from irreversible
thermodynamics to calculate the open-circuit photovoltage of
an otherwise homogeneous graded energy gap photocell (Fig. 1.1).
His result may be written

$$V_{a,a'} = \frac{1}{e} \frac{\mu_n}{\mu_p} \frac{\Delta n}{p_o} (E_{Gb} - E_{Gc}) \qquad (1.1)$$

The illumination spectrum was assumed to be such that it
resulted in a uniform density of excess electrons (Δn)
between $x = b$ and $x = c$ (see Fig. 1.1); p_o is the equilibrium
hole (majority carrier) concentration, μ_n and μ_p are the
electron and hole mobilities, respectively, and $E_{Gb} - E_{Gc}$ is
the change in energy gap between $x = b$ and $x = c$. The
assumptions made in arriving at this result are detailed in
the paper[4].

Since that time, several other analyses of graded-gap
photo-devices have appeared[2,5--10]. These vary in the
assumptions they make, in the rigor with which they are
executed, and in the conclusions which they draw. (A
discussion of these various papers is contained in reference
No. 7.) However, their results all agree that in the absence
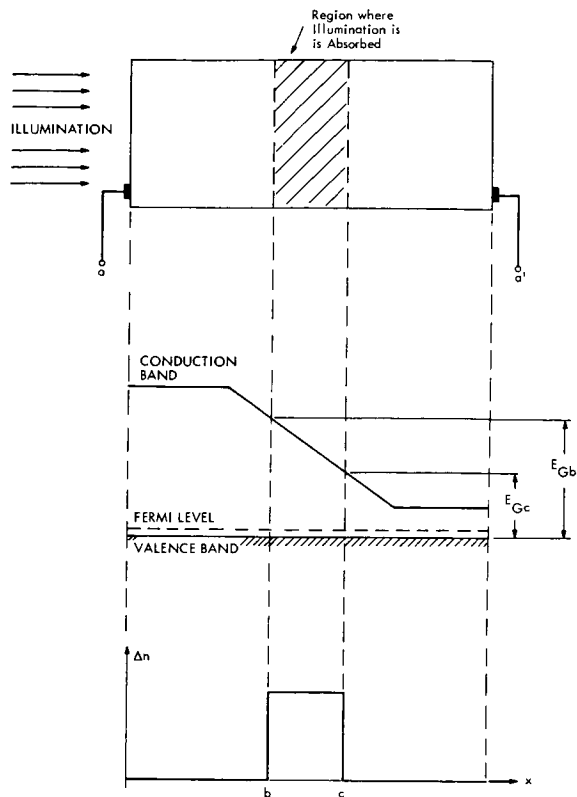
Fig 1.1: Simple Graded Energy Gap Photocell. (Adapted from Tauc (4.)

Fig 1.2: CdTe-HgTe Graded - Gap Photocell in the PEM Configuration.

Fig 1.3: CdTe Graded-Gap Photocell, Front-to-Back Measurement.
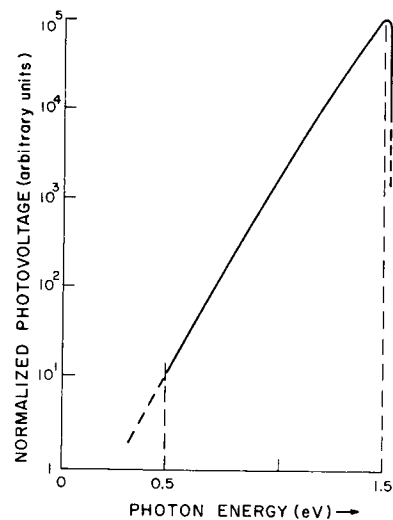
Fig 1.4: Observed Spectral Response of Front-to-Back Photovoltage.
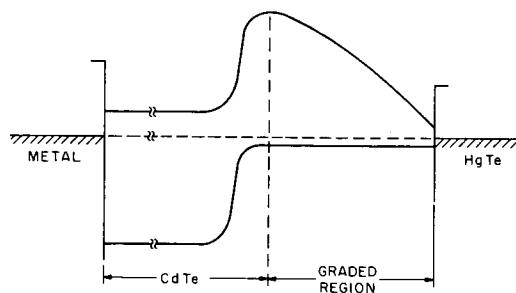
Fig 1.5: The band profile of the assumed model.

of a p-n junction in the graded region, the photovoltage will be inversely proportional to the <u>majority</u> carrier concentration in the graded region.

It can be shown from quite general considerations that efficient operation of such a device is not reached until the incident light intensity is high enough to make the open-circuit photovoltage independent of the light intensity. This condition is achieved when the density of optically generated carriers approaches the equilibrium majority carrier concentration. This same ratio of excess to equilibrium carriers determines the sensitivity of such a device used as a detector. Therefore, all other things being equal, the lower the equilibrium majority carrier concentration, the lower the light intensity required to achieve useful operation. It was with this thought in mind that the experiments to be described here were undertaken.

The fabrication procedure will be described in more detail in the next chapter, but basically it consists of the solid-state interdiffusion of HgTe and CdTe in an evacuated ampoule under a controlled partial pressure of Cd. At first, the resulting devices were tested in the Photo-Electro-Magnetic (PEM) configuration (Fig. 1.2). The photovoltage was zero for photon energies above the CdTe energy gap (1.5 eV), and more or less independent of photon energy for $h\nu < 1.5$ eV. However, the voltages were very small. The probable reason for this was the HgTe layer, which was acting as a low resistance in parallel with the PEM current source.

It seemed that this effect could be avoided by using the simpler photovoltaic configuration shown in Fig. 1.3 to measure the photovoltage between the front and back faces of the device. In addition, since Equation 1.1 indicates that for a given level of illumination, the output voltage can be increased by decreasing the equilibrium majority carrier

concentration, the diffusion conditions were chosen in the light of past annealing experiments to yield graded regions with equilibrium carrier concentrations as low as possible.

It was found that it was indeed possible to obtain devices with high small-signal impedance (indicative of low equilibrium carrier concentrations) by this method. However, the spectral response differed markedly from its anticipated behavior. It had been expected that, for equal numbers of photons, the photovoltage would be independent of photon energy, or that it would vary at most linearly with photon energy. Instead, the behavior sketched in Fig. 1.4 was observed, with the photoresponse having a maximum value at a photon energy corresponding to the CdTe energy gap (1.5 eV) and decreasing in an exponential fashion for smaller photon energies at a rate between three and nine orders of magnitude per electron-volt. In addition, the current-voltage character-istics for voltages above a few tenths of a volt were found to be strongly nonlinear.

At first, this was attributed to non-ohmic contacts at the front (CdTe) face; however, a series of experiments showed that there was always some rectification which was not associated with the contacts. Metals known to give ohmic contacts on p-type CdTe were used, as well as metals known to give ohmic contacts on n-type CdTe, and the current-voltage characteristics resulting from each were investigated from light sources specially filtered to give only photons with energies below the CdTe gap. In this way it was possible to distinguish rectification at the CdTe contact from rectifica-tion occuring elsewhere in the device. A further indication that rectification was occuring at the interface between the CdTe and the beginning of the graded gap region was provided by a junction location experiment, in which copper was photo-electroplated in a thin line along this interface.

At this point it was decided that any modification of the preparation procedure would have to await a better understanding of the physical processes in the present devices. Accordingly, a model was set up consisting of a p-n junction adjacent to a graded-gap region (Fig. 1.5), and a theoretical analysis was carried through to determine the current-voltage characteristics and spectral response to be expected from such a configuration. This analysis provided a theoretical relationship between the slope of the spectral response in Fig. 1.2 and the slope of the conduction band edge[*] in the graded region (Fig. 1.5). Using this information it is possible to construct models for individual devices which are consistent with the various data available for that particular device. These data include measurements of the spectral response, current-voltage characteristics, capacitance measurements, bulk Hall measurements, saturation open-circuit voltages, and results from contact and junction definition experiments. This model also explains another unexpected result, namely, that there is very little correlation of device characteristics with diffusion history.

It is concluded that the value of the devices as they stand as either detectors or as energy converters is marginal. The junction voltage can be used to convert energies just below the CdTe bandgap fairly efficiently, but its very narrow bandwidth makes it inefficient for any kind of a continuous illumination spectrum. By the same token its use as a detector would be limited to a very narrow range of photon energies.

The PEM voltage mentioned earlier is very small at present, but it does remain more or less independent of

---

[*] Or in general, the band edge corresponding to the carrier type being collected from the graded region by the junction.

photon energy to values of 0.1 eV and perhaps less (corresponding to wavelengths of 12μ and perhaps beyond); in addition, it may have a very fast response, since the measurements mentioned earlier indicate that the photogenerated carriers in the graded region move primarily by drift. Time response measurements are incomplete, but if the response time even approaches the room-temperature hole lifetime in CdTe[11,12] (estimates range between 10^{-8} and 10^{-9} seconds), then the device may find application as a low sensitivity but very fast long-wavelength detector which can operate at room or liquid nitrogen temperature.

The main value of the devices as they stand is in the information they provide, both on the internal mechanisms of the graded-gap region and on the avenues of development which are likely to lead to improvements. For example, it can be deduced from the behavior of the spectral response data that the photogenerated current carriers in the graded-gap region move primarily by drift. This opens up the possibility of a device whose speed is not determined by the lifetime of the excess carriers but by their transit time across the graded region.

It is concluded that the first step towards improved performance is a more precise control of equilibrium carrier concentrations.

REFERENCES

1. M. Wolf, "Photovoltaic Solar Energy Converters", Proceedings of the IRE, vol. 48, p. 1246, July 1960.

2. B. Segall and E. Pell, "An Evaluation of Graded Band Gap Photovoltaic Solar Cells", G. E. Research Laborabory Report No. 62-RL-3051G), June 1962.

3. H. Kroemer, "Quasi-Electric and Quasi-Magnetic Fields in Non-Uniform Semiconductors", R.C.A. Review, v. 18, p. 332 (1957).

4. J. Tauc, "Generation of an EMF in Semiconductors with Non-Equilibrium Current Carrier Concentrations", Review of Modern Physics, v. 29, p. 308 (1957).

5. P. Emtage. "Electrical Conduction and the Photovoltaic Effect in Semiconductors with Position-Dependent Band Gaps", Journal of Applied Physics, v. 33, p. 1950 (1962).

6. G. Almasi, "Cadmium Telluride-Mercury Telluride Graded-Gap Device", M.I.T. M.S. Thesis, 1962.

7. G. Almasi, "Graded Energy Gap Heterostructures", M.I.T. Energy Conversion and Semiconductor Laboratory Semiannual Technical Summary Report No. 3, NASA Grant NsG 496 (part), pp. 1-51, November 1964).

8. G. Cohen-Solal et al, "Effects Photoelectriques et Photo-magnetoelectriques dans les structures a largeur de bande interdite variable", Comptes Rendus, v. 257, p. 863 (1963).

9. C. Verie, "Effect des gradients de largeur de bande interdite et de masse effective dans les structures heterogenes", Comptes Rendus, v. 258, p. 6386, (1964).

10. A. Fortini and J. P. Saint-Martin, "Photomagneto-Electric Effect in Graded-Gap Semiconductors", Phys. Stat. Solid, v. 3, p. 1039 (1963).

11. M. R. Lorenz and H. H. Woodbury, "Double Acceptor Defect in CdTe", Physical Review Letters, v. 10, p. 215, March 1963.

12. D. A. Cusano and M. R. Lorenz, "CdTe Hole Lifetime from the Photovoltaic Effect", <u>Solid State Communications</u>, v. 2, p. 125, (1964).

CHAPTER 2

MATERIAL AND SAMPLE PREPARATION

2.1 Preparation of the Compounds

The CdTe ingots used for this study were the result of a program established by L.G. Ferreira, J.W. Conley, and the present author. Some 100 ingots were prepared during this study. The procedure has been described in detail by Conley[1], and so only the highlights will be described here.

Pieces of Cd wire (99.999% pure) and chunks of Te (99.999% pure) were weighed out in stoichiometric proportions and were placed in a 12 mm ID quartz tube whose inside walls had previously been carbon-coated. The tube was evacuated and sealed off when the pressure reached about 10^{-5} mm and was placed in a rocking furnace for reaction of the elements.

This reaction is strongly exothermic; rapid heating of the elements to a temperature which is sufficient to melt the compound results in a porous, inhomogeneous, and generally unsatisfactory product. To avoid this, the heating cycle shown in Fig. 2.1 has been derived empirically and has been embodied in an automatic programmed furnace control system. The cycle can be understood by the following sequence of events:

   I. First the Cd is melted

  II. then the Te is melted

 III. Temperature is increased slowly through that range where the reaction can proceed only until solid compound blocks further reaction of the melts, and then

 IV. slowly through that range of temperatures where the reaction can proceed through solution of the solid barriers. A spontaneous reaction is often observed after some time (typically one half hour) of "soaking" at 825°C.

V. The remainder of the cycle is intended to melt the compound and to allow a short period of rocking (one half hour) at 1140°C. The rocking is carried out with the ampoule oscillating slowly about the horizontal plane, followed by one or two inversions of the ampoule.

VI. Lastly, the compound is frozen with the tube in a vertical position.

The growth process is essentially a modification of the sealed ingot vertical zone process described by Lorenz[2]. The reacted ampoule is lowered through an induction-heated graphite susceptor at 1150-1175°C which creates a molten zone about one-half inch wide. Several purifying passes are made at a lowering rate of about 25 mm/hr., followed by a growth pass at 2--5 mm/hr. The result was usually a 100 gm ingot with a 12 mm diameter and about 15 cm length. About fifty ingots have been prepared by this method; single crystal regions 12 mm in diameter and three to ten cm long have been observed in at least ten of these.

Hall measurements showed carrier concentrations in the n-type samples ranging around 10^{15} cm^{-3}, with mobilities around 10^3 cm^2/v-sec. The values of carrier concentration were confirmed both by infrared free-carrier absorption data and by thermoelectric power measurements. Carrier concentrations in the as-grown p-type samples were usually higher, ranging a little above 10^{16} cm^{-3}, with mobilities around 100 cm^2/v-sec or below. (The doping is determined by small deviations from stoichiometry). Again there was some confirmation of the Hall data by thermoelectric power measurements.

The Hall measurements made on the CdTe used for the samples in this study are summarized in Table 2-1. The equipment used for these measurements is described in Chapter 3.

The HgTe used in this study was made from the same Te (99.999% pure) and from reagent grade (99.99% or better) Hg. Enough excess mercury was added to
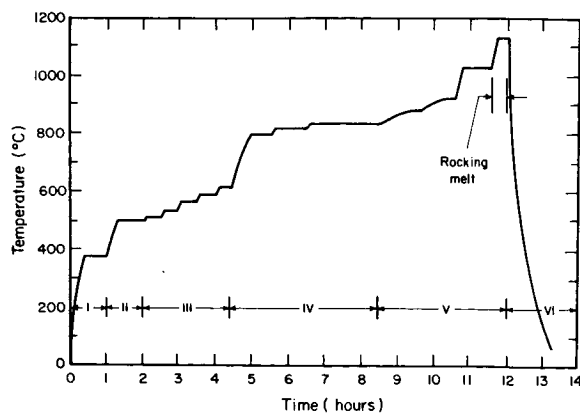
Fig 2.1: Temperature Program for Reacting CdTe
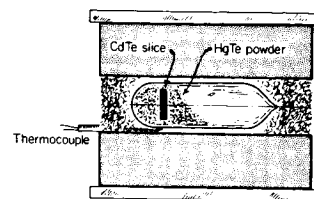
Fig 2.2a: Diffusion Sample in Furnace (not to scale).
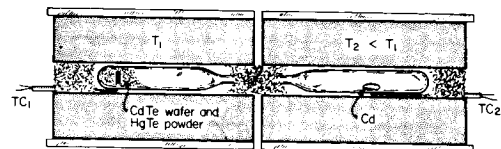
Fig 2.2b: Sample Ready for Diffusion under Cd Pressure.
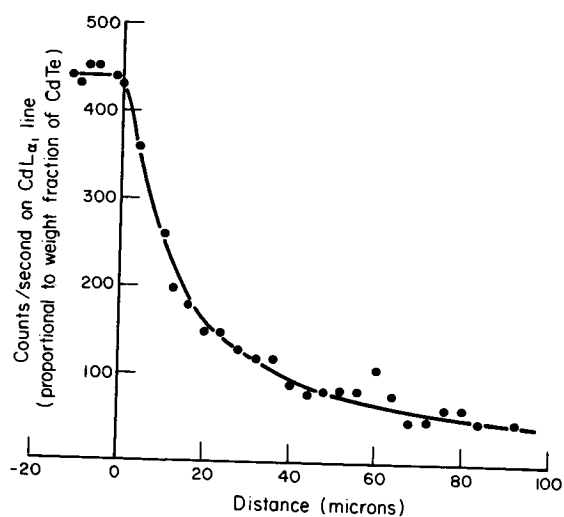
Fig 2.3: Uncorrected CdTe concentration Profile of Diffusion sample B2024-07-DI (650° C, 24h). (Corrected for Background ≡ Radiation only.)
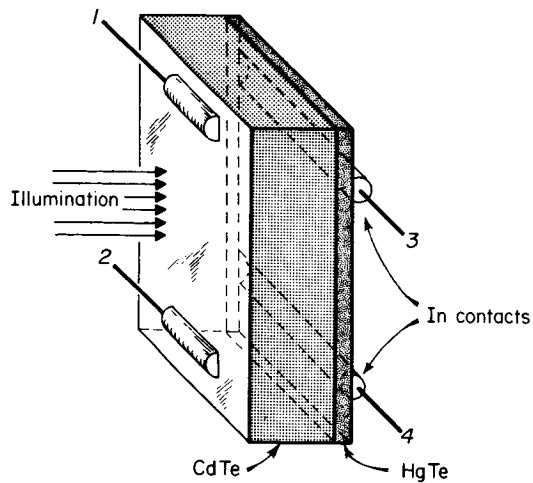
Fig 2.4: Device Configuration.

TABLE 2.1

MEASUREMENTS OF ELECTRICAL PROPERTIES (300°K)
ON CdTe INGOTS USED FOR DIFFUSION SAMPLES

Sample	Concentration (cm^{-3})	Mobility $(cm^2/v\text{-sec})$	Measurement[*]
B2081	$p = 5 \times 10^{16}$	100	HE
	$p \sim 9 \times 10^{16}$		TEP
B2085	$n = 2 \times 10^{15}$	1200	HE
	1.3×10^{15}		IR
B2089	$p = 10^{16}$	2 (?)	HE
B2098-1	$n = 1.5 \times 10^{15}$	1600	HE
B2098-2	$n = 2.2 \times 10^{15}$	2000	HE
	$n = 2.4 \times 10^{15}$		TEP

B2098A1 (This sample was annealed at 630°C for 24 hr. with no external Cd pressure imposed.)

	$p = 4.8 \times 10^{12}$	93	HE
	$p \ll 10^{14}$		TEP

B2098D8 (This sample was heated in HgTe powder at 630°C for ten minutes, after which the HgTe layer was removed.)

	$p = 9.0 \times 10^{12}$	10	HE

B2098D10 (This sample was heated in HgTe powder at 630°C for forty minutes, after which the HgTe layer was removed.)

	$p = 3.2 \times 10^{19}$	19	HE

[*] HE = Hall Effect
 TEP = Thermoelectric Power
  IR = Infrared Free Carrier Absorption

result in approximately a 5% deviation from stoichiometry. This is necessary to counteract the rejection of mercury which occurs even in samples prepared from stoichiometric proportions.[3,4] Otherwise, the precautions and procedures were very similar to those used for CdTe. The samples were reacted at 740°C for approximately ten hours, after which they were allowed to cool in the furnace. The tendency to adhere to the walls of the ampoule was much less pronounced than it was for CdTe[1], and none of the samples cracked upon cooling.

About eight 100 gm polycrystalline samples prepared in the above manner supplied most of the HgTe powder used for the diffusion samples. The few samples in which CdTe powder was diffused into HgTe wafers used slices from a single-crystal ingot prepared earlier by R. E. Nelson of this laboratory. No Hall measurements were made on HgTe.

2.2 Preparation of the Diffused Samples

The graded-gap devices were usually prepared by a solid-state diffusion process between HgTe powder and a single-crystal CdTe wafer about 1--2 mm thick and about 1 cm in diameter. The wafers were usually cleaved from the CdTe ingot with no subsequent processing except for a rinse in an acetone-alcohol mixture. Several wafers were also polished mechanically and then etched either in a modified aqua regia solution (two parts nitric, one part hydrochloric, and one part glacial acetic acid by volume) or in a Bromine etch (one part Bromine to twenty parts Methyl alcohol by volume). The second of these two etches always leaves a shiny clear surface, whereas the first sometimes leaves either a black or a whitish layer. However, no correlation was found between the characteristics of the finished device and the surface preparation technique.

The HgTe powder was ground from polycrystalline pieces using a mortar and pestle, and was then filtered through several stainless steel mesh sieves. The

final composition was such that about 95% of the particles were below 0.1 mm in diameter and 5% of the particles were between 0.1 and 0.2 mm in diameter. These were mixed uniformly.

The wafer and the powder were placed in a quartz ampoule as shown in Fig. 2.2(a), pumped down to a pressure between 10^{-4} and 10^{-5} mm Hg or below, and sealed off. The samples were then placed into a horizontal resistance furnace and heated at a temperature below the melting point of HgTe (670°C) for durations between ten minutes and four days, after which they were allowed to cool off in the furnace. (E.g., samples were heated at 630°C for 10 min, 40 min, 160 min, 1 day, and 4 days, and similarly at 560°C, 500°C, and 440°C.) Temperatures were maintained constant within $\pm$ 3 °C. (These values of temperature and time were chosen partly to correspond to the available data on the diffusion process[7,8].)

Twin line patterns visible in the CdTe "substrate" before diffusion were reproduced in the HgTe layer, which indicates that the process is epitaxial. Electron-beam microprobe measurements[5,6] show that transition regions between pure CdTe and pure HgTe with widths of several tens of microns are obtainable by this procedure. (The microprobe measurements and their interpretation are discussed in more detail in the next chapter.) A sample concentration profile is shown in Fig. 2.3. This shows the intensity of the emitted Cd $L_{\alpha 1}$ x-ray line as an electron beam about 2μ in diameter is slowly driven across a cross-section cut of the transition region between pure CdTe and pure HgTe. Since the data are not corrected for absorption, fluorescence, and atomic number effects, the intensity variation is within 10% of the true weight-fraction variation of CdTe.

The shape and width of this profile are consistent with the results of Rodot and Henoc[7], who were dealing with diffusion between two solid slabs

of CdTe and HgTe and who show results for diffusion temperatures between 400°C and 560°C[*].

Variations of the diffusion procedure used in the present study included the use of a mixture of CdTe and HgTe powder instead of pure HgTe, the addition of dopants to the HgTe powder, and diffusion under a Cd pressure using the two-zone furnace shown in Fig. 2.2(b).

2.3 Contacts

Contacts on the majority of samples were prepared as follows: After diffusion, the resulting HgTe layer was removed from all but one of the faces of the wafer by lapping and sand-blasting. The CdTe face was then polished with Linde A and B alumina powder (0.3μ and 0.05μ particles, respectively). This was followed by an etch in a 1:20 solution of Bromine in methyl alcohol (about 1 min), another polish with Linde B, and another etch (a few seconds). The Linde B polishes and the second etch were eventually discontinued, as they seemed to have negligible effect on the finished devices.

Contacts were placed as shown in Fig. 2.4 with a small ultrasonic soldering iron and pure indium solder, and were then evaluated using an I-V curve tracer. (These contact experiments are described in much more detail in the next chapter.) The high resistances of the CdTe layer after diffusion (cf Table 2.1) made ohmic contacts difficult to achieve; in general, the I-V characteristics at contacts 1-4, 2-4, and 1-2 (cf. Fig. 2.4) were high-resistance and nonlinear (zero-bias small-signal resistances were between 100K and 10M or more).

---

[*]Actually, further experiments in which the HgTe and CdTe slabs were separated by a void space indicate that the HgTe is transported to the CdTe surface in the vapor phase, and that subsequent diffusion takes place between the layer of HgTe formed in this way and the CdTe substrate. (M. Rodot, private communication). This is most probably happening in the experiments of this study also.

In some instances it was possible to decrease the resistance between some or all of the three contact pairs mentioned above by first depositing a spot of gold or silver from a salt solution (as described by deNobel[9]) onto the CdTe face and then making contact to the spot with silver conductive paint. The best results in this study were obtained using $HAuCl_4 \cdot 3H_2O$ in a water solution.

The I-V characteristics at contacts 3 and 4 on the HgTe face were linear with resistance on the order of an ohm.

The devices resulting from the preparation procedures described here are discussed in the next three chapters. The microprobe measurements (Fig. 2.3) mentioned here are discussed in more detail in Chapter 3, and the energy-gap profile is calculated from the data. This information is used in setting up the theoretical model which is analyzed in Chapter 4 and compared with other measurements in Chapter 5. In addition, Chapter 3 contains a description of how photo-effects arising at the contacts described in this chapter may be distinguished from photoeffects occurring in the graded-gap region. The latter effects are discussed in some detail and then compared to the prediction of the theoretical model in Chapter 5.

REFERENCES

1. J.W. Conley, "Absorption of Photons by Excitons with Assistance from Phonons in a Polar Semiconductor", M.I.T. Sc.D thesis, February, 1965.

2. M.R. Lorenz and R.E. Halsted, "High-purity CdTe by Sealed-Ingot Zone Refining," J. Electrochem. Soc., V. 110, p. 343 (1963).

3. R.E. Nelson, "Preparation and Electrical Transport Properties of HgTe," M.I.T. Sc.D thesis, May, 1961.

4. J. Blair, "An Investigation into the Thermal and Electrical Properties of the HgTe-CdTe Semiconductor Solid Solution System," M.I.T. Electronics Systems Laboratory, Scientific Report No. 2, Contract No. AF 19(604)-4153, June 15, 1960.

5. G.S. Almasi, J. Blair, R.E. Ogilvie, and R.J. Schwartz, "A Heat-Flow Problem in Electron-Beam Microprobe Analysis," Journal of Applied Physics, V. 36, pp. 1848-1854, June, 1965.

6. G.S. Almasi, "CdTe-HgTe Graded-Gap Device," M.I.T. MS thesis, August, 1962.

7. H. Rodot and J. Henoc, "Diffusion a l'etat Solide entre des Materiaux Semi-conducteurs," Comptes Rendus, V. 256, pp. 1954-1957, (1963).

8. F. Bailly, G. Cohen-Solal, and Y. Marfaing, "Preparation et controle a largeur de bande interdite variable," Comptes Rendus, V. 257, p. 103 (1963).

9. D. deNobel, "Phase Equilibria and Semiconducting Properties of CdTe," Philips Research Reports, V. 14, pp. 361-399 and 430-492 (1959).

CHAPTER 3

MEASUREMENTS

3.0 Introduction

This chapter describes the measurements which were made on the devices whose preparation was described in Chapter 2. The first two sections (3.1 and 3.2) deal with the effects of the diffusion procedure on the structure and material properties of the devices, as determined by electron micro-probe, Hall effect, and thermoelectric power measurements. The photovoltage as a function of photon energy is discussed in Section 3.3. Sections 3.4 and 3.5 are devoted to the current-voltage and capacitance-voltage characteristics of the devices, and the dependence of the photovoltage on the light-chopping frequency is discussed in Section 3.6. These measurements all indicate that the device contains a rectifying junction, not associated with the contacts, which is sensi-tive to photon energies below the 1.5 eV bandgap of CdTe. This is further substantiated by the junction-definition experiments described in Section 3.7, which indicate the presence of a junction at or near the interface between the CdTe and the beginning of the graded region.

These results are used to set up a model for these devices; the analysis is carried out in Chapter 4, and the predictions of the model are compared with experiment in Chapter 5.

3.1 Microprobe Measurements

The microprobe measurements discussed in this section were undertaken to determine the shape and extent of the energy-gap profile resulting from the diffusion process described in Chapter 2. The microprobe method is capable of a quantitative chemical analysis on a sample with a volume of

several cubic microns. By moving the sampling area across the diffused region, it is possible to determine the composition as a function of distance. Data on the energy gap as a function of composition can then be used to calculate the energy gap as a function of distance.

In the microprobe method[1], a finely focused electron beam (1-2μ diameter) is incident on the sample surface and causes the emission of x-ray lines which are characteristic of the elements present in the sample. The wavelength of the line identifies the element, and the intensity can be used to calculate the weight fraction of that element.

Because the characteristic x-radiation can be partly absorbed by the sample before it leaves the surface, and can also be enhanced by fluorescence effects, the measured intensity is not exactly proportional to the weight fraction of the element. Castaing[2] has developed a semi-empirical correction formula which improves the accuracy of the method to within 1% for many materials. However, the calculation is quite cumbersome and would have to be applied point-by-point in this case.

A calculation of the maximum error likely to be incurred for the HgCdTe system by assuming the weight fraction of Cd to be proportional to the intensity of the Cd L_{α_1} line yields a value of 10%. Therefore the uncorrected data of Fig. 2.3 and 3.1 may be considered to be within 10% of the true Cd weight fraction variation.

A sample result of such a scan across the diffusion inter-face was given in Fig. 2.3 and is repeated in Fig. 3.1, which also shows the resulting variation of the mole fraction β of Cd. The variation of mercury and tellurium concentration was also measured, and all three intensities were checked against reference samples of pure Cd, Te, CdTe, and HgTe. It was found that the tellurium concentration stayed constant, while the
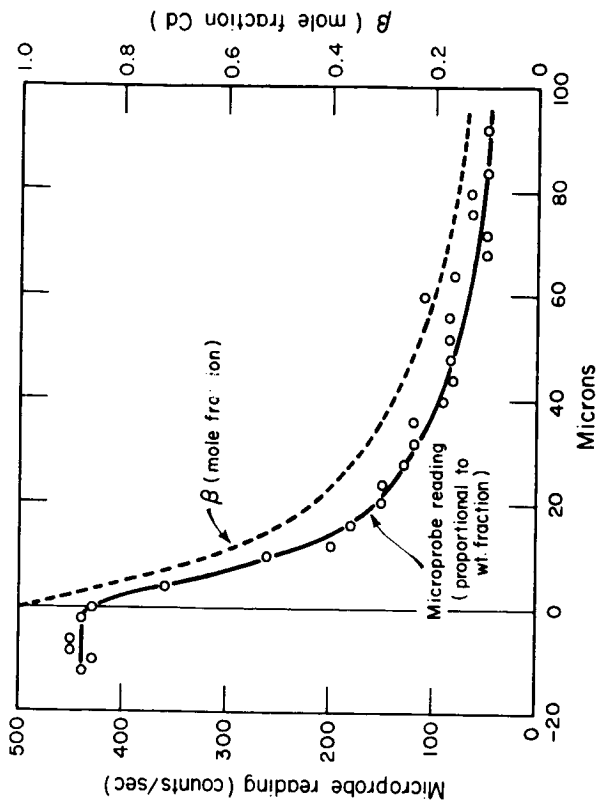
Fig 3.1: Diffusion Profile of Sample B2024-07-D1 (650°C, 27h) showing Variation of CdTe Weight Fraction and Mole Fraction.
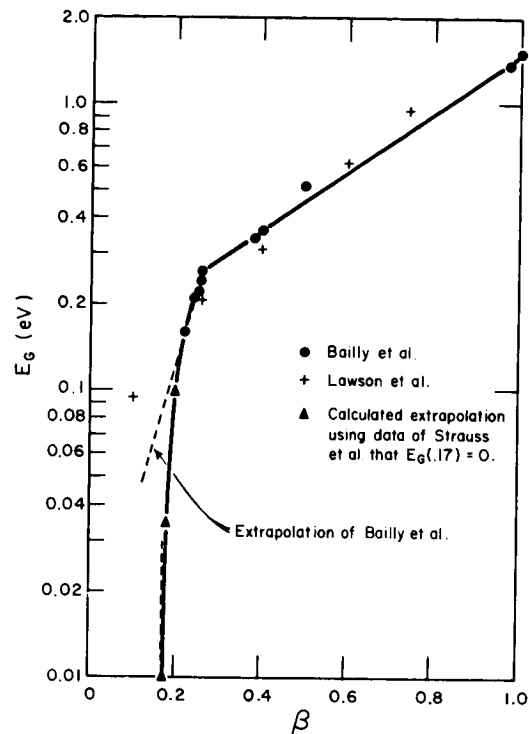
Fig 3.2:   Variation of Bandgap In $Cd_\beta Hg_{1-\beta} Te$.
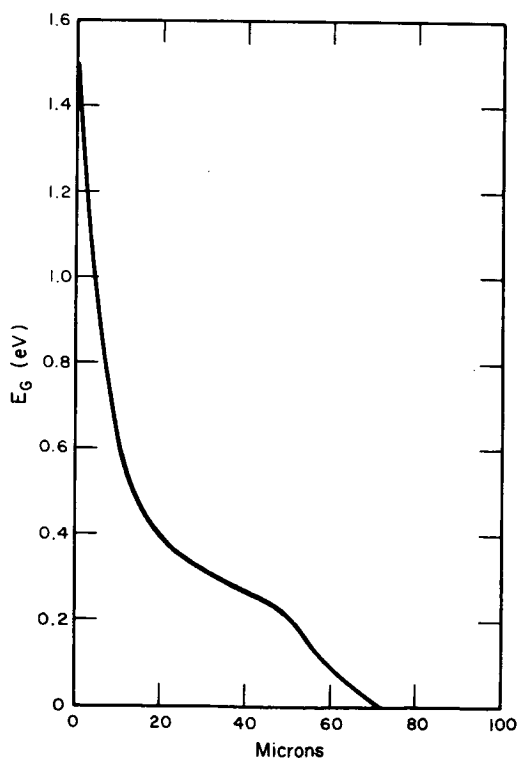
Fig 3.3: Calculated Energy Gap Variation VS. Distance for Sample 2024-07-D1. (650°C, 27h).
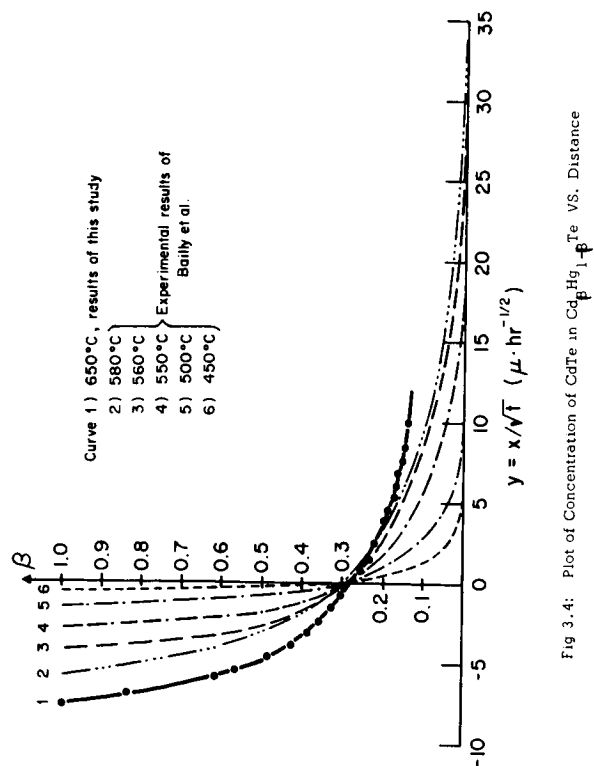
Fig 3.4: Plot of Concentration of CdTe in $Cd_\beta Hg_{1-\beta} Te$ VS. Distance

mercury concentration variation complemented that of cadmium.

The curve of energy gap vs. composition for $Cd_\beta Hg_{1-\beta} Te$ shown in Fig. 3.2 was constructed from three sets of published data on this system. Lawson et al[3] obtained their data by preparing a number of homogeneous samples with different compositions and measuring the fundamental optical absorption edge on each as a function of wavelength. Bailly et al[4] obtained their data by successively removing known thicknesses from the mercury-rich side of a diffusion sample and making optical absorption measurements each time. Magneto-optical measurements were used by Strauss et al[5] to establish that the zero-gap condition was reached at a composition of $Cd_{0.17}Hg_{0.83}Te$.

Since the value of the absorption edge becomes increasingly difficult to determine for smaller values of the energy gap, the results of both Lawson et al and Bailly et al are least reliable for the smallest values of β. Therefore the curve of energy gap vs. β for values of β between 0.25 and 0.17 was calculated by assuming a linear variation of energy gap, going from 0.25 eV to 0.00 eV, in this range.

The energy gap profile obtained from the data of Figs. 3.1 and 3.2 is shown in Fig. 3.3. Its general shape is quite similar to the sample curve shown by Bailly et al except that their curve has a much longer "tail" at small values of E_G. This is because the results of Strauss et al were not incorporated by Bailly et al, and that therefore the zero energy gap was assumed to occur for a much smaller value of β.

The data of Fig. 3.1 and similar data obtained by Bailly et al for lower diffusion temperatures are compared in Fig. 3.4. This figure is a reproduction of Fig. 2 in the paper by Bailly et al, with the data of this study drawn in for comparison. Bailly et al found that the composition at the Matano[7] interface (defined by the law of conservation of matter) was

constant at $\beta = 0.28$, and therefore chose this interface as the origin for y. The data of this study are not extensive enough to permit an independent calculation of the Matano interface, and so it is assumed to occur at $\beta = 0.28$ merely to permit a convenient comparison of the shapes of the curves. A quantitative measure of the agreement between the data of this study and the data of Bailly et al is provided in Fig. 3.5, which exhibits the distance in which the cadmium mole fraction changes from 0.14 to 0.28 as a function of the diffusion temperature. It can be seen that the point resulting from this study and the value obtained by extrapolating the results of Bailly et al differ by less than 10%. This lends weight to the hypothesis mentioned in Chapter 2 that the two processes are basically the same.

The data of Fig. 3.4 can be used to construct curves of energy gap vs. distance in the following way: From some supplementary data in an article by Rodot and Henoc[6], it can be deduced that the diffusion time for the 560°C curve in Fig. 3.4 was 24 hours. Rodot and Henoc present further data on diffusion at 560°C which shows that for diffusion times above 12 hours, the profile remains a constant function of $x/t^{1/2}$, where t is the diffusion time and x is the penetration depth, whereas for diffusion times below 5 hours, the profile is a constant function of $x/t^{1/3}$. Using this information, it is possible to construct the curves of energy gap vs. distance shown in Fig. 3.6.

Most of the spectral response data to be discussed in Section 3.3 was taken at photon energies between 1.5 and 0.5 eV. In discussing these measurements, therefore, one is interested in the region of the device in which the corresponding band-gap change occurs.

Figure 3.6 shows that at 560°C, a four-day diffusion makes this region about 12 microns wide, whereas a one-micron wide

region results from a ten-minute diffusion. The widest such region should result from the four-day diffusion at $630^\circ C$, and should be 32 microns wide, since the corresponding width for $630^\circ C$ and one day is 16 microns (Fig. 3.3), and the data of Rodot and Henoc indicate that for these temperatures and times, the penetration depth should vary as the square root of the diffusion time.

The narrowest such region should result from the ten minute diffusion at $440^\circ C$, and can be calculated from the data of Bailly et al and Rodot and Henoc as follows: it is assumed that since the $560^\circ C$ data in Fig. 3.4 are from a 24 hour diffusion, the $450^\circ C$ data are also from a 24 hour diffusion (this is not stated explicitly). The data of Rodot and Henoc indicate that at this temperature and for diffusion times below 24 hours, the penetration depth varies as the cube root of the diffusion time. Thus,

$$x(E_G = 0.5) - x(E_G = 1.5) = x(\beta = 0.54) - x(\beta = 1.0)$$

$$= [y(\beta = 0.54) - y(\beta = 1.0)] \sqrt{24} \cdot (\frac{10}{1440})^{1/3}$$

$$\approx 1/2 \ \mu$$

where the value of $[y(\beta = 0.54) - y(\beta = 1)]$ was obtained from Fig. 3.4. Thus the range of distances in which the energy gap changes from 1.5 to 0.5 eV in the devices studied here lies between 1/2 micron and 30 microns.

Appendix A of reference 8 discusses the validity of the effective mass treatment which allows the band-edge gradients to be treated as effective or "quasi-electric" fields; it is concluded that the analysis is valid for transition regions wider than 0.1 micron. Since it is unlikely that either band-edge gradient will exceed the band-gap gradient, the quasi-electric field treatment of carrier motion in the graded region should be valid for all the devices covered by this study. This is vital to the analysis carried out in Chapter 4,
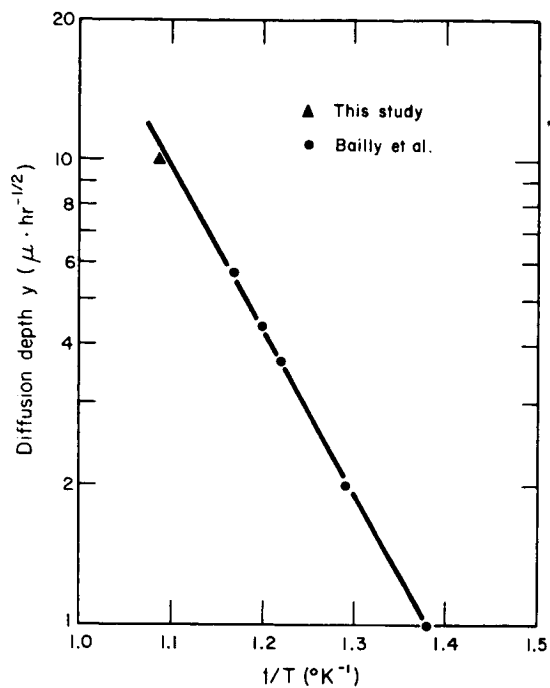
Fig 3.5: Diffusion Depth (y(β=0.14) - y(β=0.28)) as a Function of Diffusion Temperature.
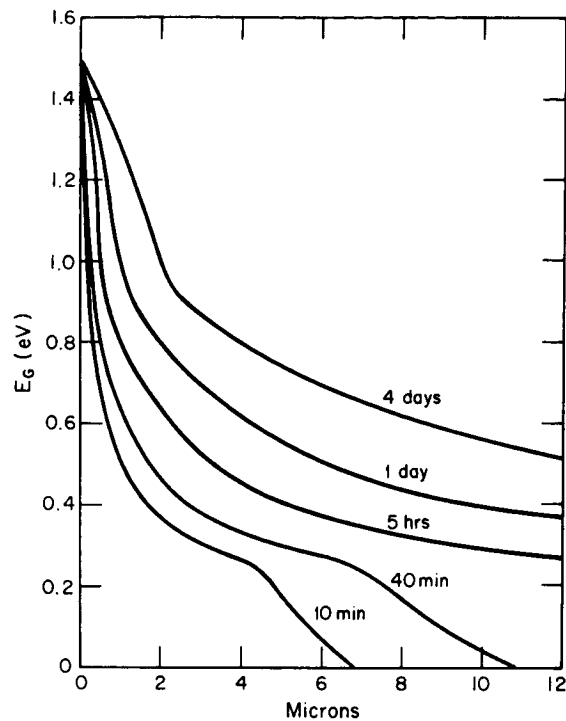
Fig 3.6: Calculated Energy Gap Profiles for 560°C Diffusion Temperature (see text for method of calculation.)
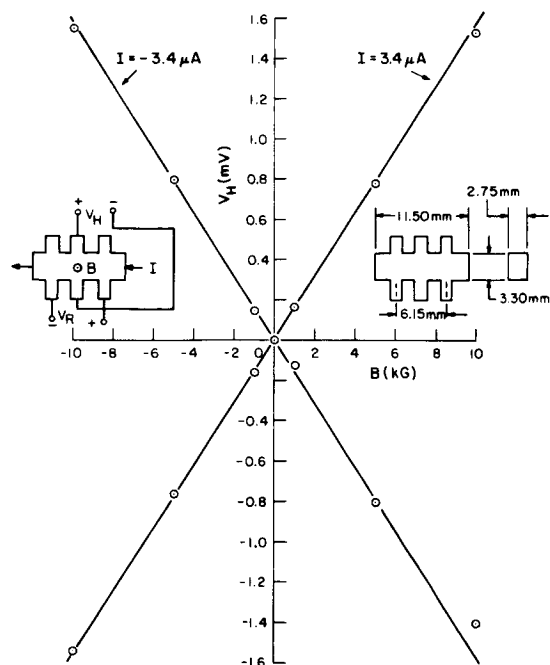
Fig 3.7: Hall Measurement on B2098 Al. (Inset: Shape of Hall Sample.)
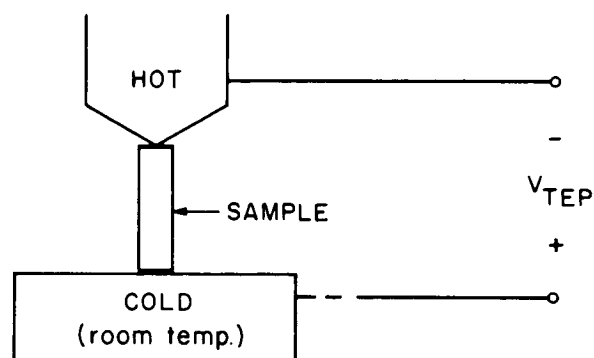
Fig 3.8: Thermoelectric power measurement (V_{TEP} positive for p-type sample.)

since it means that the graded region can be treated as a semiconductor with well-defined but position-dependent properties. Otherwise, the graded region would have to be treated as an abrupt boundary or a boundary layer between the CdTe and HgTe, and a heterojunction model would ensue.

The microprobe measurements discussed in this section can reveal the composition variation in these devices, and can be used to calculate the energy-gap variation. However, other methods must be used to determine the current carrier concentrations. This is discussed in the next section.

3.2 Bulk Carrier Concentrations

The energy-gap variation resulting from the diffusion procedure described in Chapter 2 has just been described. The next investigation to be reported concerns the effects of the diffusion procedure on the carrier concentration in the bulk CdTe portion of the sample. The results have already been summarized in Table 2.1. This section describes how these measurements were obtained.

Hall measurements[9], supplemented in several instances by thermoelectric power and infrared absorption measurements, were used to obtain the carrier concentrations. To make a Hall sample, the surface layer of the diffused slice was first completely removed by wet-lapping. The technique described by Blair[10] was then used: the Hall sample was cut using a sand-blaster, the sample was etched, and contacts were attached and checked on a curve-tracer. The sample holders were identical to those described by Blair.

Due to the high impedance of the treated samples (cf. Table 2.1), the AC system used by Blair to measure Hall and resistivity voltages proved to have too much pickup noise to give reliable results. (See Navipour[11] for a discussion of these problems). The most satisfactory procedure turned out to be a DC technique

using a Leeds-Northrup K-3 potentiometer and a Leeds-Northrup No. 2430 Galvanometer with a sensitivity of 3×10^{-9} A/mm.

The three thermo-magnetic effects which may produce errors in a DC Hall measurement are the Ettinghausen, Righi-Leduc, and Nernst effects[9]. Errors due to the last two effects can be eliminated by taking readings with both polarities of current and both polarities of magnetic field, and then averaging the four results. The Ettinghausen voltage can be calculated using a theoretical expression given by Putley[9], and can be shown to make a negligible contribution to the Hall voltage for CdTe.

The results of a typical measurement are shown in Fig. 3.7. (The insets give the dimensions of the sample and the reference polarities used.) For this particular sample, the HgTe powder in Fig. 2.2a was replaced with CdTe powder, and the process is referred to as annealing. After the sample had cooled in the furnace, about 250μ of material was removed from each side of the CdTe slice, the Hall sample was cut using a sandblaster, and the sample was etched in the modified aqua regia (Sec. 2.2) for several seconds. Indium or Indalloy contacts were attached using an ultrasonic soldering iron and were checked on a curve-tracer. Only ohmic contacts were used.

Since the results for both polarities of current and both polarities of magnetic field in Fig. 3.7 are identical, the Righi-Leduc and the Nernst effects must both be negligible, and the averaging is unnecessary. The Hall data shown in the figure and the dimensions shown in the inset lead to a current carrier concentration of 4.83×10^{12} cm^{-3}. The relative orientation of the magnetic field and current vectors indicates that the sample is p-type. Finally, a value of 320 mV across the resistivity contacts for a current of 3.4 μA results in a conductivity of 7.20×10^{-5} (ohm-cm)$^{-1}$ and a mobility of 93.1 cm^2/v-sec.

This is in good agreement with the results of Hinrichs[12], who found a value of $p = 2.2 \times 10^{12}$ cm^{-3} and $\mu = 63$ cm^2/v-sec for a sample which initially was n-type with 7.1×10^{16} carriers/cm^3 and which was annealed at 650°C for 24 hours. Hinrichs also discusses the results of deNobel[13], who presents annealing data for CdTe for higher temperatures.

The thermoelectric power measurements were made using a simple "hot probe" described by Nelson[14]. Ohmic indium contacts were attached to the ends of a bar of CdTe (usually about 10mm x 2mm x 2mm) and a temperature drop between 14 and 18°C (monitored with a thermocouple) was created in the sample by the hot probe (see Fig. 3.8). The resulting voltage was measured using a Keithley Model 150 Microvolt-ammeter. The polarity of the voltage indicates the current carrier type of the sample, and the thermoelectric power data of deNobel[13] (p. 23) can be used to calculate the magnitude of the carrier concentration. For example, for sample B2098-2 (see Table 2.1), a temperature difference of 16.0°C resulted in a negative voltage drop (cf. Fig. 3.8) of 11.4 mV. Using the data for n-type samples, a thermoelectric power of 0.713 mV/$^\circ$C is found to correspond to a carrier concentration of 2.45×10^{15} cm^{-3}, in excellent agreement with the value of 2.2×10^{15} cm^{-3} found from Hall measurements.

For the sample whose Hall measurement was described earlier in this section (B2098A1), the thermoelectric power measurement yielded a positive voltage corresponding to 4.28 mV/$^\circ$C. Since deNobel's measurements do not extend below hole concentrations of 10^{14} cm^{-3}, (corresponding to 1.14 mV/$^\circ$C), the only safe conclusion was felt to be that the hole concentration in B2098A1 was considerably below this value.

The infrared free carrier absorption measurement on B2085 is described in detail by Conley[16].

It was shown in reference 8 that the photovoltage in a

graded-gap device would depend on the ratio of the densities of excess (photon-generated) carriers and equilibrium (or "dark") carriers. The solar spectrum between 1.5 eV and 0.3 eV contains about 3×10^{17} photons/cm^2-sec.[15] If one assumes that these are uniformly absorbed in a region 10 microns wide and that the lifetime of excess carriers is 10^{-9} sec (a reasonable estimate for CdTe[17, 18], then the excess carrier concentration will be on the order of 3×10^{11} cm^{-3} (see reference 8).

These calculations are very rough estimates, but they do show that graded-gap devices with "dark" carrier concentrations on the order of 10^{12} cm^{-3} (indicated in Table 2.1) should show detectable photovoltages when illuminated with light intensities comparable to sunlight. It was therefore decided that the diffusion procedure described in Chapter 2 was satisfactory for the time being, and that it was time to investigate the photoeffects in these devices. This is described in the next five sections of this chapter.

3.3 Spectral Dependence and Other Properties of the Photo-voltage

As was mentioned in Chapter 1, photovoltages can be measured between the front and back faces of the diffused devices (V_{14} and V_{24} in Fig. 2.4), and also between two contacts on the back face when the sample is in the PEM (photo-electro-magnetic) configuration (V_{34} in Fig. 2.4 with a magnetic field perpendicular to the plane of the paper). This section describes how these two different photovoltages depend on the wavelength (or photon energy) of the incident light, and also examines the correlation between the photovoltage and the diffusion history of the samples. The experimental equipment and techniques will be described first, after which some representative data will be presented and discussed.

Experimental Procedure

Monochromatic light was obtained from a Perkin-Elmer model 112 single-beam double-pass infrared spectrometer. A NaCl prism was used with a globar source and a glass prism was used with a tungsten bulb source to cover the wavelength range between the visible (0.5 μ) and 15 μ. Measurements on the emission spectrum of a mercury lamp showed that the resolution of the instrument was within the manufacturer's specification, and a calculation following the procedure outlined in the instrument manual showed that at 100 μ slit width, the resolution throughout the range of photon energies covered was equal to or better than 0.01 eV. The NaCl prism was calibrated using Hg and Cs emission lines and H_2O, NH_3, and polystyrene absorption lines. The accuracy of the calibration curve is believed to be $\pm$0.01 eV or better in the range 0.1-1.5 eV. The resolution of the glass prism is considerably higher, being about one angstrom for a ten-micron slit width and photon energies corresponding to the mercury yellow doublet (2.1482 and 2.1404 eV).

The external optics were designed to focus the beam between the poles of an electromagnet with 6" diameter pole pieces and a 1" gap without losing any of the beam power (Fig. 3.10). Both of the front-surface aluminum mirrors were made by the World Optics Co. of Waltham, Mass. The 6" diameter mirror is flat to within 1/2 wavelength of the sodium D line; the 10" diameter concave spherical mirror has a 40" radius of curvature and is spherical to within 1/4 wavelength of the sodium D line. With the arrangement shown in Fig. 3.10, the maximum available light intensity at a slit width of 1500 μ and a globar power of 200 W was 3.16 mW/cm^2 at 3μ, as measured with a thermocouple which had been calibrated against a standard Eppley thermopile. The maximum light intensity available with the glass prism-tungsten bulb combination

Off-axis angle
$\alpha = 9.2°$

Object distance
$= 47"$

Image distance
$= 34"$

Magnification
$= 0.72X$
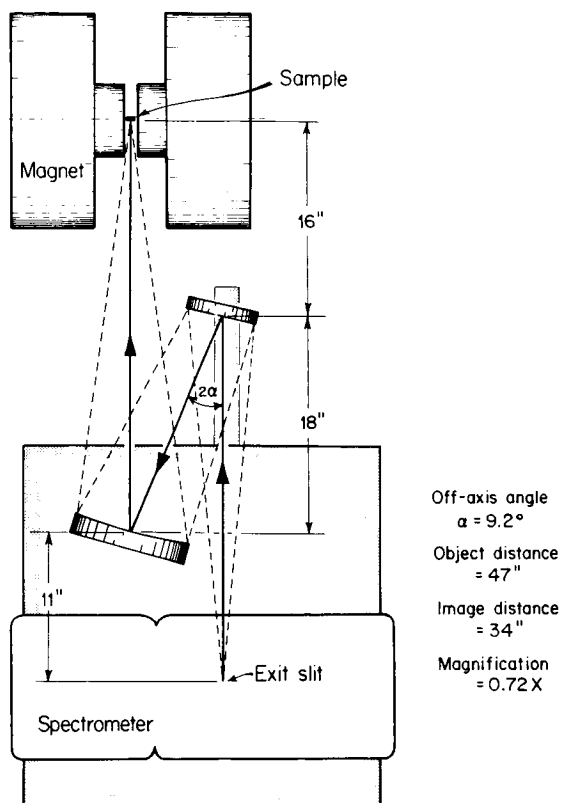
Fig 3.10: External Optical arrangement.

(a)

(b)

(c)
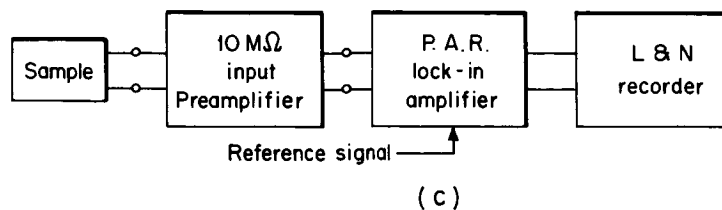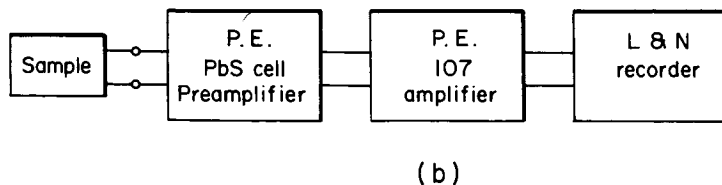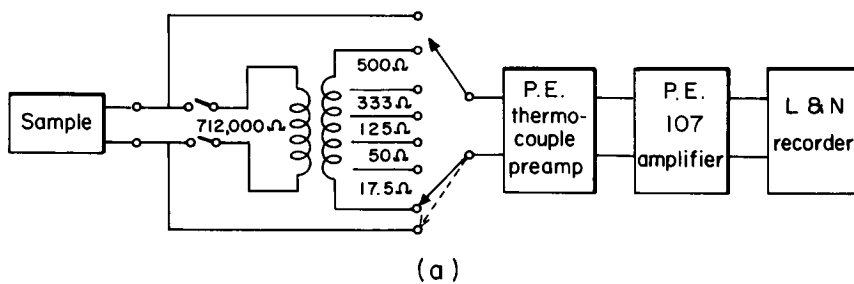
Fig 3.11: Amplification systems used to record Spectral Response
A.) PEM voltage and photovoltage.
B.) Photoconductive response.
C.) Photovoltage for high-impedance samples.

(approximately 45W input to the bulb) was about twice that available with the NaCl prism-globar combination.

Several different amplifier systems were used to record the photovoltages. The low resistance associated with the photo-electro-magnetic (PEM) voltage V_{34} (typically several ohms) made it possible to feed this signal directly into the Perkin-Elmer thermocouple preamplifier (approximately ten ohms input impedance). This was in turn connected to the Perkin-Elmer 107 amplifier and a strip-chart recorder (Fig. 3.11a) which automatically recorded the un-normalized output voltage as a function of a drum number which could be converted either to a wavelength or to a value of photon energy.

The impedance levels associated with the front-to-back voltage (V_{14} and V_{24}) are much higher, ranging between 10 K-ohm and several megohms. In some instances it was possible to use a 17.5-712,000 ohm "Geoformer" impedance-matching transformer to couple the signal into the thermo-couple preamplifier. However, impedance levels above about 100K introduced a phase shift which is difficult to compensate in the Perkin-Elmer synchronous detection system. This effect was confirmed by oscilloscope observations of the transformer input and output, which showed that in these cases the trans-former acts as a differentiator. This can lead to spurious results: Seven of the samples showed changes in the sign of the response at photon energies well below the CdTe bandgap, and in at least one case, the photon energy at which the crossover occurred was found to depend on the transformer ratio used. Four of these samples were still available for a measurement of the I-V characteristics under illumination. In all four cases it was found that the incremental resistance at zero bias was above a megohm in the dark and changed to several hundred kilo-ohms under spectrometer illumination.

This would result in a phase shift which depends on the intensity of the illumination and thus on the wavelength, and can result in an apparent sign change of the photovoltage. A check on four samples with no sign changes in their spectral response showed incremental resistances which were all above a megohm even at maximum spectrometer illumination, and would thus result in constant phase shift.

To avoid the phase-shift effect in the samples with the photo-sensitive incremental resistances, it was necessary to use the system shown in Fig. 3.11c. The 10-megohm input preamplifier was either a Tektronix Model 122 or the built-in preamplifier of a Princeton Applied Research (PAR) Model HR-8 lock-in amplifier. In addition to the HR-8, a PAR Model JB-4 lock-in amplifier was also used for chopping frequencies above 15 cps. The reference signal came either from a photo-cell mounted behind the chopping disk of the external chopping arrangement (this will be described in more detail in Section 3.6) or else from a battery and resistor connected in series with the internal chopper contacts of the spectrometer. When the lock-in amplifier was adjusted to put the reference signal in phase with the photovoltage, the sign changes in the spectral response of all four of the samples mentioned above were eliminated.

The system shown in Fig. 3.11c was also used to make some of the photoconductive measurements; the rest were made using the arrangement shown in Fig. 3.11b. The PbS photocell preamplifier has a 5-megohm input impedance in series with a 12V DC bias. The spectral dependence of the photoconductivity of a given sample was generally close to the behavior of the zero-bias photovoltage.

One of the limits on the accuracy of the measurements was set by the noise level of the recorded signal; this varied from sample to sample, but for most of the PEM measurements,

it was equivalent to a signal of approximately 10^{-9} volts peak-to-peak. The noise level with the thermocouple pre-amplifier short-circuited was between one-third and one-fourth of this value.

The peak-to-peak noise during the front-to-back photo-voltaic measurements (V_{14} and V_{24}) was usually equivalent to a signal between 0.1 and 0.3 x 10^{-6} volts. The photoconductive measurements differed only in the appearance of a current-dependent noise signal above certain current levels.

The other main limitation on the measurements is the available source power; useful data can be obtained only in wavelength regions where enough radiant power is available to create a signal photovoltage above the noise level. The effects of this will become more apparent when the data are discussed.

Normalization of the data was carried out in several ways. The spectral response for equal power input was obtained by recording the output of the source with a thermocouple detector; the data curve was then divided by the thermocouple curve point-by-point, and by taking account of the illuminated area of the sample and the area and sensitivity of the thermocouple, it was possible to present the results in units of volts/watt.

The spectral response for equal numbers of <u>photons incident per second</u> can be obtained in two ways. The simplest consists of recording the output of the source with a photon-counting detector such as a PbS cell, and then repeating the procedure outlined above. Unfortunately, the useful response of the PbS cell does not extend below 0.45 eV. In this case it is possible to <u>calculate</u> the number of photons per second from the data recorded with the thermocouple, and then use this curve to divide the data curve. The method used for the data presented here combined both these approaches. In this

case, the results are presented in units of volts per photon per second.

To insure against the possibility that the photovoltage was saturating with incident light intensity rather than reacting to changes in wavelength, the normalization procedure described above was checked by varying the slit width to keep the light intensity constant as a function of wave-length, and recording the resulting voltage. Both methods yielded identical results. In addition, spot checks at various wavelengths for a number of measurements showed that at the intensities available from the monochromator, the photovoltage was always linear with light intensity.

Because of the difficulty in determining the sensitive area associated with a front contact such as the one on these devices, spectral response data are usually in "relative" or "arbitrary" units. "Absolute" units of microvolts per photon per second are used on the data to be presented here, but the same inaccuracy prevails, and the units are used only for comparison purposes: the sensitive area was arbitrarily chosen to be equal to the illuminated area, resulting in a minimum or "worst-case" value for the sensitivity. The vertical scale of the spectral response plots may thus be in error by a large scale factor.

Experimental Results

All of the results reported in this section were obtained at 300°K. The front-to-back photovoltage available at contacts 1-4 and 2-4 was much larger than the PEM voltage available at contacts 3-4. This is shown in Table 3.1, which presents the maximum open-circuit voltage at contacts 2-4 for a number of samples when illuminated by "white" light with photon energies below 1.5 eV. This was obtained by passing light from a tungsten microscope lamp through a CdTe filter. The

Table 3.1: Maximum Open-Circuit Photovoltages for Tungsten
Bulb Light Passed Through CdTe Filter.

Sample	Diffusion Temp (^{O}C)	Diffusion Time	V_{24} (mV)	IV	$C_o/A(pf/cm^2)$
98D21	440	10 min	-410	np	108
98D23	440	40 min	-470	np	$\approx$100
98D25	440	160 min	- 16	d	-
98D20	500	10 min	- 50	d	63
98D22	500	40 min	- 2	d	11
98D24	500	200 min	-130	d	32
98D13	560	10 min	- 4	np	0
98D14	560	180 min	+ 10	d	90
98D17	560	24 hr.	+ 4	np	1.8
98D18	560	4 days	- 10	d	12
98D12	630	15 min	+440	d	35
98D6*	630	10 min	+ 80	d	12
98D11	630	170 min	+320	d	132
98D5*	640	300 min	+130	pn	279
98D16	630	24 hr.	+520	pn	120
98D19	630	4 days	<+ 40	d	7.2
81D1	630	24 hr.	+400	d	213

* These samples were annealed for 24 hours before diffusion.

voltages were measured using a Hewlett-Packard Model 3440A DC voltmeter with a 10 megohm input impedance. V_{24} would begin to saturate for intensities on the order of 0.1 watt/cm^2 (measured with an Eppley thermopile). The maximum open-circuit voltage measured in this way was 0.52 V. The maximum PEM voltage obtained under similar conditions was about 0.5 mV for a 10-kilogauss magnetic field and showed no saturation for light intensities up to 0.15 W/cm^2. However, spectrometer measurements showed that the measurable PEM voltage extended to much longer wavelengths than did the front-to-back photovoltage.

Sample results for the spectral dependence of these two photovoltages are presented in Figs. 3.12. These data are typical for most of the 30 or so samples on which such measurements were made in the sense that V_{14} and V_{24} always started at a maximum response per photon per second at a photon energy corresponding to the CdTe bandgap and decreased in a more or less exponential fashion with photon energy at a rate between three and ten orders of magnitude per electron-volt. V_{34}, on the other hand, is usually constant within 3 dB over the range between 0.2 and 1.4 eV. and is zero for energies above the CdTe bandgap[*]. The spectrometer resolution and the error due to the fixed noise level are shown by horizontal and vertical bars, respectively. The maximum photon energy at which measurements could be made was usually set by decreasing source output at high energies. Decreasing sample sensitivity usually set the lower limit on photon

[*] All the data on V_{34} reported here were magnetic-field depend-dent, and reversed sign when the magnetic field was reversed. Several samples exhibited a smaller photovoltage at contacts 3-4 even in the absence of an applied magnetic field. The spectral response of this photovoltage was quite similar to the PEM voltage, as was its frequency response (Sec. 3.6). It is believed that this effect arises when the diffusion interface and the back face of the sample are not parallel.

energies at which measurements of V_{24} could be made, whereas the lower limit on V_{34} was usually set by the decrease in source output at low energies.

The spectral response of V_{34} is in reasonable agreement with the theoretical model discussed in reference 8. However, the behavior of V_{24} and (V_{14}) was quite unexpected and was the cause of a considerable amount of puzzlement before a satisfactory explanation was reached. The sensitivities at 1.5 eV were all between 5×10^{-14} and 10^{-10} $\mu V/phot/sec$, but there was no discernible correlation with diffusion temperature and time. This is somewhat understandable in view of the previously discussed difficulty involved in determining the absolute value of sensitivity. However, the <u>slope</u> of the spectral response curve

$$\frac{d(\log V_{24})}{d(h\nu)}$$

does not suffer from the inaccuracy associated with determining the sensitive area, and yet it, too, shows very little correlation with heat-treatment history. This is shown by the data summarized in Fig. 3.13, which shows the value of this slope for photon energies between 0.9 and 1.3 eV for a number of samples. Sample 89D2 was prepared with a mixture of 80%HgTe-20%CdTe powder, while 89D5 was prepared identically and in addition was diffused under a 4mm partial pressure of Cd. The other samples have already been described in Table 3.1. As can be seen, there is no apparent correlation between slope and diffusion time, and only a very weak correlation with diffusion temperature.

A considerably stronger correlation with diffusion temperature is shown by the magnitude and sign of the open-circuit photovoltages shown in Table 3.1. This will be discussed in Chapter 5, after a theoretical model for these devices is derived in Chapter 4.
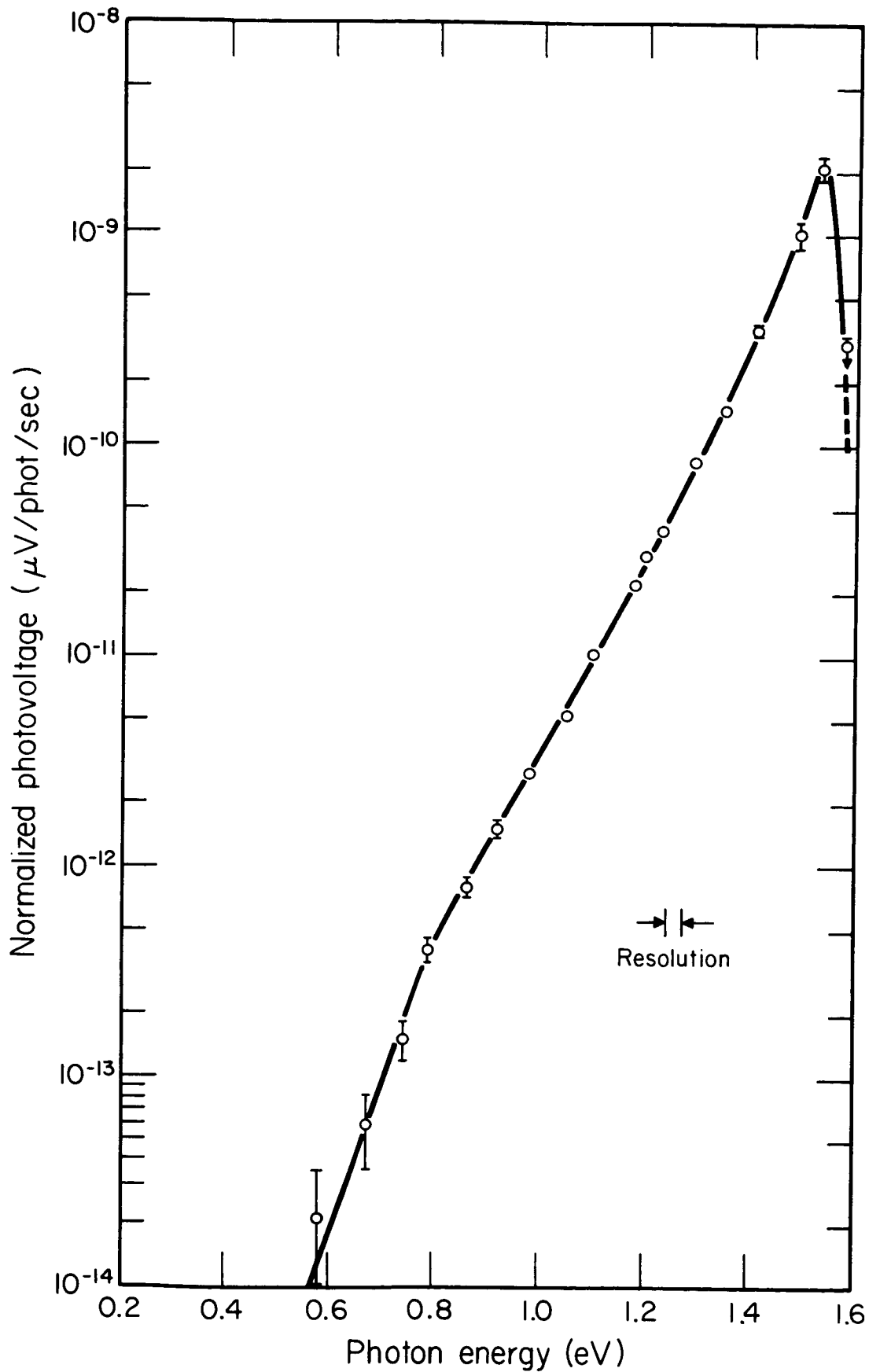
Fig 3.12a: Spectral Response of Front-to-Back Photovoltage V_{24} for B2098 DII.
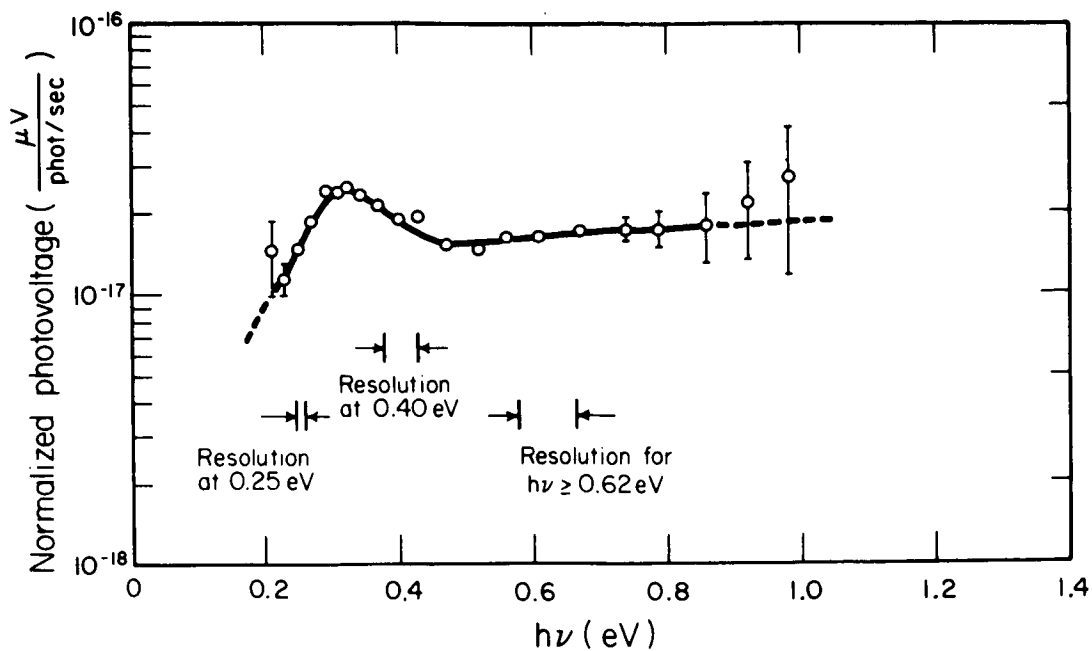
Fig 3.12b: B2098D11, Spectral Response of PEM Voltage. $V_{34}(17kG) - V_{34}(0)$.
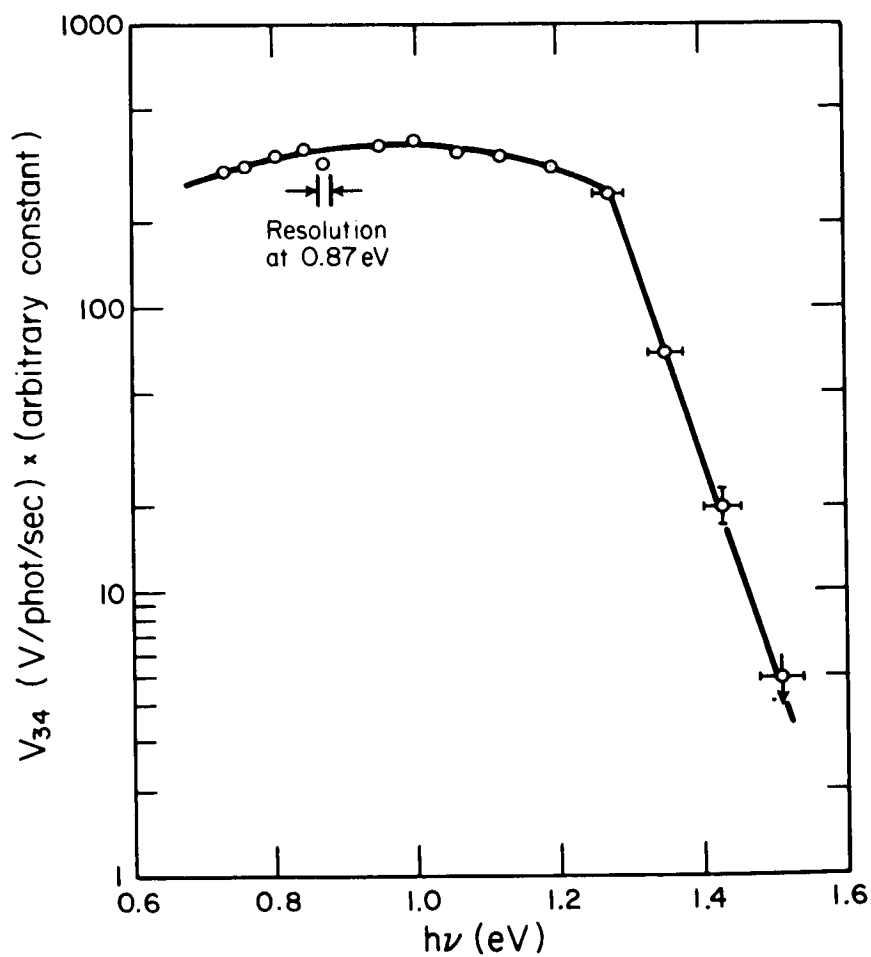
Fig 3.12c: Spectral Sensitivity of B2098D2 V_{34} PEM Voltage. B=3kG
(Taken with glass prism and tungsten source to show behavior
near CdTe gap.) Diffused at 615°C for 23 hrs.
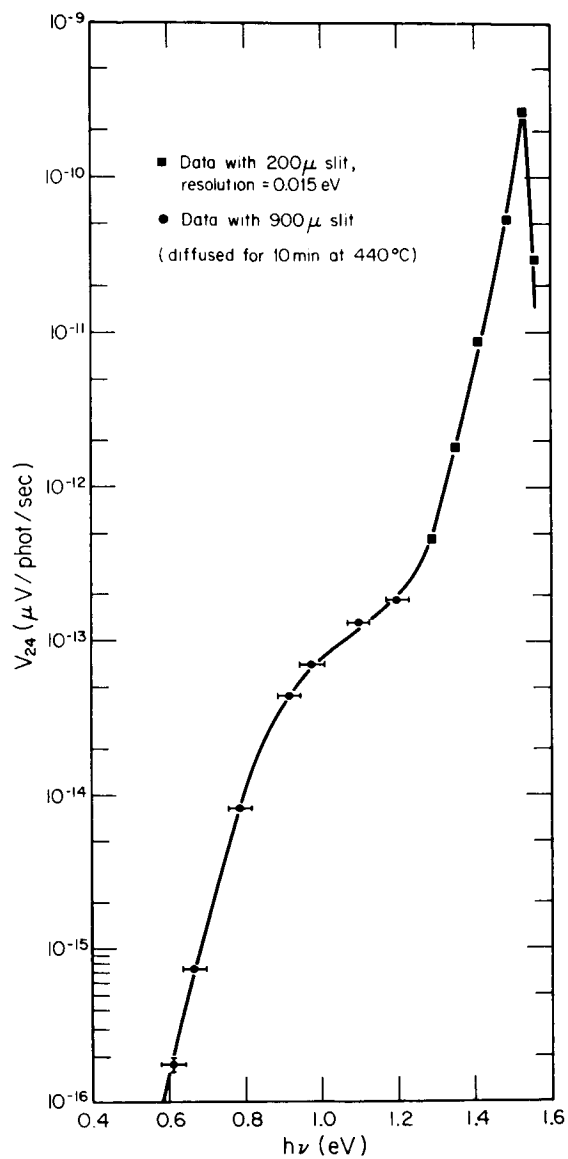
Fig 3.12d: Spectral Response of B2098D21 Front-to-Back Photovoltage V_{24}.
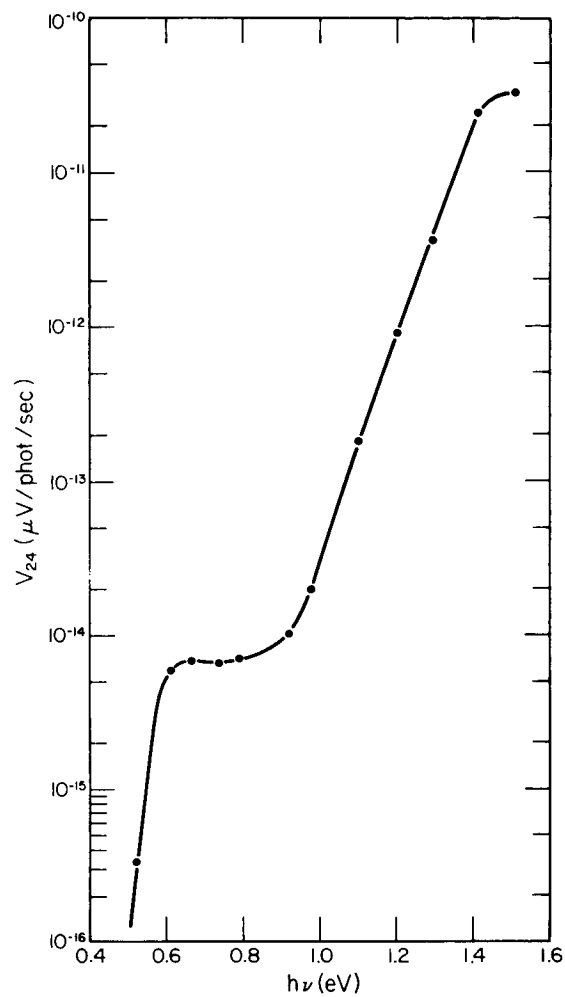
Fig 3.12e: Spectral Response of Open-circuit Photovoltage V_{24} for B2098 D16 (Diffused at 630°C for 24 hours.)
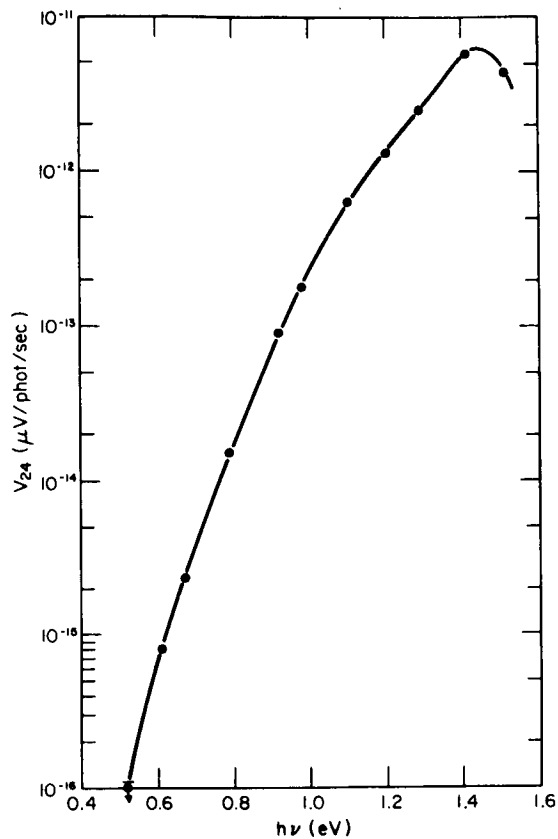
Fig 3.12f: B2098 D17 (1 day at 630 C). Spectral Response of Front-to-Back Photovoltage V_{24}.
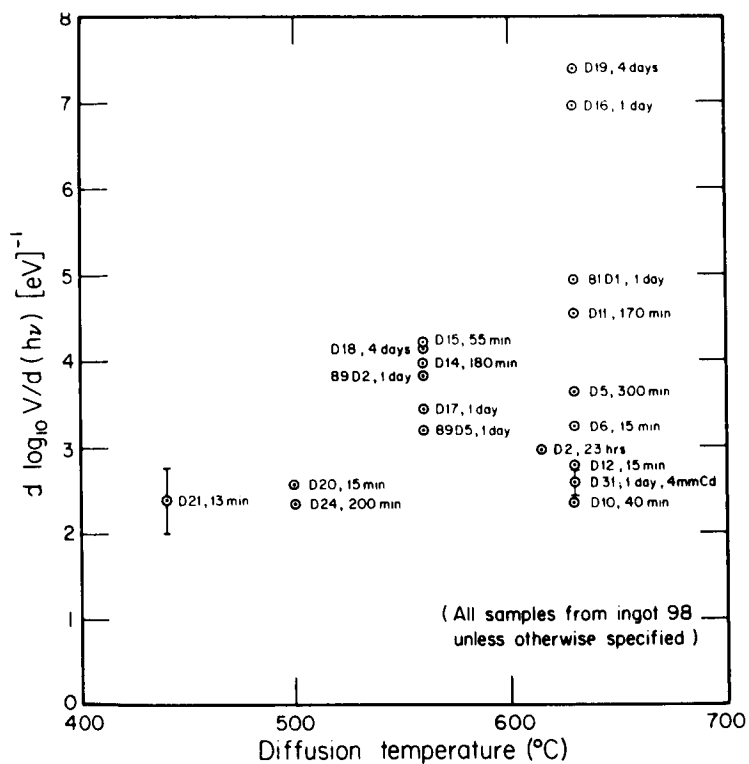
Fig 3.13: Slope of the Spectral Response between 0.9 and 1.3eV for a Number of Samples, Showing Temperature and Duration of Diffusion.
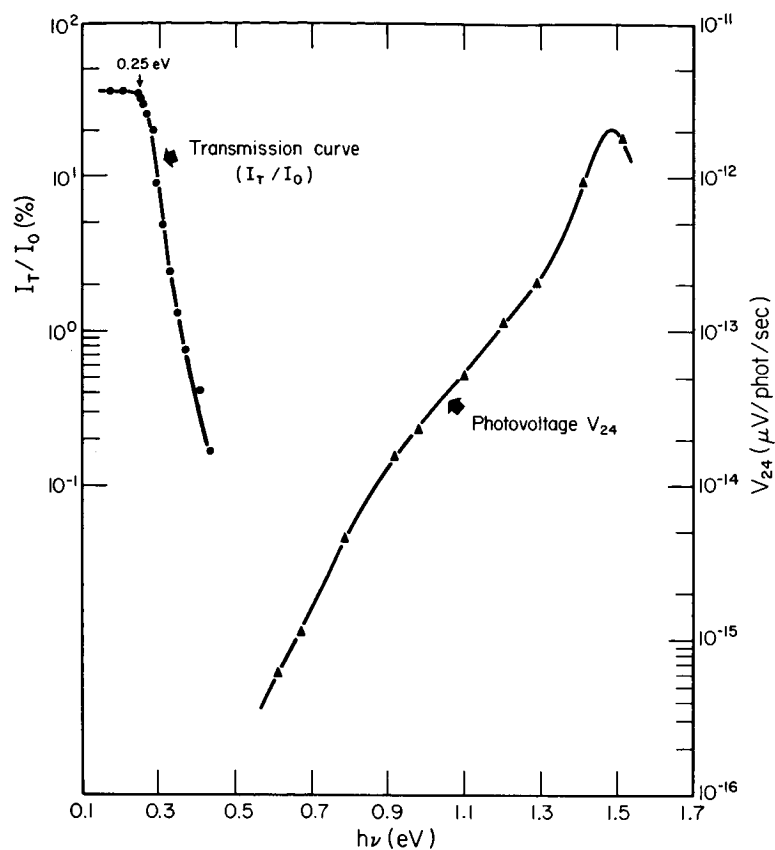
Fig 3.14: Transmission and Front-to-Back Photovoltage for 89D2, diffused with 80% HgTe-20% CdTe powder mixture.
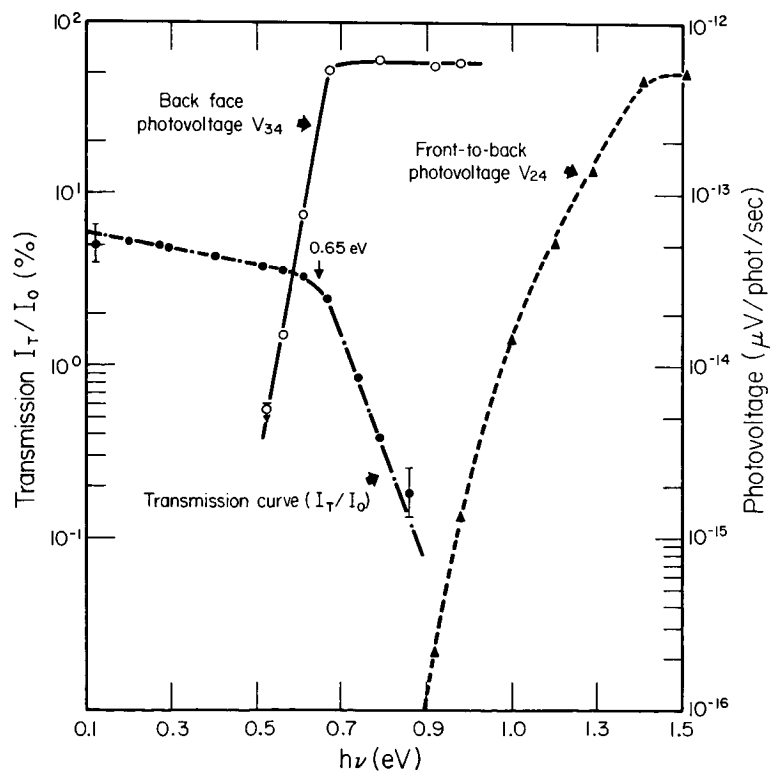
Fig 3.15: Transmission, Front-to-Back Photovoltage, and Photovoltage on Back Face for 98CH1, diffused with 50% HgTe-50%CdTe powder mixture.

One interesting variation of the diffusion procedure is the use of mixtures of CdTe and HgTe powder to obtain semiconducting layers with bandgaps below 1.5 eV on the CdTe "substrate", instead of pure HgTe layers. In preparing sample 89D2, some CdTe powder was ground in addition to the HgTe powder usually prepared for insertion in the ampoule, an 80%HgTe-20%CdTe mixture was weighed out and then thoroughly mixed, and it was this mixture which enveloped the CdTe wafer in the subsequent diffusion process. The resulting sample proved to be transparent to photon energies below 0.25 eV, as shown by the transmission curve of Fig. 3.14. The interesting thing is that the mole fraction corresponding to the above powder mixture is 0.25, and from Fig. 3.2 it can be seen that the corresponding energy gap is 0.25 eV.

This procedure was repeated for sample 98CH-1 using a 50-50 mixture of HgTe and CdTe powders. In this case both a transmission measurement and a photovoltage arising at one of the back contacts indicate that the back layer has an energy gap of 0.65 eV, whereas the front-to-back voltage cannot be measured below 0.9 eV (Fig. 3.15). (The actual value of transmission is larger than shown since part of the sample face was covered by the solder contact.) The 50-50 mixture corresponds to a mole fraction of 0.58 and (from Fig. 3.2) an energy gap of 0.56 eV.

It is possible that this may be a useful way to prepare optical low-pass filters and other semiconductor devices with a continuous range of available bandgaps.

The data discussed up to this point were all taken at room temperature. Measurements were also taken at temperatures near those of liquid nitrogen and liquid helium, but the results for V_{14} and V_{24} were difficult to interpret because the sensitivity of the devices decreased by several orders of magnitude from its room temperature value. Measurements

from three samples indicate that the slope of the spectral response ($\frac{d(\log V)}{d(h\nu)}$) remains within a factor or two of its room temperature value at 80°K, but the degradation in signal-to-noise ratio at this temperature does not allow measurements over a wide enough range of photon energies to make these results at all conclusive. The spectral response of V_{34} at 80°K remained flat within 3dB between 0.2 and 1.4 eV, although its amplitude increased by several orders of magnitude.

Discussion of Results

The reason for the difference in shape between the spectral response of the front-to-back and the PEM photovoltages was not at all clear when these measurements were begun. Transmission measurements on samples prepared with pure HgTe powder showed no radiation being transmitted for wavelengths below 15μ (i.e., photon energies above 0.083 eV), indicating that these photons were being absorbed somewhere in the device. Supplementary measurements were therefore made to learn more about the structures being produced by the diffusion process.

The I-V measurements described in the next section established not only that rectification was taking place between contacts 2-4 (and also 1-4), but also that the rectifying properties could be strongly influenced by light with photon energies below the 1.5 eV bandgap of CdTe. This would not happen for a simple junction in CdTe. The capacitance measurements described in Section 3.5 support the conclusions drawn from the I-V measurements, and give some indication of the properties of the junction responsible for the rectification. The frequency-response measurements in Section 3.6 were made to investigate the possibility that a thermal rather than a photon effect was responsible for the

PEM voltage V_{34}. This is known to be the case for PEM cells made from pure HgTe[19], but the frequency response of V_{34} is shown to be different. Finally, the junction-location experiment described in Section 3.7 supports the conclusions drawn from the I-V experiments by showing that the photo-voltage arises at the interface between the CdTe and the graded region.

The question then is whether the structure indicated by the measurements of Sections 3.4-3.7 can give rise to a front-to-back photovoltage with the exponentially varying spectral response described in this section while still showing a small PEM voltage with a relatively flat (i.e., photon-energy-independent) spectral response.

The front-to-back voltage is the subject of the theoretical analysis in Chapter 4; it is found that the structure described above can indeed give rise to the spectral responses obtained for V_{14} and V_{24}. The PEM voltage and numerical comparisons between theory and experiment are discussed in Chapter 5. It is found that all the data presented in this section are consistent with a model consisting of a sandwich of constant-gap and graded-gap material, with a p-n or n-p junction in the constant-gap material immediately adjacent to the graded region.

3.4 Current-Voltage Characteristics

The measurements described in this section show that the current-voltage characteristics associated with the front-to-back photovoltage are non-linear and are sensitive to photon energies below 1.5 eV. The effect of the illumination on the shape of the I-V curve indicates that the photons are being absorbed in the vicinity of the potential barrier responsible for the nonlinearity.

The measurements were carried out at 300°K using a

Tektronix model 575 transistor curve-tracer; DC methods were used when greater precision was required. The illumination came from the tungsten microscope lamp described in Section 3.3, and could be passed through a CdTe or other optical filter. Representative results are shown in Fig. 3.16, and will be described in more detail after a discussion of the experimental precautions necessary in making these measurements.

Because of the high resistivities involved, it is difficult to make good ohmic contact to the CdTe. Thus it is often possible to obtain rectification and a photovoltage (V_{12}) between two contacts on the front (CdTe) face of the sample. When possible, this effect was removed by using a more suitable metal for the contacts; indium is known to make good ohmic contact to n-type CdTe, while a noble metal such as gold can sometimes give an ohmic contact on p-type CdTe[13]. However, in some instances, it was necessary to use differences in spectral sensitivity to separate contact and bulk effects.

Photovoltages arising from barriers in CdTe should be affected by photons with energy above 1.5 eV (the CdTe bandgap) but not by those with energy below 1.5 eV. Thus by successively illuminating the sample with unfiltered light and then with light passed through a filter which absorbs all photons with energy above 1.5 eV, it is possible to deduce whether or not the observed photoeffect is arising at the contacts. The most convenient filter was a thick (2 mm) slice of single-crystal CdTe, although silicon and multiple-dielectric-layer filters were also used. All of the final results reported in this section were obtained for photon energies below 1.5 eV.

The conductivity type of the CdTe at the front face as deduced from the direction of rectification associated with

the contact was in agreement with the results of Hall measurements where these were available. For example, when indium was used for contact No. 1 for B2098D5, the I-V characteristic between contacts 1 and 4 in the absence of illumination was a horizontal line corresponding to a resistance greater than 2 megohms. Use of a gold spot for contact No. 2 produced the characteristic between contacts 2 and 4 shown in Fig. 3.16a. Since the gold results in a contact with lower resistance for at least one polarity of applied voltage, the implication is that the CdTe is p-type.

This is substantiated by measurements at contacts 1-2; the I-V characteristics there exhibit rectification, the easy-current-flow condition corresponding to V_{21} positive (Au positive with respect to In). Furthermore, for open-circuit conditions, V_{21} was positive for unfiltered light and zero for CdTe-filtered light. This is all in agreement with a p-type CdTe layer on which an indium contact creates an inversion layer and on which gold makes a more or less ohmic low-resistance contact.

P-type CdTe would be in agreement with the Hall measurements made on this sample: B2098D5 was prepared at 630°C from the annealed slice B2098A1, which according to Table 2.1 is p-type. Since Table 2.1 also shows that the diffusion process at 630°C results in p-type CdTe even when the starting slice is n-type, it is most probable that the bulk CdTe of sample B2098D5 is indeed p-type.

Equal intensities of unfiltered and CdTe-filtered light were found to have identical effects on the I-V characteristics at contacts 2-4 (Fig. 3.16a). Since the front contacts are not sensitive to CdTe-filtered light, the implication is that the rectification shown in Fig. 3.16a is not occuring at the contact. Furthermore, the "dark" I-V curve is not only shifted by the light, but shows a non-saturating

a) B2098D5 with Au contact

b) B2098D23 with In contact

c) B2098D12 with Au contact

d) B2098D24 with Au contact
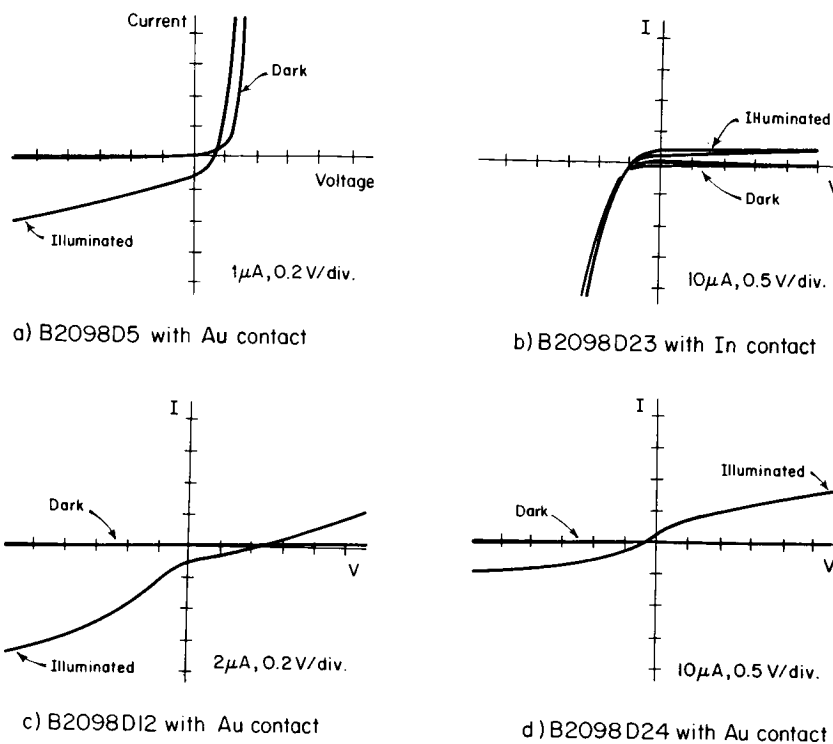
Fig 3.16: Effect of CdTe-filtered light on the I-V characteristics between
contacts 2 and 4 for four types of sample. (Voltage reference
taken positive at CdTe.)
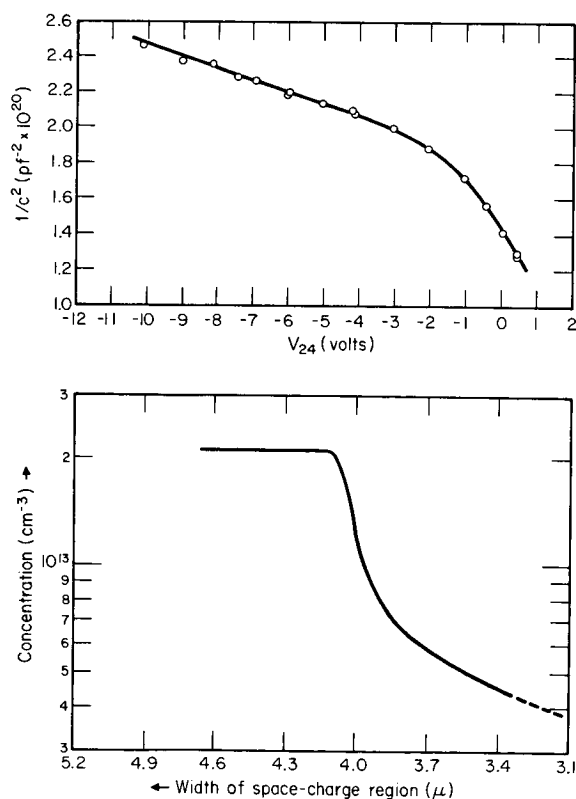
Fig 3.17: Capacitance-Voltage Behavior and Deduced Impurity Distribution

behavior for reverse bias which is characteristic of generation in the space charge region of a pn junction. Thus the junction responsible for the rectification shown in Fig. 3.16a must be near enough to the graded region to collect at least some of the excess current carriers which are being generated there.

An entirely analogous discussion holds for sample B2098D23, which was diffused at 440°C for 40 minutes. In this case, indium made a better contact that gold, implying that the CdTe is n-type. Since the loss of Cd and the resulting creation of cadmium vacancies should be considerably less at 440°C than at 630°C, it is not unreasonable that the bulk CdTe should remain n-type in this case. Again the I-V characteristic shown in Fig. 3.16b was identical for both unfiltered and CdTe-filtered illumination, and again the implication is that of a junction near the graded region.

The characteristics shown in Fig. 3.16c and 3.16d also show identical behavior for unfiltered and CdTe-filtered light. The implication here is that of two opposing junctions in series, the one nearest to the graded region determining the sign of the photovoltage. These are shown only for the sake of completeness and will not be analyzed in detail.

The classification of the I-V characteristics for the samples in Table 3.1 is based on the four types of behavior shown in Fig. 3.16. Curves similar to 3.16a are designated "pn" (since this would be the direction of rectification exhibited by a p-n junction with the p-side positive), curves similar to 3.16b are designated "np", and curves similar to 3.16c and 3.16d are designated "d".

The main implication of the measurements described in this section is that the devices as they are being prepared contain rectifying junctions in the bulk CdTe which interact with the graded-gap region. The capacitance measurements

described in the next section were carried out to learn more about the structures resulting from the diffusion procedure.

3.5 Capacitance Measurements

Voltage-dependent capacitances at terminals 1-4 and 2-4 were found in a good number of the devices, although the multi-junction structure present in many of these makes the exact interpretation of the voltage behavior difficult. In the few cases in which a simple C-V behavior was observed, the direction of rectification indicated by the capacitance measurement was in agreement with the result of the I-V measurement. It was noted in passing that the capacitances were sensitive to light with no photon energies above 1.5 eV, the effect of illumination being to increase the capacitance.

The C-V measurements were obtained using a Boonton model 75B-S8 (1 Mc) direct capacitance bridge with a maximum sensitivity of 1.0000 $\pm$0.0001 pf full scale in conjunction with a Hewlett-Packard 3440A digital voltmeter whose 3443A high-gain plug-in unit had a maximum sensitivity of 100.00 $\pm$0.01 mV full scale. The sample was kept in a small light-tight cardboard box. Lead lengths were always kept short enough to make the measured residual capacitance a negligible fraction of the sample capacitance.

Zero-bias capactiances for about 15 samples ranged between 1 and 100 pf, 30 pf being a typical value. Obtaining the capacitance per unit area is more difficult, since the front face of the sample is not an equipotential plane due to the shape of the front contact. The back face, however, would be an equipotential plane due to the low resistance of the HgTe layer. The procedure adopted here was to calculate the capacitance per unit area as if the entire front face were metal-coated and thus an equipotential. This results in a minimum estimate of the capacitance per unit area of the

device. Using this procedure, the sample capacitances ranged between 10 and 300 pf/cm^2, the average value being near 100 pf/cm^2. There was no discernible correlation with either diffusion time or temperature.

Sample results are presented in Fig. 3.17a, which shows the capacitance-voltage curve of the sample whose current-voltage characteristics are shown in Fig. 3.16a. The capacitance decreases as V_{24} becomes more negative, indicating that this is the direction for reverse bias. This is seen to be in agreement with Fig. 3.16a.

It is possible to obtain some information about the width of the space charge region of the junction and also about the doping variation at the edge of the junction from the capacitance data. Assuming that the depletion approximation[20] is valid for these junctions, the width w of the space charge region for any doping profile is given by the simple parallel-plate capacitor formula

$$w = \frac{\epsilon}{C/A}$$

where ϵ is the dielectric constant of the material and C/A is the capacitance per unit area. The value of w calculated from the data shown in Fig. 3.17a is about 3.4μ. This value will be used in Chapter 5 in constructing a model for these devices. Zero bias capacitances for some of the other devices are given in Table 3.1.

If it is assumed that the junction is strongly asymmetric, and that therefore most of the depletion-layer-width change occurs on one side of the junction, then the equation

$$\frac{d(\frac{1}{C/A})^2}{dv} = \frac{Q}{eN_{A,D}\epsilon}$$

derived by Schottky[21] can be used to infer the doping variation $N_{A,D}$ on that side of the junction.

The results of this calculation are shown in Fig. 3.17b for the C-V characteristics of Fig. 3.17a; it has been assumed that the CdTe dielectric constant $\epsilon = 11\epsilon_o$ holds throughout the device. It can be seen that the magnitude of the calculated doping density is within an order of magnitude of the value obtained from the Hall measurement made on the sample before diffusion ($p = 4.8 \times 10^{12} cm^{-3}$). However, these results should be accepted with caution, both because of the aforementioned uncertainty in the area used to normalize the capacitance, and because there is no way to tell whether a donor or an acceptor density variation is being measured.

Nevertheless, the existence of a light-sensitive capacitance which indicates the same direction of rectification as do the I-V measurements does support the conclusions drawn from those measurements regarding the existence of a junction and its proximity to the graded-gap region.

3.6 Frequency Response Measurements

It was shown in Section 3.3 that the front-to-back photovoltage was a strong exponential function of photon energy, whereas the PEM voltage was constant within 3 dB for photon energies between 0.1 and 1.4 eV. One possible explanation for this difference in the spectral responses is that the PEM voltage is not a photon effect at all but rather is thermal in origin (i.e., the absorbed photons create a temperature gradient which then results in a thermoelectric voltage). Kruse et al[19] concluded that this was the case for the PEM effect in HgTe, where they found a photoresponse which, when normalized with respect to incident power, was constant for wavelengths between 4 and 12μ, decreased with wavelength between 2 and 4μ, and increased for wavelengths beyond 12μ. In addition, the frequency response varied as $f^{-1/2}$, in agreement with the expected behavior of the Nernst

effect, the thermal effect which competes with the photon effect in the PEM configuration[*].

Since the spectral response of a graded-gap PEM device can be anywhere between that of a pure photon counting detector (independent of photon energy) and that of a thermal detector (proportional to photon energy), depending on internal parameters (see Appendix C), it is difficult to use the spectral response data of Section 3.3 to decide which of the two effects dominates. However, the measurements of this section show that V_{34} in the devices studied here differs from the "PEM" effect in HgTe in being independent of chopping frequency up to 600 cps.

The measurements were obtained by mounting a small AC motor in such a way that a chopping disk attached to the motor shaft modulated the beam just before the monochromator entrance slit. The speed of the motor could be varied between 900 and 2400 rpm by driving it with a high-power audio amplifier which in turn was driven by a variable-frequency audio oscillator. The range between 15 cps and 1 KC was covered by using several chopping disks with different numbers of teeth. The sample was illuminated with light from the monochromator, and the resulting photovoltage was detected by the lock-in amplifier system shown in Fig. 3.11c. A photocell mounted behind the chopping disk provided a reference signal of the correct frequency.

Sample data are shown in Figs. 3.18a and b. The first of these shows the front-to-back photovoltage V_{24} of sample B2098D24 under 1.4 eV illumination. The scatter of data is increased by the fact that it is necessary to correct the

----

[*] Similar results have been observed for both the frequency response and the spectral response of the "PEM" effect in HgTe in the course of this study.
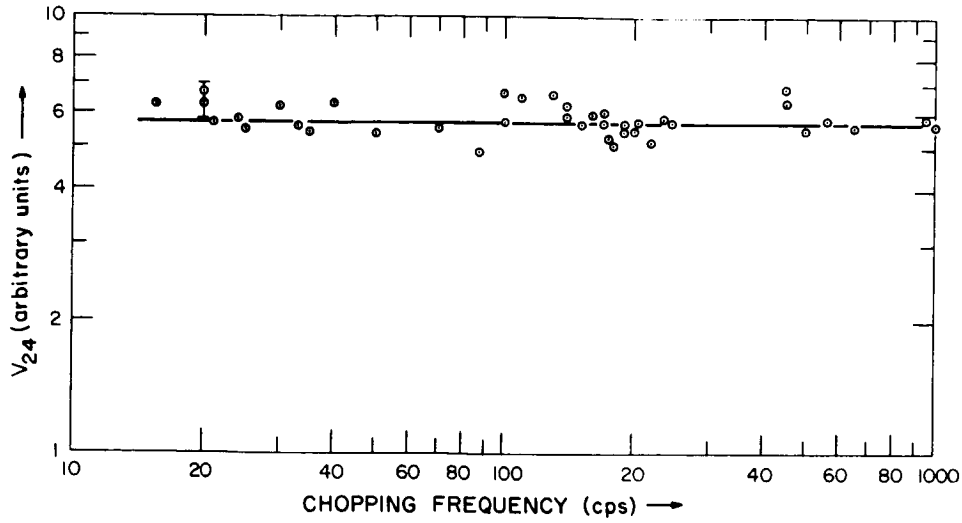
Fig 3.18a: Open-Circuit Voltage V_{24} for 1.4eV Radiation as a function of Chopping Frequency for 98D24.
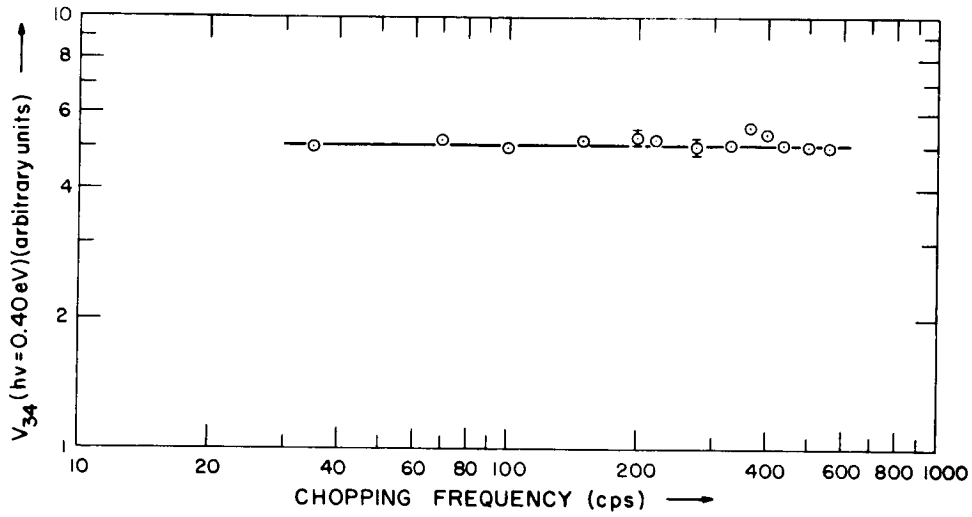
Fig 3.18b: PEM Voltage V_{34} for B=17 kG as a function of chopping frequency for sample B2098 D11.
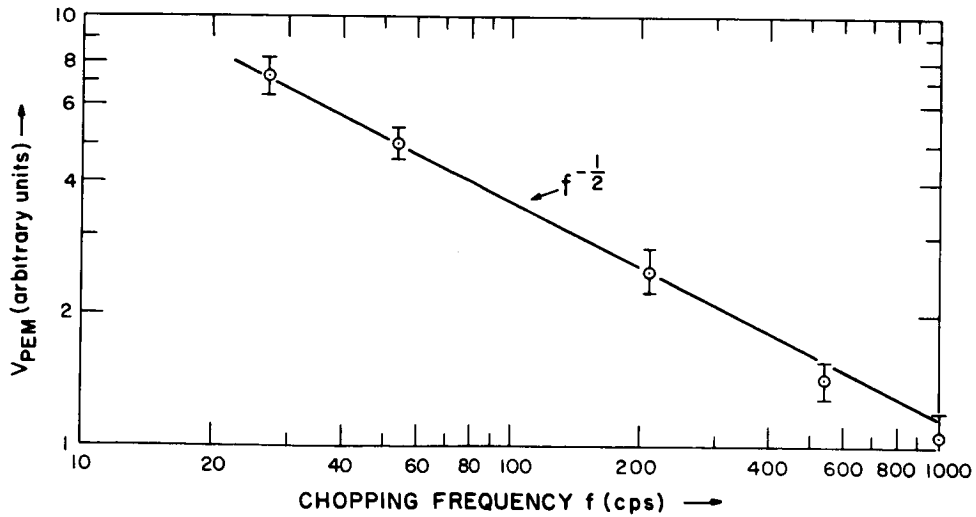
Fig 3.18c: Frequency dependence of Photovoltage from HgTe Sample in PEM Configuration (B=17kG, 2μ Radiation.)

photovoltage for the capacitance of the sample holder. It can be seen that the photovoltage is independent of chopping frequency up to 1 KC. This is in agreement with some incomplete measurements of the speed of the front-to-back photovoltage made on another sample using a Xenon flash lamp, which showed a response faster than or equal to the 1 microsecond duration of the light pulse.

The real purpose of these measurements, however, is to investigate the frequency response of the PEM voltage at contacts 3-4. This is shown in Fig. 3.18b for sample B2098D11 under 3.1μ (0.40 eV) illumination, and in Fig. 3.18c for a sample prepared in an identical manner from a slice of pure single-crystal HgTe. It can be seen that, unlike the PEM effect in HgTe[19], the photovoltage in the diffused sample is independent of chopping frequency between 30 and 600 cps*. It will be recalled that the spectral response of this sample (Fig. 3.12b) also differed from the HgTe PEM effect in being constant within 3 dB for photon energies between 0.2 eV and 1.4 eV. Thus it seems safe to say that the magnetic-field-dependent photovoltage at contacts 3-4 in these devices is not caused by the same mechanism as the corresponding voltage in pure HgTe, which is believed to be thermal in origin[19].

The theory of the PEM voltage in these devices is discussed in Appendix C and in reference 8. In the next section of this chapter, attention is again focused on the front-to-back photovoltage V_{24}, as some experiments are described whose purpose is to locate the region of the device in which this photovoltage arises.

---

* This is in agreement with time response measurements obtained on another sample (B2098D18) using the chopped output of a CO_2 laser (10.6μ). These measurements showed an exponential decay with a time constant of approximately 10^{-3} seconds at room temperature which became less than 5×10^{-5} seconds (the rise time associated with the chopper) when the sample was cooled with liquid nitrogen.

3.7 Junction Location Experiments

The behavior of the I-V curves under illumination reported in Section 3.4 indicated the presence of a pn junction which interacts with the graded-gap region. It was therefore decided to try to locate the junction by one of the conventional techniques used for this purpose. This section reports on some copper photo-electroplating experiments which support the conclusions drawn from the I-V measurements by indicating the presence of a junction very near to the CdTe-graded gap region interface and sensitive to photon energies below the CdTe bandgap.

The sample used in these experiments was made by making a cross-section cut on one of the diffused devices (B2089D1) and polishing the cross-section surface using the techniques described in Section 2.2. This was followed by a 10--20 second etch in the 1:20 solution of Bromine in methyl alcohol. After a rinse, the sample was placed in a solution consisting (by volume) of one part saturated $CuSO_4$ solution, one part demineralized water, and one part HF. The sample was then illuminated with a tungsten microscope lamp for a period between a few seconds and a few minutes, removed from the solution while still illuminated, and rinsed in water. The resulting pattern of deposited copper was then photographed on color film using a microscope. This is a technique commonly used to delineate junctions in silicon and germanium[22]--the copper is deposited on the n-type side, and the edge of the deposit corresponds to the edge of the junction*. The color film is necessary in this case to

---

* The argument may be raised that these are not really junction location experiments but rather are photovoltage-location experiments, the photovoltage being assumed due to a junction, and that in this case the photovoltage could equally well arise from the energy-gap gradient. A comparison

distinguish copper from HgTe, since both appear shiny on a black-and-white photograph. The data presented in Fig. 3.19 are sketched from color photographs.

Under CdTe-filtered illumination, the use of the plating solution described above resulted in a fairly thick, uniform copper deposit on the HgTe (Fig. 3.19). When the solution was diluted to approximately 25% of its original strength by the addition of demineralized water, a thin (approximately 3μ) copper line appeared at the visually observed boundary between CdTe and HgTe. (CdTe appears bluish-black to the naked eye, HgTe is silvery-grey.) No copper deposits appeared when the sample was left in either of the two solutions in the dark for periods up to ten minutes.

To pinpoint more precisely the location of the copper deposits with respect to the CdTe boundary, the sample was illuminated from behind with an infrared source, and an infrared-sensitive "DetectIRscope" was substituted for the microscope eyepiece. The DetectIRscope sensitivity was found to be maximum at a photon energy of 1.36 eV, and to be down to 10% of this value at a photon energy of 1.06 eV. Thus all areas having a bandgap greater than approximately 1 eV are transparent under these conditions, while all other areas are opaque.

The edge of the thick, uniform copper deposited onto the HgTe was found to be in the opaque region and about ten microns from its edge. The thin copper line obtained with the more dilute solution was right at the edge of the opaque

---

(Continued from previous page)

of the expressions derived for the junction photovoltage in Chapter 4 and for the graded-gap voltage in reference 8 and Appendix C shows, however, that in this configuration, the ratio of graded-gap to junction photovoltage is approximately the same as the ratio of minority to majority carriers on the graded-gap side of the junction, and is therefore negligible.

CdTe   HgTe

a) Observation with DetectIRscope before Photoelectroplating

boundary between regions transparent and opaque to infrared

Cu

10μ

b) Copper Deposit resulting from use of Concentrated Solution

3μ

Cu

c) Copper Deposit resulting from use of Dilute Solution
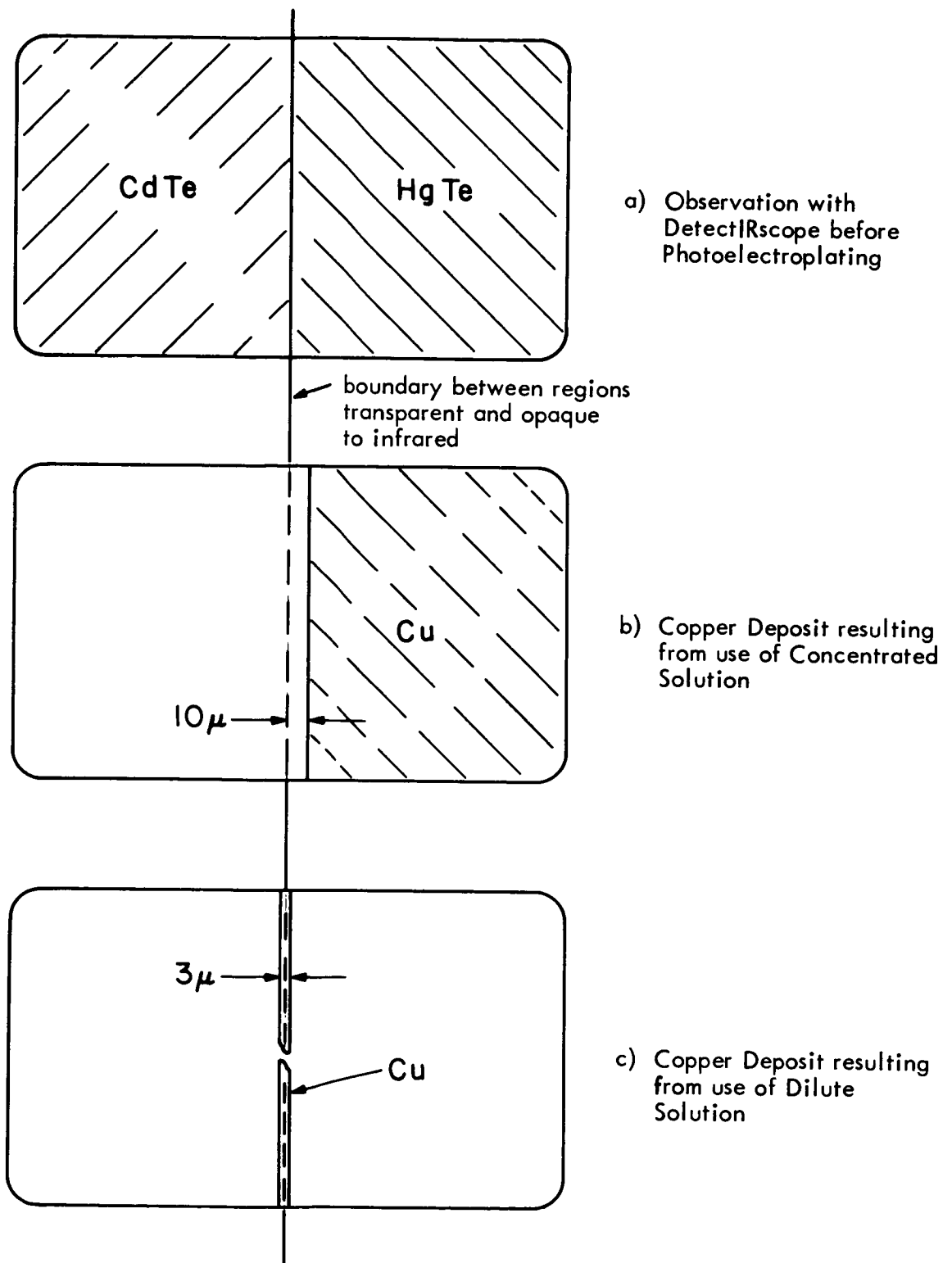
Fig 3.19: Sketches of Microscope Observations of Cu Photodepositions. (400X)
a.) Observation with DetectIRscope before Photoelectroplating,
b.) Copper Deposit resulting from use of Concentrated Solution.
c.) Copper Deposit resulting from use of Dilute Solution.

region, and even at 400X magnification it was impossible to resolve which side of the edge it was on. However, since the edge of the opaque region corresponds to material with an energy gap of about 1 eV, this probably means that the copper is being deposited on the graded-gap side of the interface between CdTe and the graded-gap region.

If the mechanism of copper deposition is the same here as it is for silicon and germanium, this would indicate that the graded-gap region is on the n-type side of a pn junction in CdTe, the bulk CdTe being p-type. This would agree with the Hall measurements made on this sample before diffusion ($p = 10^{16} cm^{-3}$, see Table 2.1) as well as with Hall, I-V, and C-V measurements made on other samples diffused at the same temperature (B2081D1, B2098D5, B2098D11).

3.8 Conclusions

The measurements of the I-V and C-V characteristics and their behavior under illumination (Sections 3.4 and 3.5) and the junction location experiments of Section 3.7 all point to the presence of a rectifying junction in the bulk CdTe which is near enough to the graded-gap region to collect some of the excess current carriers generated by the photons absorbed there. The question is whether such a structure could give rise to the spectral response curves seen in Section 3.3. The theoretical analysis of Chapter 4 answers this question in the affirmative, after which the data of all seven sections of this chapter are used to synthesize tentative band models for several of the devices described here.

REFERENCES

1. R. E. Ogilvie, "Electron Beams in Microanalysis", in Bakish, R., ed., <u>Introduction to Electron Beam Technology</u>, 1962, pp. 413-431.

2. R. Castaing and J. Descamps, <u>Comptes Rendus Acad. Sci.</u>, v. 237, p. 1220 (1953).

3. W. Lawson, S. Nielsen, E. Putley, and A. Young, "Preparation and properties of HgTe and Mixed Crystals of HgTe-CdTe", <u>J. Phys. Chem. Solids</u>, v. 9, pp. 325-329, 1959.

4. F. Bailly, G. Cohen-Solal, and Y. Marfaing, "Preparation et controle de structures a largeur de bande interdite variable", <u>Comptes Rendus Acad. Sci.</u>, v. 257, p. 103, 1963.

5. A. J. Strauss, T. C. Harman, J. G. Mavroides, D. H. Dickey, and M. S. Dresselhaus, "Optical and Electrical Properties of $Cd_xHg_{1-x}Te$ Alloys", <u>Proceedings of the International Conference on Semiconductor Physics</u>, Exeter, 1962, p. 703.

6. H. Rodot and J. Henoc, "Diffusion a l'etat solide des materiaux semi-conducteurs", <u>Comptes Rendus Acad. Sci.</u>, v. 256, 1963.

7. Jost, <u>Diffusion in Solids, Liquids, and Gases</u>, Academic Press, New York, 1960.

8. G. Almasi, "Graded Energy Gap Heterostructures", <u>M.I.T. Energy Conversion and Semiconductor Laboratory Semiannual Technical Summary Report No. 3</u>, NASA Grant NsG 496 (part), pp. 1-51, November, 1964.

9. E. H. Putley, "The Hall Effect and Related Phenomena", Butterworths, London, 1960.

10. J. Blair, "An Investigation into the Thermal and Electrical Properties of the HgTe-CdTe Semiconductor Solid Solution System", <u>M.I.T. Electronics Systems Laboratory Scientific Report No. 2</u>, Contract No. AF 19(604)-4153, June 15, 1960.

11. W. A. Navipour, "The Hall Effect in the Lower Oxides of Titanium", M.I.T. M.S. thesis, 1959.

12. R. A. Hinrichs, "Impruity Control in CeTe", M.I.T. B.S. thesis, June, 1963.

13. D. deNobel, "Phase Equilibria and Semiconducting Properties of CdTe", Philips Research Reports, v. 14, pp. 361-399 and 430-492 (1959).

14. R. E. Nelson, "Preparation and Electrical Transport Properties of HgTe", M.I.T. Sc.D. thesis, May, 1961.

15. M. Wolf, Proc. IRE, v. 48, pp. 1246-1263, July, 1960.

16. J. W. Conley, "Absorption of Photons by Excitons with Assistance from Phonons in a Polar Semiconductor", M.I.T. Sc.D. thesis, February, 1965.

17. M. R. Lorenz and H. H. Woodbury, "Double Acceptor Defect in CdTe", Phys. Rev. Letters, v. 10, pp. 215-217, 15 March 1963.

18. D. A. Cusano and M. R. Lorenz, "CdTe Hole Lifetime from the Photovoltaic Effect", Solid State Communications, v. 2, pp. 125-128, 1964.

19. P. Kruse, M. Blue, J. Garfunkel, and W. Saur, "Long-Wavelength Photoeffects in HgSe, HgTe, and HgTe-CdTe", Infrared Physics, V. 2, pp 53-60, 1962.

20. A. K. Jonscher, Principles of Semiconductor Device Operation, John Wiley & Sons, Inc, 1960.

21. W. Schottky, Z. Physik 118, 539 (1942).

22. P. A. Iles and P. J. Coppen, "Location of p-n and 1-h Junctions in Semiconductors", British Journal of Applied Physics, vol. 11, p. 177 (1960).

CHAPTER 4

THEORETICAL ANALYSIS

4.0 Introduction

As was mentioned in Chapter 1 and described in more detail in Chapter 3, the experimental evidence strongly suggests that the graded-gap region in these devices is interacting with a p-n junction. Consequently, the model shown in Figure 4.1 was chosen. The purpose of the following analysis is to find the excess carrier concentration at the edge of the junction under monochromatic illumination as a function of the photon energy of the illumination. Once this is known, it is easy to calculate the variation of the junction photo-voltage as a function of photon energy.

The starting point for the analysis are the expressions for the partial currents in the graded region $(x > 0)$. Simplifying assumptions are made about the variation of such parameters as the absorption constant, the bandgap, the mobility, and the lifetime. It is found that under certain conditions, the minority carrier drift current can be neglected; the minority carrier current and continuity equations may then be combined to yield a second-order diff-erential equation for the excess minority current carrier concentration in the graded region.

The boundary conditions necessary to solve this equation depend upon the assumptions made about the junction whose edge is at $x = 0$ and about the contact at $x = t$ as well as upon the function describing the excess generation rate due to photons. The assumptions made about the junction are conventional ones, e.g., no generation in the space charge region and low injection conditions (see for example Jonscher,[1] Chapter 4). Open-circuit conditions are assumed.

The contact is assumed ohmic. A simple generation function is assumed for the portion of the graded region in which the photon energy exceeds the energy gap.

Once these boundary conditions are combined with the equation derived earlier, it is possible to find the excess carrier concentration at any point in the graded region. However, the quantity of interest here is the excess concentration at the edge of the junction. This is found as a function of the photon energy and the parameters of the graded region, and under the assumptions mentioned earlier, is directly proportional to the junction voltage.

The special cases corresponding to various relationships among the parameters of the graded region are discussed in some detail, and it is shown that this model can indeed be used to explain the exponentially varying spectral responses described in Chapter 3.

A more detailed comparison between theory and experiment is given in Chapter 5.

4.1 Equation for Excess Carrier Distribution

It is assumed that the excess carrier lifetime is position-independent and that the mobility is either position-independent or can be treated by using an average value as discussed in reference 2. Then for the region $x > 0$ in the structure shown in Fig. 4.1, the partial currents to first order in Δn and Δp may be written

$$J_{xn} = e\Delta n \mu_n \left(\frac{kT}{e} \frac{d\delta_o}{dx} - \frac{4kT}{eE_G} \frac{dE_G}{dx}\right) - en\mu_n \frac{d}{dx}(\phi-\phi_o) + eD_n \frac{d\Delta n}{dx} \qquad (4.1a)$$

$$J_{xp} = e\Delta p \mu_p \left(-\frac{kT}{e} \frac{d\gamma_o}{dx} + \frac{4kT}{eE_G} \frac{dE_G}{dx}\right) - ep\mu_p \frac{d}{dx}(\phi-\phi_o) - eD_p \frac{d\Delta p}{dx} \qquad (4.1b)$$

where

$\dfrac{d\delta_o}{dx}$ is the variation of the conduction band in equilibrium referred to the fermi level E_F.

$\frac{d\gamma_o}{dx}$ is the variation of the valence band in equilibrium referred to the fermi level E_F.

The term $\frac{4kT}{eE_G} \frac{dE_G}{dx}$ reflects effective mass variations and was derviced by assuming effective masses proportional to the energy gap. It can usually be neglected for $E_G >> kT$. $n = n_o + \Delta n$ is the non-equilibrium electron concentration, $p = p_o + \Delta p$ is the non-equilibrium hole concentration. ϕ_o is the equilibrium electrostatic potential and is determined by the electron affinity variation as well as by the doping.

$\phi - \phi_o$ is the photopotential due to the excess carriers and must in general be found from Gauss' Law

$$\nabla \cdot (\vec{\varepsilon} - \vec{\varepsilon}_o) = - \frac{d^2}{dx^2} (\phi - \phi_o) = \frac{e}{\epsilon} (\Delta p - \Delta n)$$

Other symbols may be found in the List of Symbols. It is assumed that the material is extrinsic enough (in this case, $p_o >> n_o$) and that the injection is everywhere low enough ($\Delta n << p_o$, $\Delta p << p_o$) that the two continuity equations may be written

$$\nabla \cdot J_n = - eg + e \frac{\Delta n}{\tau} \qquad (4.2a)$$

$$\nabla \cdot J_p = eg - e \frac{\Delta n}{\tau} \qquad (4.2b)$$

where g is the net generation rate of carriers due to photons.

Quasi-neutrality is not a good assumption to make in this case, since (as discussed in reference 2) the extrinsic Debye length will in general be long enough so that the fraction of the band-edge changes which occur in a Debye length are large enough to violate quasi-neutrality.

Instead, it will be assumed in eq. 4.1a that the majority carriers are

plentiful and mobile enough so that the <u>minority carrier</u> drift current can be neglected.[*] Specifically, it is assumed that

$$\Delta n \frac{d}{dx} (\phi - \phi_o) \ll \Delta n \frac{kT}{e} \frac{d\delta_o}{dx}$$

$$n_o \mu_n \frac{d}{dx} (\phi - \phi_o) \ll \Delta n \mu_n \frac{kT}{e} \frac{d\delta_o}{dx} + D_n \frac{d\Delta n}{dx}$$

Then if it is also assumed that $E_G \gg kT$ everywhere, and that the band edge gradients are constant and equal to

$$\frac{d\delta_o}{dx} = \frac{\delta_o(t) - \delta_o(0)}{t} = \frac{e[\phi(t) - \phi(0)] + E_c(0) - E_c(t)}{tkT} = \frac{\Delta\delta_o}{t}$$

$$\frac{d\gamma_o}{dx} = \frac{\gamma_o(t) - \gamma_o(0)}{t} = \frac{-e[\phi(t) - \phi(0)] - E_v(0) + E_v(t)}{t\,kT} = \frac{\Delta\gamma_o}{t}$$

$$\frac{dE_G}{dx} = \frac{\Delta E_G}{t} = \frac{[E_c(0) - E_c(t)] - [E_v(0) - E_v(t)]}{t}$$

then 4.1a and 4.2a may be combined to obtain the following equation for Δn:

$$\frac{d^2\Delta n}{dx^2} - \underline{\varepsilon} \frac{d\Delta n}{dx} - \frac{\Delta n}{L_n^2} = - \frac{g(x)}{D_n} \tag{4.3}$$

where $L_n^2 = D_n \tau$

and where $\underline{\varepsilon}$ has been defined as

$$\underline{\varepsilon} = \frac{d\delta_o}{dx} = \frac{\Delta\delta_o}{t}$$

---

[*]This assumption is self-consistent in that the only way that the minority current can be on the same order of magnitude as the majority current is if the minority drift current is indeed a small fraction of the total minority current. If the assumption is incorrect, the minority carrier current is negligible compared to the majority current and the error is of no consequence.

4.2 Homogeneous Solution

The homogeneous solution to 4.3 may be written

$$\Delta n_h = C_1 e^{r_1 x} + C_2 e^{r_2 x}$$

where

$$r_{1,2} = \frac{\epsilon \pm \sqrt{\epsilon^2 + 4/L_n^2}}{2}$$

or

$$r_{1,2} = \frac{1}{L_n} \left(\frac{L_n \epsilon}{2} \pm \sqrt{\frac{L_n^2 \epsilon^2}{4} + 1} \right)$$

but

$$L_n \epsilon = \frac{L_n^2 \epsilon}{L_n} = \frac{D_n \tau \epsilon}{L_n} = \frac{\mu_n \tau \frac{kT\Delta \delta_o}{et}}{L_n} = \frac{L_{dr}}{L_n}$$

where L_{dr} is a drift length analogous to that discussed by Jonscher[1] p. 60.

Thus,

$$L_{dr} = L_n^2 \frac{\Delta \delta_o}{t} \tag{4.4}$$

Then,

$$r_{1,2} = \frac{1}{L_n} \left(\frac{1}{2} \frac{L_{dr}}{L_n} \pm \sqrt{1 + \frac{1}{4} (L_{dr}/L_n)^2} \right)$$

$$r_1 = \frac{1}{L^+} \qquad \text{where } L^+ \text{ is a "drift-reduced diffusion length"}$$

$$r_2 = \frac{-1}{L^-} \qquad \text{where } L^- \text{ is a "drift-enhanced diffusion length".}$$

The radial can be expanded for two special cases:

Case 1: Diffusion dominates, $\dfrac{L_{dr}}{L_n} << 1$

$$\sqrt{1 + \frac{1}{4} \left(\frac{L_{dr}}{L_n} \right)^2} = 1 + \frac{1}{2} \cdot \frac{1}{4} \left(\frac{L_{dr}}{L_n} \right)^2 - \frac{1}{8} \cdot \left[\frac{1}{4} \left(\frac{L_{dr}}{L_n} \right)^2 \right]^2 + \ldots$$

$$\boxed{r_1 = \frac{1}{L_n} \left(1 + \frac{1}{2} \frac{L_{dr}}{L_n} \right), \quad r_2 = - \frac{1}{L_n} \left(1 - \frac{1}{2} \frac{L_{dr}}{L_n} \right)} \tag{4.5a}$$

Case 2: Drift dominates, $\dfrac{L_{dr}}{L_n} \gg 1$

$$r_{1,2} = \frac{1}{2} \underline{\varepsilon} \ (1 \pm [1 + 2(L_n/L_{dr})^2 + ---])$$

$$\boxed{r_1 = \underline{\varepsilon} \ [1 + (L_n/L_{dr})^2], \quad r_2 = -\ 1/L_{dr}} \tag{4.5b}$$

4.3 Particular Solution

The generation function is chosen based on the assumption of a simple exponential photon absorption process which can be characterized by an absorption constant α. (Absorption processes in which α was a linear or a quadratic function of x were also considered, but did not significantly change the results [see Appendix B].) The generating function and the subdivision of the band model into appropriate regions are shown in Fig. 4.2. The analytical expression is

$$g(x) = \alpha q_0 \ e^{-\alpha(x-x_\nu)} [u_{-1}(x-x_\nu) - u_{-1}(x-t)] \tag{4.6a}$$

where $u_{-1}(x)$ is the unit step function,

q_0 is the total photon flux in $cm^{-2}\ sec^{-1}$,

and x_ν is the point at which absorption begins.

$$(x_\nu = t \ \frac{E_G(o)-h\nu}{E_G} \ ) \tag{4.6b}$$

(The scale factor αq_0 was chosen to make the area under the curve equal to q_0 for large t.)

Now in general, in region I $(0 < x < x_\nu)$, $g(x) = 0$, and

$$\Delta n_I = C_1^I \ e^{r_1 x} + C_2^I \ e^{r_2 x}$$

4.1a Energy-Band Model for Analysis

4.1b Energy-Band Levels at a Point in the Graded Region, Showing References for the Various Quantities.

SPACE CHARGE LAYER

$$x_\nu = t\left(\frac{E_G(o) - h\nu}{\Delta E_G}\right)$$

4.2 Generation Function for Particular Solution

4.3 Piecewise-Linear Modification of Fig. 4.1

In region II ($x_\nu < x < t$),

$$\Delta n_{II} = C_1^{II} e^{r_1(x-x_\nu)} + C_2^{II} e^{r_2(x-x_\nu)} + C_p e^{-\alpha(x-x_\nu)}$$

and as long as $\alpha \neq -r_2$,

$$C_p = \frac{-\alpha q_o/D_n}{(\alpha + r_1)(\alpha + r_2)} \tag{4.7}$$

In region III ($x < -a$),

$$\Delta p_{III} = \Delta p(-a)e^{(x+a)L_p}$$

where the boundary condition

$$\Delta p_{III}(-\infty) = 0$$

has been applied, and $\Delta p(-a)$ is related to $\Delta n(0)$ by[*]

$$\Delta p(-a) = p_o(-a)(e^{qV_{jn}/kT} - 1) = p_{IIIo}(e^{qV_{jn}/kT} - 1)$$

$$= \left(\frac{p_{IIIo}}{n_{Io}(o)}\right) \Delta n(o)$$

Four more boundary conditions are required to evaluate the four remaining constants.

It will be assumed that the open circuit condition is being treated. $J_{TOT} = J_n(o) + J_p(o) = 0$. Then in the absence of recombination in the space charge layer, $J_p(o) = J_p(-a)$ and

$$J_{TOT} = J_n(o) + J_p(-a) = 0$$

---

[*]This follows from the normal low-injection treatment of a p-n junction; see, for example, Jonscher[1] pp 85-86.

or

$$-e\, D_p\, \frac{d\Delta p_{III}}{dx}\bigg|_{x=-a} = e\, D_n\left(\frac{d\Delta n_I}{dx} - \underline{\varepsilon}\, \Delta n_I\right)\bigg|_{x=0} \tag{4.8a}$$

since III is assumed to be a homogeneous, field-free region.
It is assumed that the contract at $x = t$ is ohmic so that

$$\Delta n_{II}(t) = 0 \tag{4.8b}$$

The electron current at x_ν is continuous, giving

$$J_n^I(x_\nu^-) = J_n^{II}(x_\nu^+) \tag{4.8c}$$

Since the driving function $g(x)$ contains a step at $x = x_\nu$, $d^2\Delta n/dx^2$ may contain at most a step, which means that $d\Delta n/dx$ must be continuous; thus

$$\frac{d\Delta n_I}{dx}\bigg|_{x_\nu^-} = \frac{d\Delta n_{II}}{dx}\bigg|_{x_\nu^+} \tag{4.8d}$$

Solution of the equations resulting from these boundary conditions requires a non-trivial amount of algebra, but the result for the excess minority carrier concentration at the edge of the junction can be shown to be

$$\Delta n(o) = \frac{\alpha q_o/D_n}{a_1 e^{r_2 t} - a_2 e^{r_1 t}}\left[\frac{e^{r_1(t-x_\nu)}}{r_1 + \alpha} - \frac{e^{r_2(t-x_\nu)}}{r_2 + \alpha} + \frac{(r_1-r_2)e^{-\alpha(t-x_\nu)}}{(r_1 + \alpha)(r_2 + \alpha)}\right] \tag{4.9}$$

where

$$a_1 = r_1 - \underline{\varepsilon} - \frac{D_p}{D_n}\, \frac{P_{IIIo}}{n_{Io}(o)}\, \frac{1}{L_p} \tag{4.10a}$$

$$a_2 = r_2 - \underline{\varepsilon} - \frac{D_p}{D_n} \frac{P_{IIIo}}{n_{Io}(o)} \frac{1}{L_p} \qquad (4.10b)$$

The term in the brackets represents the functional dependence on photon energy through the functional dependence of x_ν on the photon energy $h\nu$ (Eq. 4.5b). It will be noted that the exponent of the first term is always positive whereas the exponents of the other two terms are always negative. However, because of the differences in the denominators of the three terms, it is necessary to consider all the possible relationships between r_1, r_2, α, and t. This is done in Appendix A, and the result is that _if_ there is any significant dependence of $\Delta n(0)$ on x_ν, then the dominant term will be $e^{r_1(t-x_\nu)}$.

Now, the junction voltage V_{oc} (i.e. the change in electrostatic potential drop across the junction) can be found from

$$\frac{\Delta n(0)}{n_{Io}(0)} = (e^{qV_{oc}/kT} - 1) \qquad (4.11)$$

and for $V_{oc} \ll \frac{kT}{e}$ (a condition which is true for all the spectral response measurements reported here),

$$V_{oc} = \frac{kT}{e} \frac{\Delta n(0)}{n_{Io}(0)} \qquad (4.12)$$

thus $\ln(V_{oc}) = \ln(\text{const}) + r_1(t - x_\nu)$

and

$$\frac{d \ln V_{oc}}{d(h\nu/kT)} = kT \, r_1(t - x_\nu) \qquad (4.13)$$

For drift dominant, the term $r_1(t - x_\nu)$ becomes

$$r_1(t-x_\nu) = \frac{\Delta\delta_o}{t} \cdot t \left(\frac{\Delta E_G - E_G(0) + h\nu}{\Delta E_G}\right)$$

$$= \frac{kT\Delta\delta_o}{\Delta E_G} \left(\frac{\Delta E_G - E_G(0) + h\nu}{kT}\right)$$

and therefore

$$\frac{d \ln V_{oc}}{d(h\nu/kT)} = \frac{kT\Delta\delta_o}{\Delta E_G} \qquad (4.14)$$

Thus the slope of the spectral response when plotted on semilogarithmic coordinates is directly proportional to the fraction of the bandgap change which is due to conduction band edge change.

For diffusion dominant, the term in the exponent becomes

$$r_1(t - x_\nu) = \frac{1}{L_n} \cdot t \left(\frac{E_G - E_G(0) + h\nu}{\Delta E_G}\right)$$

thus

$$\frac{d \ln V_{oc}}{d(h\nu)} = - \frac{t}{L_n} \frac{1}{\Delta E_G} \qquad (4.15)$$

One somewhat surprising feature of Eq. 4.14 is that it predicts that the slope of the spectral response should be independent of t, the width of the graded region, and thus of the heat-treatment history of the sample. It also predicts that the slope should vary linearly with temperature.

Equation 4.15 differs from 4.14 in that it predicts that the slope of the spectral response should vary linearly with the width of the graded region. Thus one would expect steeper slopes for samples with longer diffusion times.

4.15 differs from 4.14 also in that the temperature dependence of the slope

is now a function of the excess carrier diffusion length L_n, which can be a very weak function of temperature.[*]

The ratio of the slopes resulting from the two different assumptions may be written

$$\frac{\left[\dfrac{d \ln V_{oc}}{d(h\nu/kT)}\right]_{diff}}{\left[\dfrac{d \ln V_{oc}}{d(h\nu/kT)}\right]_{drift}} = \frac{1}{\Delta\delta_o} \frac{t}{L_n} = \frac{L_n}{L_{dr}} > 1 \quad \text{for diffusion to dominate}$$

Thus, in the absence of a knowledge of which mechanism dominates, one may state that

$$\frac{kT\Delta\delta_o}{\Delta E_G} \leq \left| \frac{d \ln V_{oc}}{d(h\nu/kT)} \right| \tag{4.16}$$

or in other words, the measured slope gives the maximum possible band edge variation.

It has been shown that in the absence of a minority carrier band-edge gradient in the graded gap region, the excess minority carriers generated in the graded-gap region arrive at the junction by a process of diffusion; if the minority carrier band-edge gradient is large enough, then the drift component due to this gradient becomes the dominant term in the expression for excess

---

[*] For example, since $L_n = \sqrt{D_n \tau} = \sqrt{\dfrac{kT}{e} \mu_n \tau}$, if the excess carrier lifetime τ is relatively independent of T, and since $\mu(T) = \mu(300°K) \left(\dfrac{T}{300°K}\right)^{-n}$ where n depends on the scattering mechanism but is generally between 1 and 2.5, then

$$L_n \sim T^{\frac{1-n}{2}}$$

minority carrier current (eq. 4.1a). To determine which process is dominant in the devices studied here, it is necessary to calculate the ratio L_{dr}/L_n.

From equation 4.4 it follows that

$$\frac{L_{dr}}{L_n} = \frac{L_n}{t} \, \Delta\delta_o \qquad (4.17)$$

Assuming that the mobility $\mu_n = 10^3$ cm^2/v-sec is applicable and that the lifetime is 10^{-8} sec results in

$$L_n = (\frac{kT}{e} \mu_n \tau)^{1/2} = 5\mu.$$

If it is assumed that $\tau = 10^{-10}$ sec, then $L_n = 1/2 \, \mu$.

If one considers a change in E_G from 1.5 ev to 0.5 ev, the distance t was shown in Chapter 3 to be at most about 5-10μ. Thus the minimum value of L_n/t occurs for $L_n = 1/2 \, \mu$ and t = 10μ and is 1/20. The maximum value of L_n/t occurs for $L_n = 5\mu$ and t = 5μ or less and is certainly greater than or equal to unity. Thus it is safe to say that the limits on L_n/t are

$$\frac{1}{20} < \frac{L_n}{t} < 1.$$

If the valence band remains flat in the graded gap region, then $\angle\gamma_o = 0$ and kt $\Delta\delta_o = \Delta E_G = 1$ev = 40 kT at rm. temperature, making $\Delta\delta_o = 40$. Now, if the graded region is to remain p-type throughout, then $\Delta\gamma_o$ cannot exceed $\frac{1}{2} E_G$(CdTe) = 0.75 ev = 30 kT at room temperature. This would set a lower limit on $\Delta\delta_o$ of approximately 10.

The minimum value of L_{dr}/L_n would then occur for $L_n/t = 1/20$ and $\Delta\delta_o = 10$ and is equal to 1/2, whereas the maximum value occurs for $L_n/t = 1$ and $\Delta\delta_o = 40$.

Thus

$$\frac{1}{2} < \frac{L_{dr}}{L_n} < 40.$$

Since the dividing line between the drift dominant and diffusion dominant regions is $L_{dr}/L_n = 1$, this result indicates that drift is the more probable dominant mechanism but that diffusion cannot be neglected.

These conclusions are based on a model with linear band-edge variations. If one considers the non-linear band-edge variations which are possible, the determination of the dominant mechanism becomes even more difficult. Consider, for example, the piecewise-linear modification of Fig. 4.1 shown in Fig. 4.3. In this case, $\Delta\delta_o$ is zero for the entire region A, which makes L_{dr}/L_n zero also. Thus if one considers non-linear variations of the band edges, it is by no means possible to have the diffusion current be completely dominant in at least a limited region of the device.

Based on these considerations, the safest conclusion which can be drawn is that both drift and diffusion may be significant.

The experimental results discussed in Chapters 3 and 5 are in agreement with this conclusion in the sense that the slope of the spectral response shows neither the strong correlation with heat-treatment history predicted by the "diffusion dominant" theory and eq. 4.15, nor the strong temperature dependence predicted by the "drift dominant" theory and eq. 4.14.

The next chapter will also show how the information derived in this chapter may be used in constructing quantitative models.

REFERENCES

1. A.K. Jonscher, <u>Principles of Semiconductor Device Operation</u>, John Wiley, 1960.

2. G. Almasi, "Graded Energy Gap Heterostructure," <u>M.I.T. Energy Conversion and Semiconductor Laboratory Semiannual Technical Summary Report No. 3</u>, NASA Grant NsG 496 (part), pp 1-51, November 30, 1964.

CHAPTER 5

COMPARISON BETWEEN THEORY AND EXPERIMENT

5.0 Introduction

The main purpose of this chapter is to compare the experimental results of Chapter 3 with the theoretical model derived in Chapter 4. This model, it will be recalled, consists of a sandwich structure of constant-gap and graded-gap material (Fig. 4.1), with a p-n junction in the constant-gap material which is near enough to the graded-gap region to collect some of the excess charge carriers which are generated by the photons absorbed in the graded-gap region.

The comparison between theory and experiment is done by using the data of Chapter 3 to construct quantitative band profiles for several of the diffused devices (Sec. 5.1). The main purpose of this is not to determine the exact structure of these devices, but rather to show that the various data are all compatible with the model and with each other.

The next section (5.2) deals with several alternate models which at first glance offer an explanation for the exponential spectral response of the front-to-back voltage described in Section 3.3. The theoretical shortcomings of these explanations are discussed first, followed by a description of the experimental checks whose results also weigh against them.

Section 5.3 discusses a specific prediction of the model in Chapter 4 concerning the effect of monochromatic light of various wavelengths on the I-V characteristics of the front-to-back voltage, and shows that this effect may actually be observed experimentally. Finally, Section 5.4 discusses the behavior of the PEM voltage V_{34} under monochromatic illumination.

5.1 Quantitative Band Profiles

The steps used in constructing quantitative models are best illustrated by an example. The data available in Chapter 3 for sample B2098D5 will be used to obtain numbers for the various distances and energy levels of the model shown in Fig. 4.1a. (It should be re-emphasized here that the resulting band profile will only be an approximation, whose main purpose is to show the compatibility of the various data with the model and with each other.) The result may be seen in Fig. 5.1, and the method by which it was obtained is as follows.

The most obvious difference between Fig. 5.1 and Fig. 4.1a is the direction of rectification--the I-V data of Fig. 3.16a indicate a p-n junction, and so the bulk CdTe is drawn as being p-type. This is in agreement with the Hall effect measurement made on this sample before diffusion, since this showed a hole concentration of $4.8 \times 10^{12} cm^{-3}$ (Sec. 3.2 and Table 2.1), and since the data of Sec. 3.2 indicate that diffusion at this temperature leads to increased acceptor concentrations. The above value of hole concentration can thus be used to calculate an upper limit on the spacing between the Fermi level and the valence band edge in Fig. 5.1; according to DeNobel[1], $p = 4.8 \times 10^{12} cm^{-3}$ corresponds to $E_F - E_V = 0.36$ eV. (Bulk p-type CdTe is also in agreement with the thermoelectric measurements of Sec. 3.2 and the contact experiments of Sec. 3.4.)

The width of the junction space charge region was calculated in Sec. 3.5 from capacitance data using the depletion assumption, and the value obtained for this sample was 3.4μ. This is subject to the errors involved in finding the true junction area, as discussed in Sec. 3.5, but with this precaution in mind, this value is used for the junction width in Fig. 5.1.

E_G (eV)

1.0

0.5

5.0   2.5   0   2.5   5.0   7.5   x(μ)

(a) from capacitance (sec. 3.5)

(b) from microprobe data (3.1)

(c) from Hall measurement (3.2)

(d) from spectral response (3.3)

(e) from photovoltage this must be > 0.13 eV (3.3)

(f) direction of rectification from 3.4

CB

(f)

E_F

0.36 eV (c)

VB

0.43 eV (e)

0.28 eV (d)

3.4 μ (a)   4.5 μ (b)
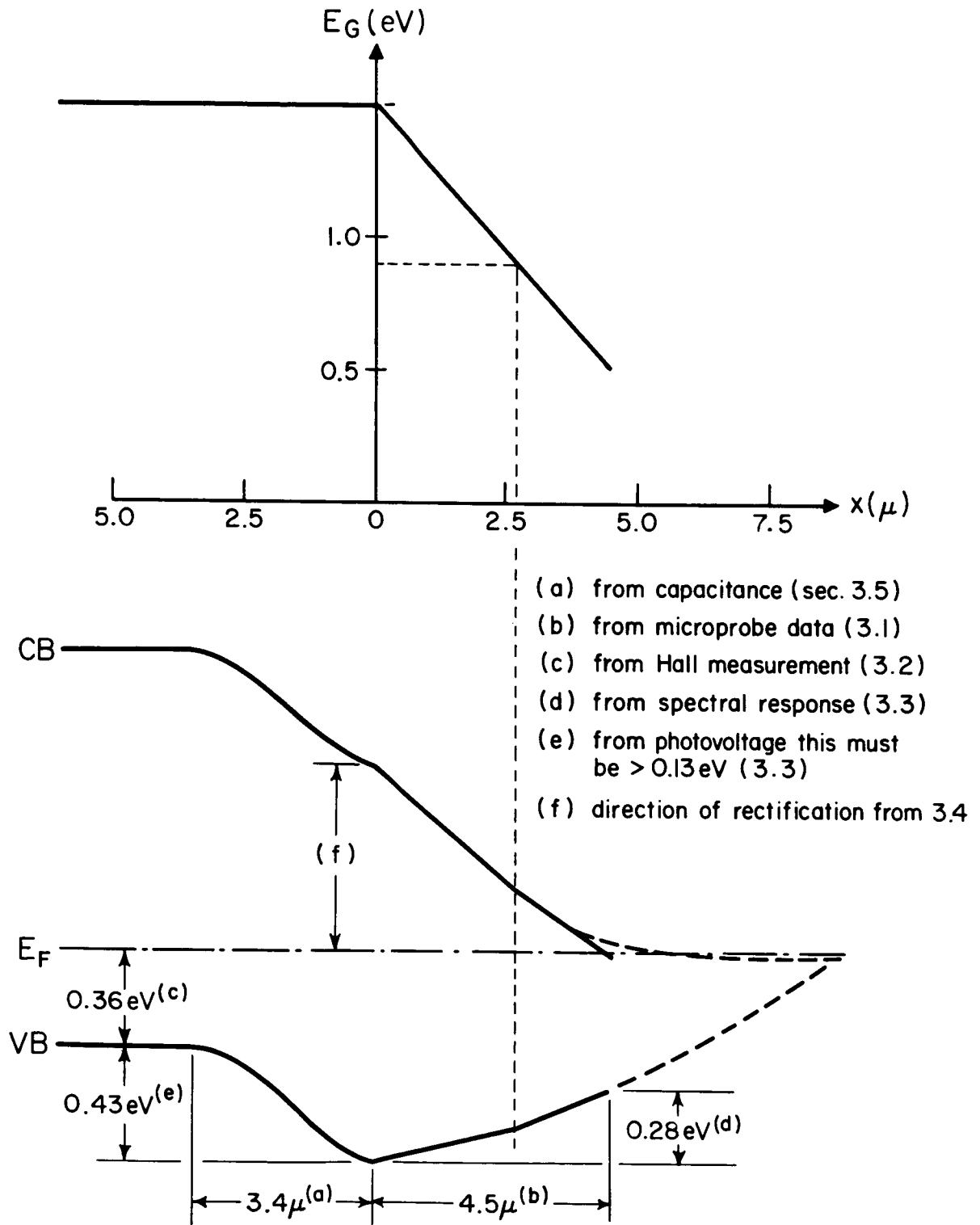
5.1   Band Model for B2098 D5 Based on Theory of Chapter 4 and Data of Chapter 3

A lower limit on the barrier height of a junction can usually
be obtained from the saturation open-circuit photovoltage
available for high intensity light[2]. In this case, this
voltage is only 0.13 V, although higher voltages are obtained
for other, similar samples (Table 3.1). However, when the
graded-gap region of this device is considered, it will be
shown that a higher barrier is indicated.

The energy gap profile of this sample may be calculated
from the profile shown in Fig. 3.1 for a 27-hour diffusion
and from the data discussed in Sec. 3.1 which shows that at
this temperature, the penetration depth varies as the square
root of the diffusion time. The result is shown in Fig. 5.2a,
along with the linear approximation which will be used for
these calculations between 1.5 and 0.5 eV, the range over
which data was obtained.

It was shown in Chapter 4 that the slope of the spectral
response was related to the band-edge change by Equation 4.16,

$$\frac{kT\Delta\delta_o}{\Delta E_G} \leq \left| \frac{d \ln V_{oc}}{d(h\nu/kT)} \right| \qquad (5.1)$$

where the equal sign applies for the case when drift is
dominant. In terms of the sample being discussed here, this
expression gives an upper limit on the change in valence
band edge over any given distance in the graded-gap region.
This valence band-edge change is equal to (or less than) the
band-gap change which occurs over that distance, multiplied
by a fraction which is equal to the measured slope of the
logarithm of the photovoltage with respect to normalized
photon energy. The calculation proceeds as follows.

The spectral response curve of B2098D5 was not included
in Sec. 3.3 because of its strong similarity to the curve for
B2098D11 (Fig. 3.12a). For B2098D5, the photovoltage decreases
at a rate of 3.8 orders of magnitude per electron-volt for

photon energies above 0.9 eV, and at a rate of 6.7 orders of magnitude per electron-volt for photon energies below 0.9 eV. This means that the "slope" term on the right-hand side of Equation 5.1 is equal to

$$\frac{3.8(2.3)}{40} = .218$$

for photon energies above 0.9 eV and is equal to 0.384 for photon energies below 0.9 eV. This in turn means that while the energy gap changes by 0.6 eV in going from 1.5 eV to 0.9 eV, the valence band edge changes by $(0.60)(.218) = .13$ eV, whereas an energy gap change from 0.9 eV to 0.5 eV results in a corresponding valence-band-edge change of $(0.40)(.384) = .15$ eV. The total valence-band-edge change over the measurable range of photon energies (1.5 eV to 0.5 eV) is therefore ≤ 0.28 eV. This is shown in Fig. 5.1; the conduction-band-edge variation is found by subtracting the valence-band-edge variation from the energy gap variation.

Since the measurements could not be extended below photon energies of 0.5 eV due to noise problems, this method leaves an uncertainty of 0.5 eV in the position of the Fermi level in the graded-gap region. Figure 5.1 was drawn with an n-type graded region to agree with the direction of rectification shown by the I-V data of Sec. 3.4. One result of this assumption is that all material with energy gap below 0.5 eV is degenerate. This is by no means impossible. However, the assumption that the p→n transition takes place entirely in the bulk CdTe was made only for convenience in analysis, and lowering the Fermi level by 0.1 eV or so should not significantly affect the measured properties of the device.

It is interesting to note in Table 3.1 that both B2098D16 and B2081D1 have considerably larger saturation photovoltages than found here (.52 and .40 volts, respectively, vs. .13 volts here). Both of these samples were diffused for a longer

time at the same temperature as B2098D5, which should result
in a larger hole concentration in the bulk CdTe. As a matter
of fact, B2081D1 was prepared from a CdTe ingor which was
originally p-type with 5×10^{16} holes/cm^{-3} (Table 2.1). If
this values is assumed to be valid for the bulk CdTe of the
device, and when an analysis similar to the one for B2098D5
is carried out, a maximum barrier height of 0.90 eV is
obtained for B2081D1, compared to 0.43 eV for B2098D5. This
is within 50% of the ratio of saturation photovoltages (0.40 V
to 0.13 V). If the bulk CdTe hole concentration for B2098D16
is also assumed to be 5×10^{16} cm^{-3}, the maximum barrier height
is 0.65 eV, compared to a maximum photovoltage of 0.52 V.

The preliminary indication of the data discussed up to
this point is that (at least for this temperature) the Fermi
level in the graded region is a more or less independent of
the diffusion time, the main effect of increased diffusion
time being to increase the hole concentration in the bulk
CdTe, which brings the Fermi level closer to the valence
band edge and thus results in a higher barrier. One way to
check this is to decrease the loss of cadmium and the conse-
quent formation of acceptor centers by lowering the diffusion
time and temperature. Since B2098 was originally n-type, it
may even be possible to obtain devices with n-type bulk CdTe;
these should show rectification in the opposite direction and
negative photovoltages.

A glance at Table 3.1 will show that, except for the
cases where the effect is obscured by the formation of
secondary junctions, this is exactly what seems to be happen-
ing; the samples prepared at 440°C show large negative photo-
voltages and np-type rectification (Fig. 3.16b), the samples
prepared at 630°C show large positive photovoltages and
pn-type rectification (Fig. 3.16a), and the samples prepared
at 500°C and 560°C show small or intermediate photovoltages

and rather poor rectification (Fig. 3.16b).

It is also interesting to note the correlation of the zero-bias capacitance per unit area (C_o/A) with the diffusion temperature: Taking into account again the secondary junctions which tend to obscure the effect, it can be seen that the capacitance is large where the photovoltage is large and is small where the photovoltage is small. It is difficult to be more quantitative than this because of the problems involved in determining the proper area to use in calculating C_o/A. However, this is in qualitative agreement with the processes which were postulated to occur during the diffusion: If the Fermi level in the graded-gap region is indeed relatively independent of the diffusion process, then a short diffusion at low temperature will leave the electron concentration in the bulk CdTe unchanged and result in a thin np junction (with a large capacitance) which is relatively efficient at collecting photogenerated excess carriers from the graded-gap region (an example would be sample B2098D21). As the diffusion time and temperature are increased, the increased loss of cadmium creates more cadmium vacancy acceptor sites, the electron concentration decreases , the depletion width increases, and the net result is a wide junction (hence a small capacitance) which is relatively inefficient at collecting the photogenerated excess carriers from the graded-gap region (an example of this is sample B2098D17). As the diffusion time and temperature are increased still further, the bulk CdTe eventually acquires an acceptor concentration large enough to make the space charge region of the junction narrow again (hence a larger capacitance), resulting in a pn-junction which again is an efficient collector of photogenerated excess carriers from the graded region.

To show that the process discussed above is feasible,

the procedure used to construct a model for a "pn" sample (B2098D5) is repeated for an "np" sample (B2098D21) and for an "intermediate" or "d" sample (B2098D17). The energy gap profiles and their linear approximations are shown in Fig. 5.2b and c, and the models are shown in Figs. 5.3 and 5.4.

The assumption made in setting up the model for B2098D21 (Fig. 5.3) was that the carrier concentration in the bulk CdTe is unchanged from its pre-diffusion value of $n = 2 \times 10^{15} cm^{-3}$ (Table 2.1). This results in a spacing between the Fermi level and the conduction band edge of 0.16 eV. The zero-bias capacitance of 108 pf/cm^2 (Tabel 3.1) results in a depletion-layer width of 8.8μ. Since this junction collects electrons and not holes from the graded-gap region to its right, the spectral response data of Fig. 3.12d now reflects conduction band edge changes instead of valence band edge changes. With this variation, the method used for B2098D5 results in a conduction band edge change of 0.33 eV for the energy gap range between 1.5 eV and 0.5 eV. The maximum barrier height can be seen to be about 0.70 eV, which compared with a maximum open-circuit photovoltage of -0.41 V (Table 3.1).

The method used to construct the model for B2098D17 shown in Fig. 5.4 is essentially identical to the method used for the other two samples, with the exception that the small capacitance (1.8 pf/cm^2) of Table 3.1 indicates such a wide space charge region that the final value of electron concentration in the CdTe to the left of the junction is really immaterial. (The fact that the bulk CdTe is n-type is indicated by the "np" I-V characteristic (Table 3.1).) The conduction-band-edge change deduced from the spectral response curve of Fig. 3.12f is 0.29 eV for an energy gap range between 1.5 and 0.5 eV. The probable reason for the very small photo-voltage is that most of the excess current carriers from the

graded-gap region recombine before they even get part-way across the junction.

In summing up this section, it can be said that the data of the various sections of Chapter 3 are consistent and/or compatible with each other in terms of the model derived in Chapter 4, and that furthermore the model makes possible an explanation of the effects of the diffusion process on the characteristics of the resulting devices.

5.2 Alternate Explanations

There are several models which are simpler than the one developed in Chapter 4 and which at first glance seem to offer an explanation for the exponential behavior described for the spectral response of the front-to-back voltage in Sec. 3.3. This section considers the theoretical aspect of these explanations first, and then discusses the experimental evidence which led to their rejection.

The first and simplest explanation for an exponentially decreasing photovoltage is an exponentially decreasing absorption constant. Moss[3] mentions CdS and CdSe among the materials for which a plot of log α vs photon energy gives a slope of $1/kT$ for values of α between 1 mm^{-1} and 10^3 mm^{-1} (i.e., for photon energies below the bandgap). The transmission curve of Fig. 3.14 and some of our unpublished transmission data on CdTe indicate that this behavior occurs in these materials also, since these data show a 10:1 decrease in about 0.06 eV, which corresponds to an e:1 decrease in $0.06/2.3 = 0.0026$ eV, whereas kT at room temperature is 0.025 eV. However, this would mean that the decrease in photoresponse between photon energies of 1.5 eV and 0.5 eV should be about 17 orders of magnitude, whereas even under the highest resolution (0.01 eV or better) the highest slope observed corresponded to about 7-1/2 orders of magnitude per

electron-volt, and as is shown by Fig. 3.13, the average is closer to 3-1/2 orders of magnitude per electron-volt. Thus the slope predicted by this model is much too steep.

Furthermore, experimental checks were made as a safeguard against the possibility that a CdTe effect was being observed by measuring front-to-back photovoltages on un-diffused CdTe samples, on CdTe "control" samples in which CdTe powder had been substituted for HgTe powder, and on diffused samples from which the graded-gap layer was carefully removed. In no case was there a detectable photovoltage below a photon energy of 1.4 eV, nor was there a PEM voltage at contacts 3-4 with the properties described in Secs. 3.3 and 3.6. The explanation that the spectral response of the front-to-back photovoltage is due to an absorption constant which is an exponential function of photon energy was therefore ruled out.

Another explanation which was considered in some detail involved a doping gradient in the graded-gap region. A change in current carrier concentration of five orders of magnitude corresponds, after all, to only 0.3 eV change in band-edge with respect to the Fermi level, and it seemed possible that the spectral response of a graded-gap photocell under monochromatic illumination would reflect the spatial variation of the equilibrium current carrier concentration at the point where the photons are being absorbed. However, it can be shown from the analysis of the PEM effect carried out in Appendix C that this can only come about when the excess current carrier distribution which results from the photon absorption process is so narrow compared to the width of the graded-gap region that it takes on some of the properties of an impulse function. In order for this to come about, both the drift length and the diffusion length of excess carriers must be small compared to the width of the graded-gap region. Since the considerations near the end of Sec. 4.3 showed that
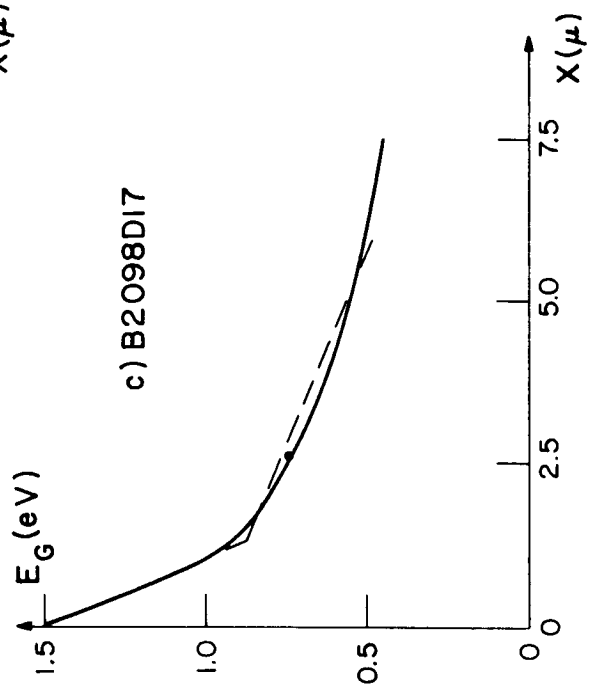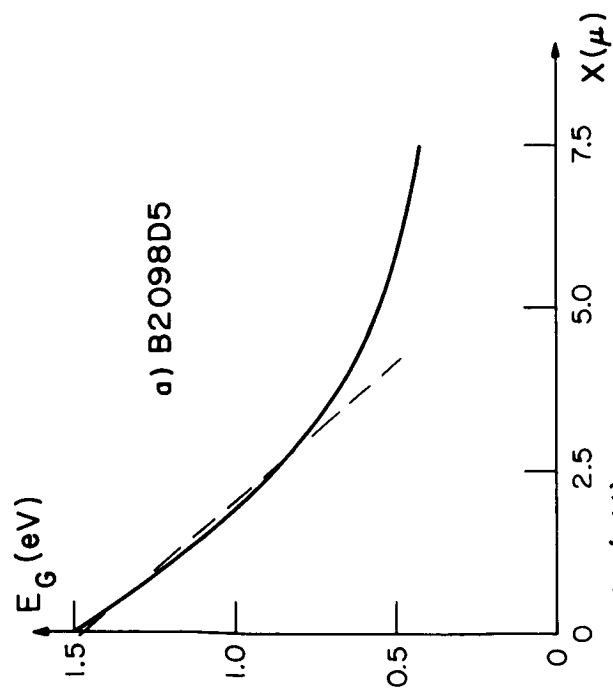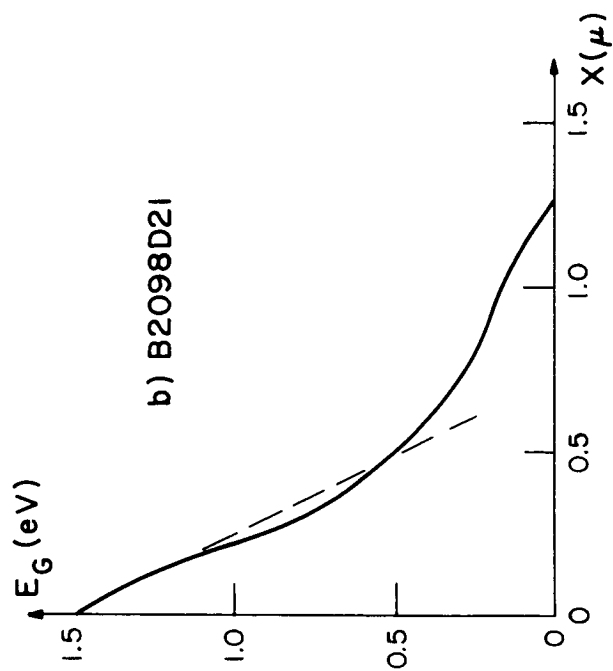
5.2 Calculated Energy Gap Profiles and Linear Approximations

5.3   Band Model for B2098 D21
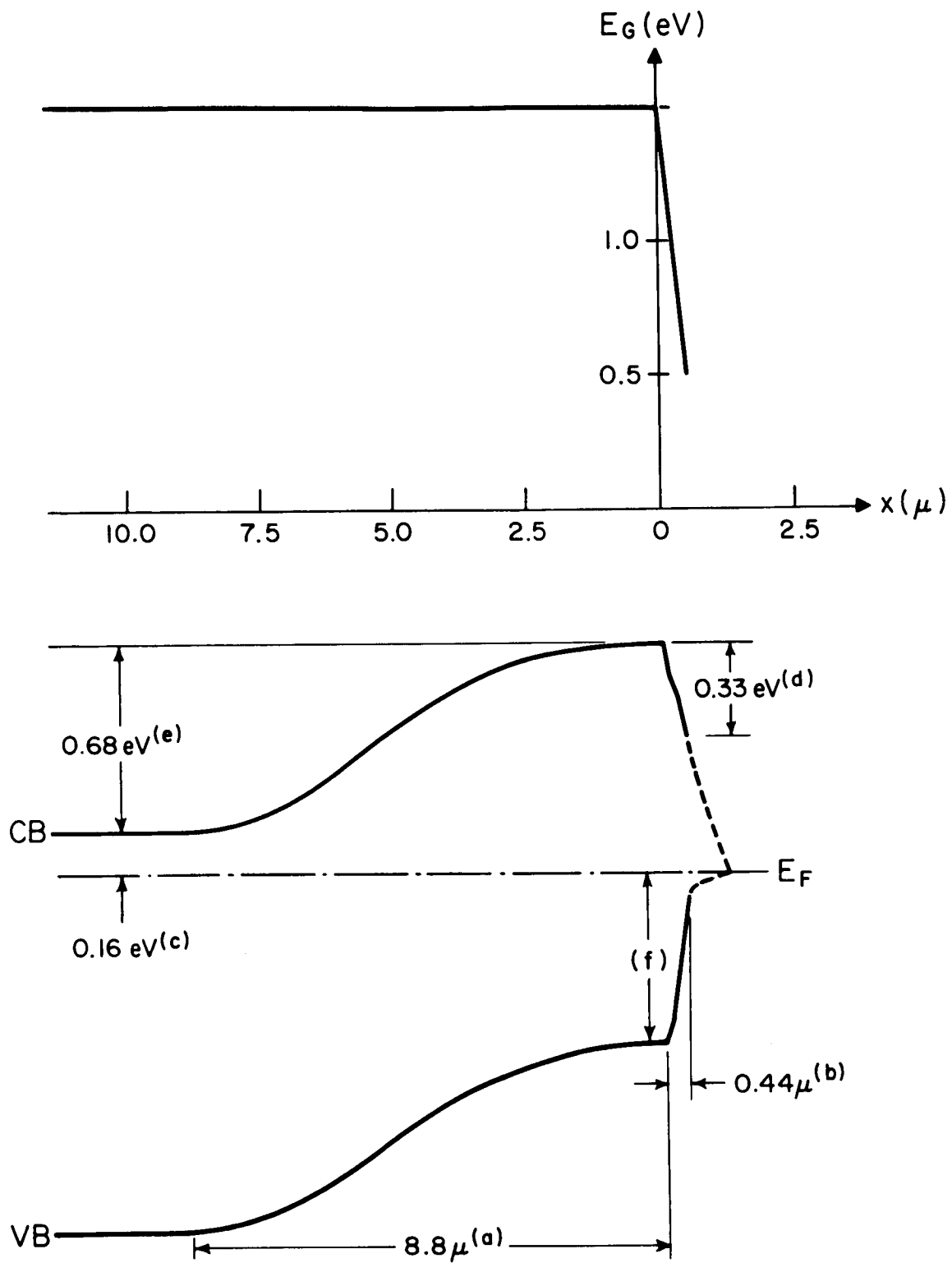
it was very unlikely that the drift length would be much smaller than the diffusion length, and that the diffusion length would probably be between 0.5μ and 5μ, the assumption of an impulse-like excess carrier distribution might be reasonable for a sample like B2098D19, for which the energy gap changes from 1.5 eV to 0.5 eV in 30μ, but it would be completely unjustified for a sample like B2098D21, for which the corresponding distance is 0.5μ. Yet there is no drastic difference in the slopes of the spectral responses of these two samples, and Fig. 3.13 shows very little correlation for any of the samples between the slope of the spectral response and the expected width of the graded-gap region.

Add to this the fact that the I-V data definitely shows current carriers generated by photons with energy below the CdTe bandgap being collected by a rectifying junction, that the model being discussed here predicts no difference in the spectral behavior of the front-to-back and PEM voltages, and that it furthermore predicts a maximum negative output voltage of -0.14 V (see Appendix C) because of the mobility ratio in these materials, and this explanation involving a doping gradient in the graded-gap region can also be discarded.

The next section describes one more check on the validity of the model derived in Chapter 4: an experiment to determine the effect of monochromatic light of different wavelengths on the I-V characteristics of the front-to-back voltage. It is shown that the effect predicted by the model can be observed experimentally.

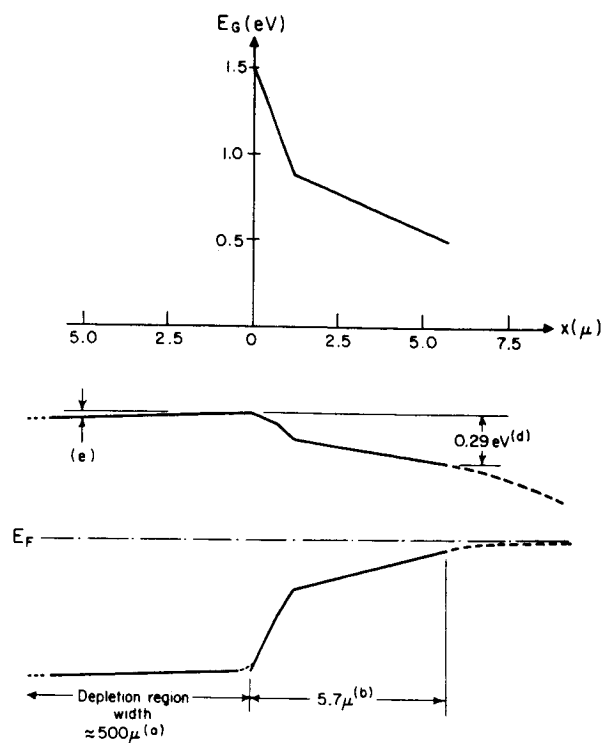5.3 Dependence of I-V Characteristics on Photon Energy of Illumination

The model of Fig. 4.1 shows a p-n junction immediately

adjacent to the large-gap end of the graded-gap region. It seems reasonable that by reverse-biasing the junction it should be possible to extend the junction space charge layer into the graded-gap region, thus influencing the collection of photogenerated carriers from that region. Since the applied field should help excess minority carriers to drift toward the junction, it may now be possible to collect excess carriers generated by low-energy photons which are absorbed so far away from the junction that the excess carriers they create would normally recombine before reaching the junction. Thus, crudely speaking, one should see an increase in reverse photo-current when that voltage is reached for which the edge of the space charge region begins to approach the point where the photons are being absorbed. Since the model of Fig. 4.1 predicts that lower energy photons should be absorbed farther away from the junction, this threshold of photo-current should correspond to larger and larger values of reverse bias as the photon energy is lowered[*].

The main problem in observing this effect experimentally is getting enough intensity from the monochromator. Never-theless, the effect was observed in B2098D16, one of the most sensitive devices produced during this work. The results are shown in Fig. 5.5.

The I-V characteristic for this sample in the absence of illumination is shown in Fig. 5.5a. An expanded portion of this characteristic for reverse bias is shown in Fig. 5.5b, which also shows the effect of monochromatic light with a photon energy of 1.10 ±.04 eV. It can be seen that the

---

[*] An alternate method of investigation is to take spectral response curves for increasing values of reverse bias and to look for increased sensitivity at long wavelengths. This effect was observed qualitatively in one or two samples, but quantitative data are nor available.

E_G(eV)

1.5

1.0

0.5

5.0   2.5   0   2.5   5.0   7.5 $x(\mu)$

0.29 eV$^{(d)}$

(e)

E_F

Depletion region width $\approx 500\mu^{(a)}$

5.7$\mu^{(b)}$

5.4   Band Model for B2098 D17

I (mA)

4

3

2

1

10 20 30 40 50 V_{24}(volts)

Expanded in fig. 5.5b
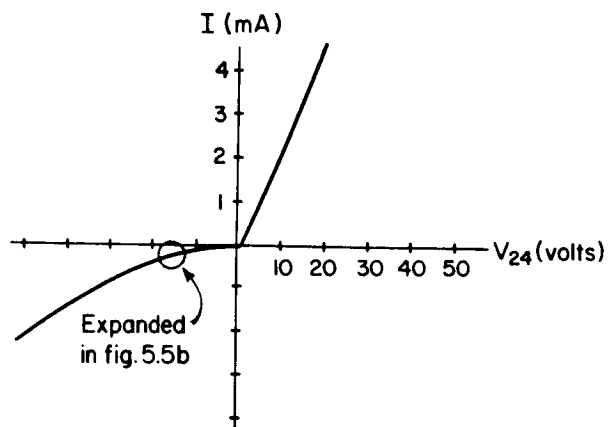
5.5a   Current-Voltage Characteristics for B2098 D16 in the Absence of Illumination

I (μA)

-40

-50

-15   -14   -12   -11   V(volts)

-70

-80

Dark
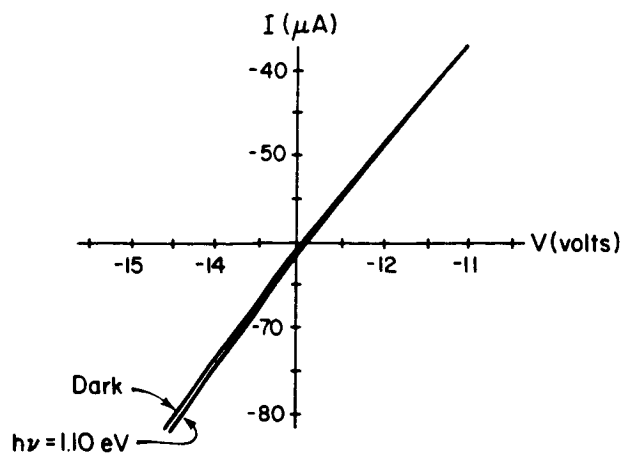
$h\nu$ = 1.10 eV

5.5b   Expanded Portion of B2098 D16 I-V Characteristic under 1.10 eV Monochromator Light

photocurrent seems to begin when a reverse bias of about
15 V is reached.

The effect of other values of photon energy is shown in
Fig. 5.5c. It can be seen that as the photon energy is
increased, the threshold moves to smaller values of reverse
bias, the magnitude of the effect being very roughly
1.5V/0.10 eV. Since the distance corresponding to a bandgap
change of 0.10 eV should be (from Fig. 3.3) roughly 1 micron
for this sample, and since the zero-bias capacitance of
120 pf/cm^2 (table 3.1) implies a junction depletion layer
width of about 8 microns, the implication is that a reverse
bias of 1.5 volts should cause about a 10% change in
capacitance. This is not unreasonable in view of the results
for B2098D5 (Fig. 3.17a).

Thus the results of the experiment described in this
section may be interpreted as lending further support to the
model developed for the physical processes in these devices
in Chapter 4.

5.4 Spectral Response of the PEM Voltage

It was assumed in Chapter 4 that the voltage measured
between the two ohmic contacts in Fig. 4.1 was essentially
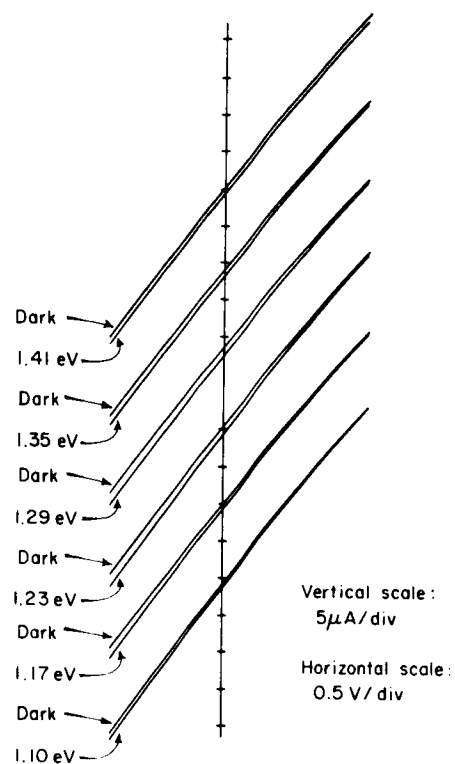equal to the junction voltage. This is justifiable because
it will be shown shortly that photovoltage arising in the
graded-gap region is inversely proportional to the equilibrium
majority carrier concentration in that region, whereas the
junction photovoltage is inversely proportional to the
minority equilibrium concentration at the graded-gap side of
the junction (Equation 4.12). However, the Hall component of
the photovoltage arising in the graded region should be avail-
able at two contacts on the back face of the device (contacts
3 and 4 of Fig. 2.4) and is the subject of this section.

The expression derived for the open-circuit junction

Dark
1.41 eV
Dark
1.35 eV
Dark
1.29 eV
Dark
1.23 eV
Dark
1.17 eV
Dark
1.10 eV

Vertical scale:
5 μA/div

Horizontal scale:
0.5 V/div

5.5c   Effect of the Photon Energy of the Monochromatic Light
on I-V Characteristics of B2098 D16

I_{jn} I_{GG}

P
N

R_{GG}

1   3   4
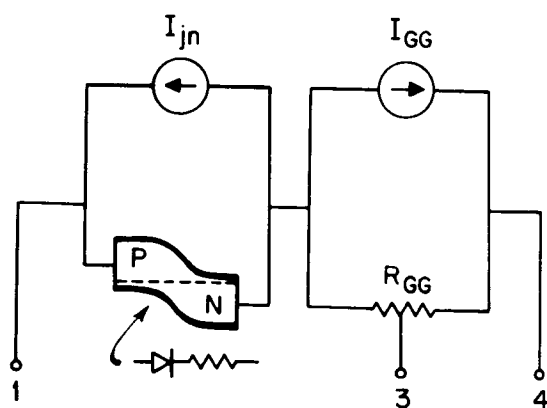
5.6   Circuit Model for Discussion of Sec. 5.4

$\dfrac{V_{oc}}{g_o(h\nu)}$

$\left(\dfrac{\tau}{p_o} \dfrac{\mu_n}{\mu_p} \dfrac{\Delta E_G}{e} \right)$

$\tau_d = \dfrac{1}{10} \tau$

$\tau_d = \tau$

$\tau_d = 10\tau$

$h\nu$

ΔE_G
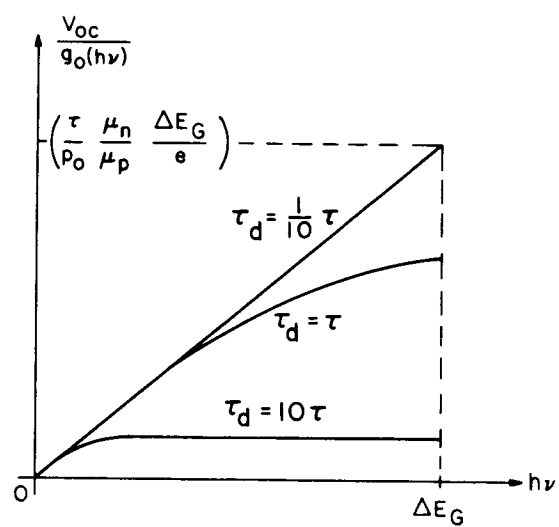
Spectral Dependence of PEM Voltage in Graded-Gap Region
for Several Values of Transit Time τ_d

photovoltage is given in Equation 4.12 for low illumination
as

$$V_{oc} = \frac{kT}{e} \frac{\Delta n(0)}{n_{IO}(0)}$$

where $\Delta n(0)$ is the excess electron concentration at the edge
between the space-charge region of the junction and the
p-type graded-gap region, and n_{IO} is the equilibrium minority
(electron) concentration at the same point. By comparison,
the photovoltage arising in the graded region alone (i.e.,
between $x = 0$ and $x = t$ in Fig. 4.1a) for "white" light
which results in a uniform distribution of excess carriers Δn
throughout the graded region can be shown to be [4,5,6]

$$V_{oc} = \frac{\mu_n}{\mu_p} \frac{\Delta n}{P_o} \frac{\Delta E_G}{e}$$

for a sample with uniform equilibrium hole concentration P_o
(ΔE_G is the change in energy gap which occurs between $x = 0$
and $x = t$). Since $n_o P_o = n_i^2 = 1.76 \times 10^{11} cm^{-6}$ for CdTe, the
ratio of majority to minority equilibrium carriers is so
large that at least for photon processes occuring in the
graded-gap material near the CdTe, the junction photovoltage
should completely overwhelm the graded-gap photovoltage.

Another way to look at this is in terms of the circuit
model of Fig. 5.6; the graded-gap impedance is so low compared
to the junction impedance that it tends to short out the
graded-gap voltage. In practical terms, this means that the
graded-gap signal is difficult to measure because of the large
noise signal associated with the high impedance between
contacts 1 and 4. This is the consideration which led to the
neglect of the voltage developed across the graded-gap region
in the development of the theoretical model, and the experi-
mental evidence of Chapter 3 seems to justify the assumption.

However, as discussed in reference 4, it should be

possible to measure the PEM component of the graded-gap photovoltage. Since it is shown in reference 4 that the PEM voltage is merely the Hall component of the front-to-back graded-gap voltage, only the latter effect will be discussed here.

For the purposes of this analysis, the graded-gap region is assumed to be quasi-neutral with a uniform equilibrium hole concentration p_o. It is assumed that there are no junctions in the bulk CdTe.

The analysis is carried out in Appendix C. It is shown that if the photons are absorbed within a very small distance of the point where their energy matches the bandgap (i.e., if $\alpha \approx \infty$) and if drift current dominates ($L_{dr}/L_n \gg 1$), then the open-circuit voltage between $x = 0$ and $x = t$ of Fig. 4.1 is given by

$$V_{oc} = \frac{g_o(h\nu)\tau}{p_o} \frac{\mu_n}{\mu_p} \frac{\Delta E_G}{e} \frac{\tau}{\tau_d}(1 - e^{-(\tau_d/\tau)h\nu/\Delta E_G}) \qquad (5.2)$$

where $g_o(h\nu)$ is the number of photons per cm^2 per sec at the photon energy $h\nu$

τ is the lifetime of excess carriers

$\Delta E_G = E_G(0) - E_G(t)$ is the bandgap change and would be 1.5 eV in this case

τ_d is the drift transit time across a graded region of width t and is given by

$$(\tau_d = \frac{et^2}{\Delta E_G \mu})$$

The spectral dependence of this photovoltage is shown in Fig. 5.7 for several values of τ_d. It can be seen that a transit time long compared to the lifetime can result in a "flat" spectral response usually associated with photon counting, whereas a transit time short compared to the lifetime results in a signal proportional to the photon

energy, usually associated with thermal detectors such as thermocouples. The PEM spectral responses shown in Figs. 3.12b and 3.12c seem to correspond to an intermediate case.

5.5 Conclusions

The main result of this chapter is that the data of Chapter 3 can be explained using the model in Chapter 4. This was shown first by constructing quantitative models for several of the devices described in Chapter 3. The result was not only that the various data were consistent with the model and with each other, but that it was possible to gain some insight into what was happening during the diffusion process used to prepare these devices. Some alternate explanations were discussed and their failings were pointed out. A prediction of the model was shown to be experimentally observable. Finally, an expression was derived for the PEM voltage V_{34} which was in satisfactory agreement with the data of Chapter 3.

The next chapter discusses conclusions to be drawn from this work as a whole, and makes recommendations for future work.

REFERENCES

1. D. de Nobel, "Phase Equilibria and Semiconducting Properties of CdTe", Philips Research Reports, vol. 14, pp 361-399 and 430-492 (1959).

2. M. Wolf, "Photovoltaic Solar Energy Convertors", Proceedings of the IRE, vol. 48, pp 1246-1263 (1960).

3. T. S. Moss, "Optical Properties of Semiconductors", Butterworth's, 1961.

4. G. S. Almasi, "Graded Energy Gap Heterostructures", M.I.T. Energy Conversion and Semiconductor Laboratory Semiannual Technical Summary Report No. 3, NASA Grant NsG 496 (part), pp. 1-51, November, 1964.

5. P. Emtage, Journal of Applied Physics, v. 33, p 1950 (1962).

6. J. Tauc, Review of Modern Physics, v. 29, p 308 (1957).

CHAPTER 6

CONCLUSIONS AND RECOMMENDATIONS

At this point, it is appropriate to ask what the research reported here means to someone interested in the potentialities of a graded-energy-gap structure either as an energy converter or as a photodetector. After this is discussed, the course of the future research is considered.

As they stand, the devices produced in the course of this study have very limited advantages over existing devices. The conversion efficiency corresponding to the maximum PEM voltage in Section 3.3 is about 10^{-3}% at best. The front-to-back voltage obtained in some of these devices for photon energies just below the CdTe bandgap (1.5 eV) is considerably higher-- the 10^3 $\mu V/\mu W$ sensitivity obtained for sample B2098D10 under 1.4 eV monochromator illumination, combined with its impedance of 10^6 ohms, yields a conversion efficiency of approximately 0.1% when extrapolated to a power level of 10^{-3} watts/cm^2-- but this efficiency exists over such a narrow range of photon energies that the overall conversion efficiency of a continuous spectrum such as the sun's would be very poor (observed efficiencies are about 10^{-3}% at best). Thus, from the standpoint of solar energy converters, the devices as they stand offer no improvement over present semiconductor photocells.

From the standpoint of photodetectors, the picture for the devices in their present form is a little less bleak, but they would be limited to special applications. For example, the sensitivity associated with the front-to-back photovoltage is still near maximum for photon energies near 1.4 eV, the value for GaAs injection laser radiation. For the optimum values quoted in Chapter 3, the calculated noise-equivalent-power (NEP) for sample B2098D10 operating at room temperature

is about 10^{-9} W/cps for 1.5 eV photons[*]. A possible advantage might be that the active region can be protected from high-energy particle damage by the thick CdTe window which is an integral part of the device.

Another application might take advantage of the long-wavelength response of the PEM voltage at contacts 3-4 to detect the output of a Q-switched CO_2 laser at 10.6μ. The room-temperature sensitivity associated with this photovoltage (maximum 2×10^{-3} V/W) is several orders of magnitude smaller than that obtainable from a thermocouple, as is the NEP (maximum 10^{-7} W/cps)[+]. However, if the speed of the device even approaches the 10^{-8}--10^{-9} second hole lifetime estimated for n-type CdTe[1,2] at room temperature, the low sensitivity might be tolerable, since present-day detectors in this wave-length region must be cooled with liquid helium to achieve nanosecond response times[3,4].

The main value of the devices as they stand is in the information they furnish about the experimental difficulties which must be overcome in further development work on graded-gap photodevices, as well as the information they furnish about the internal mechanisms of the graded-gap regions which exist in these devices. The model derived for the structures studied here illustrates that doping control is probably the main problem to overcome in designing an efficient graded-gap photodevice. Furthermore, since it was possible to resolve the discrepancies between the results predicted by analyses

---

[*] Calculated on the basis of an 0.11 cps bandwidth for the amplifier settings used.

[+] As mentioned in Chapter 3, cooling our samples with liquid nitrogen increased the sensitivity by three orders of magnitude for certain wavelengths, resulting in a NEP of 10^{-10} W/cps, but since the behavior of these devices at low temperatures is not fully understood, this data was not presented. See reference 8.

of simple graded-gap devices[5,6,7] and the results obtained
here by using a model of an undesirable CdTe pn junction
which interacts with the graded-gap region, these measurements
support the assumptions made in those theoretical treatments.
Finally, even though the present device configuration is far
from optimum, it is still possible to obtain useful informa-
tion about the graded-gap region from these measurements.
This will be discussed briefly.

The dominant photocurrent mechanism in the graded-gap
region is determined by the ratio of drift to diffusion length
(L_{dr}/L_n), while the spectral response and efficiency of a
simple graded-gap device[*] is determined by the larger of the
two quantities L_{dr}/t or L_n/t, where t is the width of the
graded region. As discussed in Chapter 4, the lack of corre-
lation between the slope of the spectral responses of these
devices and their heat-treatment history is a strong indica-
tion that $L_{dr}/L_n \gg 1$ and that drift is the dominant mechanism.
However, the fact that the PEM voltage in these devices is
more or less independent of photon energy is interpreted in
Section 5.4 to mean that $L_{dr}/t \ll 1$, i.e., that the lifetime
in the graded region is so low that photogenerated carriers
recombine after drifting a distance which is only a small
fraction of the width of the graded region. This would be
in agreement with the very poor conversion efficiencies
available at light intensities comparable to that of sunlight.

It is doubtful if a simple graded-energy gap converter
will ever be a competitive solar cell, for the basic reason
that its linear I-V characteristics[3,4] result in a maximum

---

[*] A simple graded-gap device in this discussion is taken to
mean one which contains no p-n junctions and in which the
main motive force is due to the energy-gap gradient.

theoretical conversion efficiency[*] of 25% for any illumination spectrum, while the limit conversion efficiency for silicon solar cells, including the losses due to the nature of the solar spectrum, is 22%, and 15% efficiencies have been observed experimentally[9].

From the standpoint of a photodetector, the future of graded energy gap devices looks considerably more promising. The long wavelength response of the PEM voltage has already been mentioned. However, if the p-n junctions in these devices can be eliminated while still maintaining a low equilibrium carrier concentration, this long-wavelength response should also be available from the front-to-back photovoltage.

In addition, it was just pointed out that the behavior of the spectral response data indicates that the photo-generated excess carriers in the graded-gap region move primarily by drift. This opens up the possibility of a device whose speed is determined by the transit time of excess carriers across the graded region, rather than by their lifetime.

It is suggested that the next step which is necessary is to make measurements on devices in which the equilibrium carrier concentration is controllable. This probably will make it necessary to separate the investigatory and device

---

[*] Emtage[4] has made a calculation for a GaAs-InAs graded-gap photocell which incorporates a pn junction in the material with the smaller gap (InAs) in the hope of avoiding this source of inefficiency; considering present-day technology in these materials, he finds a maximum conversion efficiency of 43% for an idealized spectrum with a total number of photons which is 2×10^3 times the number found in sunlight at the earth's surface, and 3% for a number of photons equivalent to sunlight at the earth's surface. Using amplified sunlight instead of the idealized spectrum, he finds a maximum conversion efficiency of about 20% for these materials. Using an ideal semiconductor alloy system, a conversion efficiency of 35% under direct sunlight is calculated.

development aspects of this problem, since it will probably be necessary to introduce a large amount of foreign impurities[*] in the beginning at least, which will result in an inefficient device with a small output. It will be a simpler device, however, and permit better comparison with theory.

Once this control has been achieved, it is suggested that some time response measurements be carried out, since the main interest in such a device would be as a high-speed long-wavelength detector. This will require matching a high-speed or high-frequency amplifier to the low impedance of the device. A CO_2 laser would make a good high-power source of long-wave-length radiation, and either Q-switching or high-frequency modulation might be employed to test the speed of the device. Then if the speed is high enough to be of interest, it would be appropriate to return to the problem of improving the efficiency of the device by lowering the equilibrium carrier concentration. This could be done either by compensation experiments with foreign impurities or by using a precisely controlled annealing scheme. Once this is accomplished, there should probably be a study of the noise in these devices.

Another potentially interesting problem is an investigation of the properties of the intermediate-bandgap semiconductor layers which can be achieved on a CdTe substrate by the

---

[*] Since the band-edge variations in a device consisting of two interdiffused semiconductors are determined not only by the doping variation but also by the electron-affinity variation as a function of distance[5], it is valid to ask whether the rectifying junctions obtained in the bulk of these devices are really due to cadmium vacancy and interstitial sites, or whether they are a manifestation of this electron affinity variation. Unfortunately, the electron affinity as a function of composition is not known. However, the fact that both directions of rectification may be obtained is a fairly strong indication that the structure is being controlled by the doping. Doping control, therefore, looms as the major problem in further development work on graded-gap devices.

method described in Section 3.3. One of the main problems in making good long-wavelength detectors by growing homogeneous mixed crystals of CdHgTe is that the energy gap near 0.10 eV is varying very rapidly with composition, and is thus very sensitive to inhomogeneities in the device. This may be a good alternate way to make small-bandgap photovoltaic or photoconductive devices.

In conclusion, the results of this chapter may be summarized briefly as follows: the assumptions made in the analysis of a graded gap device are applicable to the devices prepared here if allowance is made for the undesirable p-n junctions which appear in the bulk CdTe during the HgTe diffusion. These junctions interact with the graded-gap region and collect some of the optically generated carriers from that region. Elimination of this junction should make it possible to develop these devices into long-wavelength photodetectors which may have very short response times.

REFERENCES

1. M. R. Lorenz and H. H. Woodbury, "Double Acceptor Defect in CdTe", _Physical Review Letters_, v. 10, p. 215, March, 1963.

2. D. A. Cusano and M. R. Lorenz, "CdTe Hole Lifetime from the Photovoltaic Effect", _Solid State Communications_, v. 2, p. 125 (1964).

3. R. A. Smith, "Detectors for Ultraviolet, Visible, and Infrared Radiation", _Applied Optics_, vol. 4, p. 631, June, 1965.

4. J. Lavine, private communication.

5. G. S. Almasi, "Graded Energy Gap Heterostructures", _M.I.T. Energy Conversion and Semiconductor Laboratory Semiannual Technical Summary Report No. 3_, NASA Grant NsG 496 (part), pp. 1-51, November 30, 1964.

6. P. R. Emtage, _Journal of Applied Physics_, vol. 33, p. 1950 (1962).

7. J. Tauc, _Review of Modern Physics_, vol. 29, p. 308 (1957).

8. G. S. Almasi, "Graded Energy Gap Heterostructures", _M.I.T. Energy Conversion and Semiconductor Laboratory Semiannual Technical Summary Report No. 2_, June 30, 1964, and _Report No. 4_, June 30, 1965.

9. M. Wolf, _Proceedings of the IRE_, vol. 48, p. 1246, July, 1960.

APPENDIX A

BEHAVIOR OF $\Delta n(0)$

This appendix considers the relationships which are possible between r_1, r_2, α, and t in equation 4.9, and shows that __if__ these is any significant dependence of $\Delta n(0)$ on x_ν, then the dominant term in equation 4.9 must be $e^{r_1(t-x_\nu)}$.

The various combinations can be broken down into two main cases:

1) $r_1 = -r_2$ for various values of α.

2) $r_1 \gg -r_2$ for various values of α.

Case 1: "Diffusion Dominant", $r_1 = -r_2 = 1/L$

In this case, equation 4.9 becomes

$$\Delta n(0) = \frac{\alpha q_o/D_n}{a_1\left(e^{-t/L}-e^{t/L}\right)(\alpha + 1/L)}\left[e^{\left(\frac{t-x_\nu}{L}\right)} - e^{-\left(\frac{t-x_\nu}{L}\right)}\right.$$
$$\left. + \frac{2/L}{1/L + \alpha}\, e^{-\alpha(t-x_\nu)}\right] \tag{A1}$$

Since the coefficient of the last exponential in the bracket varies between zero and two as α varies between infinity and zero, it can be shown that the magnitude of the sum of the last two terms in the bracket never exceeds unity. The dominant term in the brackets is therefore the first term with its positive exponent.

Case 2: "Drift Dominant," $r_1 \gg -r_2$

    a) $\alpha \gg r_1 \gg -r_2$

In this case, equation 4.9 becomes

$$n(0) = \frac{q_o}{D_n} \left[\frac{e^{r_1(t-x_\nu)} - e^{r_2(t-x_\nu)}}{a_1 e^{r_2 t} - a_2 e^{r_1 t}} \right] \qquad (A2)$$

Since $r_1(t-x_\nu) \geq 0$ and $r_2(t-x_\nu) \leq 0$, the term $e^{r_1(t-x_\nu)}$ dominates. This function is sketched in Fig. A.1.

b) $r_1 \gg - r_2 \gg \alpha$

In this case, equation 4.9 becomes

$$\Delta n(0) = \frac{\alpha q_o/D_n}{a_1 e^{r_2 t} - a_2 e^{r_1 t}} \left[\frac{1}{r_1} e^{r_1(t-x_\nu)} - \frac{1}{r_2} \left\{ e^{r_2(t-x_\nu)} - e^{-\alpha(t-x_\nu)} \right\} \right] \qquad (A3)$$

The term in the square brackets may be re-written

$$\frac{1}{r_1} e^{r_1(t-x_\nu)} \left[1 - \frac{r_1}{r_2} \left\{ e^{(r_2-r_1)(t-x_\nu)} - e^{-(r_1+\alpha)(t-x_\nu)} \right\} \right]$$
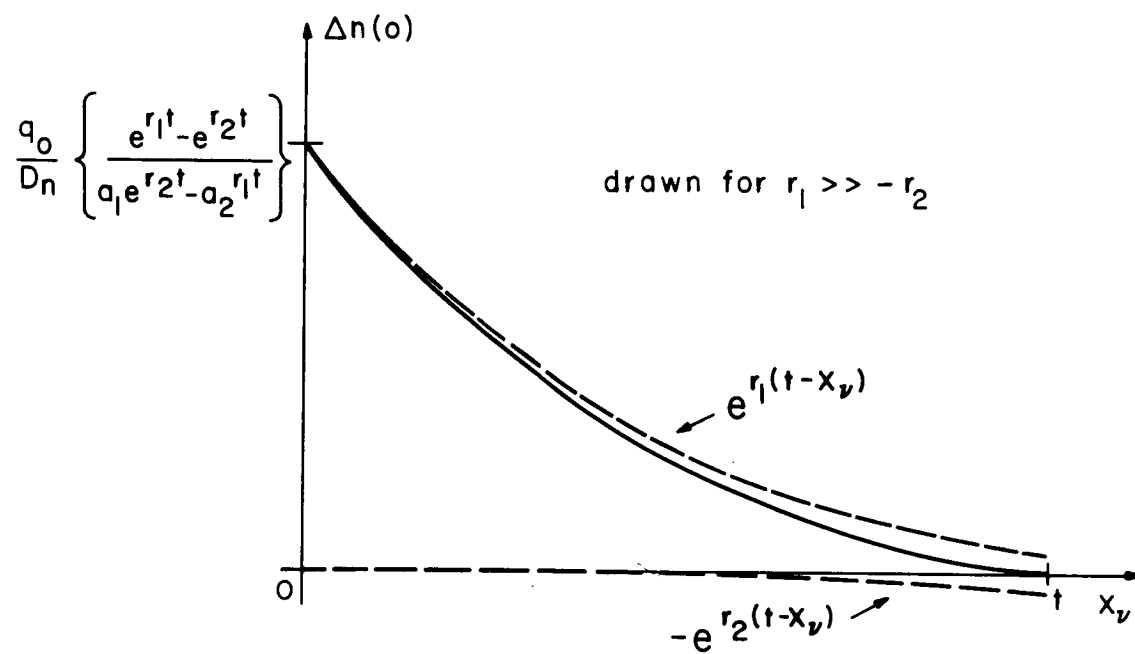
and since $r_1 \gg - r_2$ and $r_1 \gg \alpha$, this becomes

$$\frac{1}{r_1} e^{r_1(t-x_\nu)} \left[1 - \frac{r_1}{r_2} \left\{ e^{-r_1(t-x_\nu)} - e^{-r_1(t-x_\nu)} \right\} \right]$$

$$= \frac{1}{r_1} e^{r_1(t-x_\nu)}$$

Thus again the term $e^{r_1(t-x_\nu)}$ dominates.

c) $r_1 \gg \alpha \gg -r_2$

In this case, equation 4.9 becomes

The figure shows a graph with vertical axis labeled $\Delta n(o)$ and horizontal axis labeled x_ν.

The y-intercept is labeled:

$$\frac{q_o}{D_n} \left\{ \frac{e^{r_1 t} - e^{r_2 t}}{a_1 e^{r_2 t} - a_2 e^{r_1 t}} \right\}$$

Annotation in graph: drawn for $r_1 >> -r_2$

Curves labeled $e^{r_1(t - x_\nu)}$ and $-e^{r_2(t - x_\nu)}$, with origin marked 0 and point t on the horizontal axis.

A.1 Excess Carrier Distribution at x= 0 for a >, r_1

$$\Delta n(0) = \frac{\alpha q_o/D_n}{a_1 e^{r_2 t} - a_2 e^{r_1 t}} \left[\frac{1}{r_1} e^{r_1(t-x_\nu)} - \frac{1}{\alpha} \left\{ e^{r_2(t-x_\nu)} - e^{-\alpha(t-x_\nu)} \right\} \right] \quad (A4)$$

The proof is identical to that for the case b) above, and the result again is that $e^{r_1(t-x_\nu)}$ is the dominant term.

Thus it has been shown that both for drift and diffusion cominant and for large, intermediate, and small values of absorption coefficient, the dominant exponential term in the square brackets of equation 4.9 is $e^{r_1(t-x_\nu)}$.

APPENDIX B

PHOTON-ENERGY-DEPENDENT ABSORPTION COEFFICIENTS

The main purpose of this section is to show that absorption coefficients with a simple dependence on energy or on position do not significantly alter the photon-generation function used in section 4.3.

The number of photons absorbed per unit time in a thin strip of unit area and a thickness dx normal to the light flux is equal to $\alpha F dx$, where F is the photon flux and α is the absorption coefficient[1]. Thus

$$\frac{dF}{dx} = \alpha F \tag{B1}$$

and if it is assumed that the absorption of photons of energy $h\nu$ begins at a point x_ν in the graded-gap region where $E_G(x) = h\nu$, then the probability P_c that the photon is absorbed <u>somewhere</u> in the graded-gap region between $x = x_\nu$ and $x = t$ is given by

$$P_c = \int_{x_\nu}^{t} \alpha F(x) dx. \tag{B2}$$

For constant α, $F(x) = F(x_\nu) e^{-\alpha(x-x_\nu)}$

and

$$P_c = 1 - e^{-\alpha(t-x_\nu)} \tag{B3}$$

If a linear energy-gap variation with distance is assumed, i.e.,

$$E_G = E_{Go} \left(1 - \frac{x}{t}\right) \tag{B4}$$

and since x_ν is defined by

$$E_g = h\nu = E_{Go} \left(1 - \frac{x_\nu}{t}\right) \tag{B5}$$

the probability that a photon of energy $h\nu$ is captured in the graded region is given by

$$P_c = (1 - e^{-\alpha t \frac{h\nu}{E_{Go}}}).$$

(B6)

This function is plotted in Fig. B.1 for several values of αt.

In general, α is a function of photon energy even in homogeneous semi-conductors, varying with powers of photon energy between 1/2 and 3/2, depending on the specific absorption mechanism[1]. The effect of such a functional dependence of α on photon energy is investigated first by assuming α still independent of x explicitly but linearly dependent on $[h\nu - E_G(x)]$. Thus

$$\alpha = \alpha_o \left(\frac{h\nu - E_G(x)}{E_{Go}}\right).$$

(B7)

Combining this with (B3) and (B4) gives α as an implicit function of x:

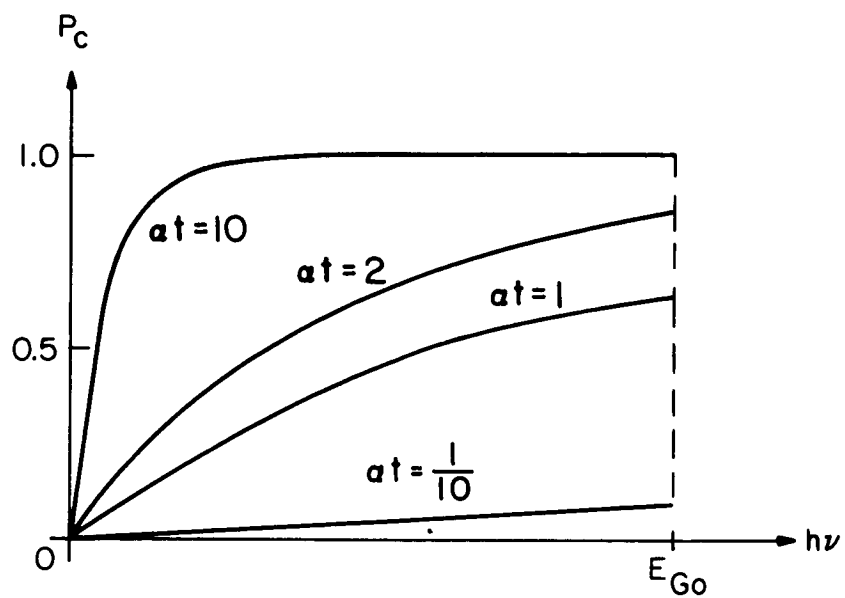$$\alpha = \alpha_o \frac{(x - x_\nu)}{t} \qquad \text{for } x > x_\nu$$

$$\alpha = 0 \qquad \text{for } x < x_\nu$$
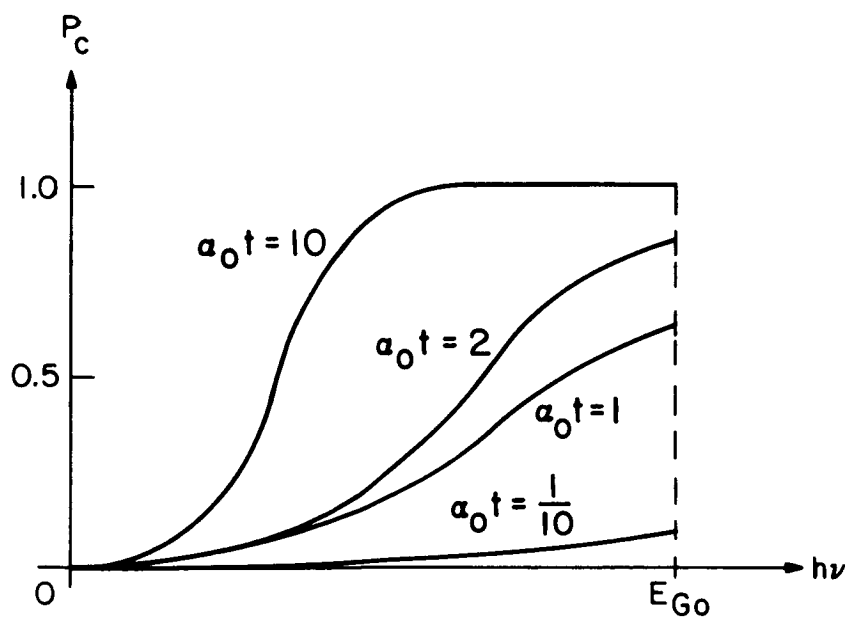
(B8)

Integration of equation (B1) in this case yields

$$F(x) = F_o \, e^{-\alpha_o \frac{(x - x_\nu)^2}{2t}}$$

(B9)

and use of equation (B2) gives the probability of capture in the graded-gap region as

$$P_c = 1 - e^{-\alpha_o t \left(\frac{h\nu}{E_{Go}}\right)^2}$$

(B10)

B.1   Probability of Photon Capture in Graded Region of Thickness
       t for α Constant

B.2   Probability of Photon Capture in Graded Region of Thickness
       t for α Linearly Related to Photon Energy

This function is plotted in Fig. B.2 for several values of $\alpha_0 t$. It can be seen that the functional dependence on photon energy is not drastically different from the behavior shown in Fig. B.1.

The value of α_0 in equation B7 may depend on position in the graded-gap region, since the effective masses decrease as the energy gap decreases, resulting in a increase in the densities of states in each band and thus resulting in an increase in α_0. If α_0 is assumed to be an explicit linear function of x,

$$\alpha = \alpha_{oo} \left(\frac{x-x_\nu}{t}\right) \left(\frac{h\nu - E_G(x)}{E_{Go}}\right) \tag{B11}$$

then the preceding analysis can be repeated to show that the capture probability will now have the form

$$P_c = \left(1 - e^{-\alpha_{oo} t \left(\frac{h\nu}{E_G}\right)^3}\right). \tag{B12}$$

This will differ from the function plotted in Fig. B.2 mainly in its behavior for low-energy photons, which will be cubic rather than quadratic.

It is clear that neither of these position-dependent absorption processes lead to an exponential function of photon energy with a slope anywhere near the values found for the photovoltaic spectral responses described in section 3.3. It was therefore decided that the photon absorption process was adequately represented for the purposes of this analysis by a constant absorption coefficient.

REFERENCES

1. R.A. Smith, "Wave Mechanics of Crystalline Solids," John Wiley and Sons, 1961.

APPENDIX C

SPECTRAL RESPONSE OF THE PEM VOLTAGE

The methods and results of Chapter 4 can be adapted to calculate the photo voltage that arises in the graded-gap region, with a generality which is equal to the results for the junction photo voltage. However, in view of the relative lack of emphasis placed on the PEM data, such a general treatment seems neither warranted nor appropriate at this point. Therefore, it is only outlined briefly, followed by an analysis of a simpler model which nevertheless fulfills the purposes of this discussion.

The general procedure to be sketched here assumes that CdTe to the left of the graded-gap region is infinitely wide, and that the entire structure has a uniform equilibrium hole concentration p_o. The results quoted without proof here are from unpublished work by the present author, and are included for the convenience of others who may be interested either in comparing or in extending this work.

The only boundary condition which differs from those used in Chapter 4 is that $\Delta n_I(x = -\infty) = 0$. Region III, of course, does not exist in this case. The open-circuit voltage V_{oc} is found by integrating equation 4.1 for the case where the total current is zero. The result is

$$V_{oc} = \frac{1}{\sigma_p} \left[e(D_p - D_n)\Delta n(0) - e\, D_n\, \underline{\varepsilon} \int_o^t \Delta n(x)\, dx \right] \tag{C1}$$

where $\sigma_p = e\mu_p\, p_o$.

$$\Delta n(0) = \frac{\alpha q_o / D^*}{\alpha + r_2} \left[\frac{(1 - e^{-(r_1 - r_2)(t - x_\nu)})}{r_1 - r_2} - \frac{(1 - e^{-(\alpha + r_1)(t - x_\nu)})}{\alpha + r_1} \right] e^{-r_1 x_\nu}$$

where D* is the ambipolar diffusion coefficient, and

$$\int_0^t \Delta n(x) dx = \frac{\alpha q_o / D^*}{(\alpha + r_1)(\alpha + r_2)(r_1 - r_2)} \cdot$$

$$\left[\frac{r_1 - r_2}{r_1} \{ e^{-\alpha(t - x_\nu)} - 1 + e^{r_1 x_\nu} (1 - e^{-(\alpha + r_1)(t - x_\nu)}) \} \right.$$

$$- \frac{\alpha + r_1}{r_1} \{ e^{r_2(t - x_\nu)} - 1 + e^{r_1 x_\nu} (1 - e^{-(r_1 - r_2)(t - x_\nu)}) \}$$

$$\left. + \frac{r_1 - r_2}{\alpha} (e^{-\alpha(t - x_\nu)} - 1) + \frac{\alpha + r_1}{r_2} (e^{r_2(t - x_\nu)} - 1) \right]$$

The behavior of the open-circuit photovoltage as a function of photon energy can be elucidated using the techniques, of Appendix A and it can be shown that no matter what the relationship between r_1, r_2, and α, the shape of the spectral response will not differ markedly from the results of the simplified analysis to follow. (See also Figure 5.7)

The analysis to be worked out here assumed that $r_1 \gg -r_2$ (drift dominates) and that $\alpha \gg r_1$ and $\alpha t \gg 1$ (thick graded region). The generation function in equation 4.3 is then an impulse-like function

$$g(x) = g_o(h\nu) \, \mu_o (x - t + \frac{h\nu}{E_{Go}} t)$$

where $g_o(h\nu)$ is the number of photons per cm^2 per second at the photon energy $h\nu$, and μ_o is the unit impulse function. The solution for Δn is

$$\Delta n = g_o(h\nu) e^{\frac{-(x - t[1 - h\nu / E_{Go}])}{L_{dr}}} \mu_{-1}(x - t[1 - h\nu / E_{Go}]) \qquad (C2)$$
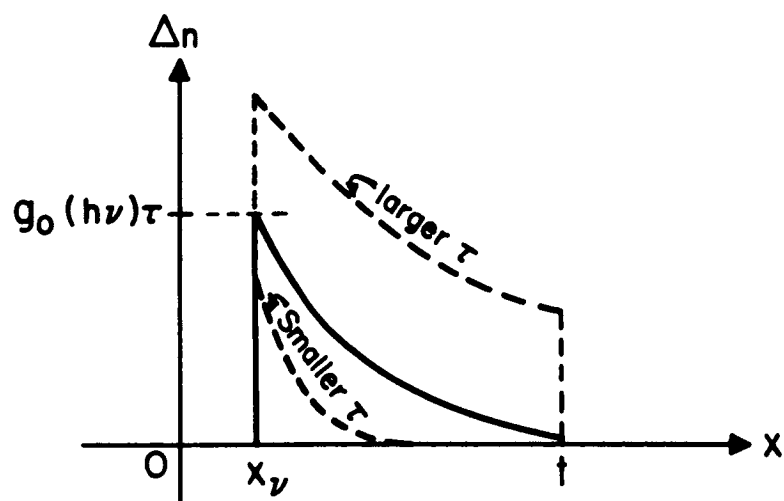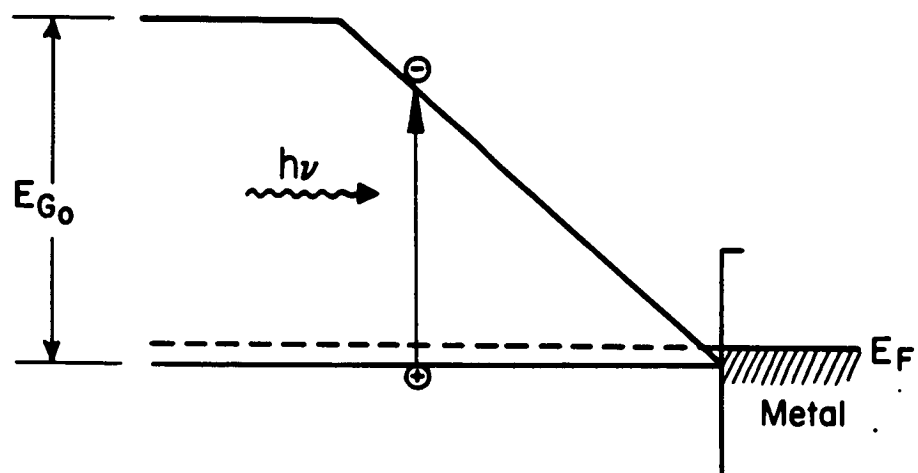
C.1   Band Model Used for Analysis and Excess Carrier
      Concentration Resulting form Assumption that
      Drfit Dominates

where E_{Go} is the energy gap at $x = 0$, the "drift length" L_{dr} is still defined by eq. 4.4 as

$$L_{dr} = L_n^2 \frac{\Delta\delta_o}{t}$$

and μ_{-1} is the unit step function. The excess carrier distribution in this approximation is sketched in Fig. C.1.

The open-circuit photovoltage is calculated by adding equations 4.1a and 4.1b to obtain the total current, setting this equal to zero, and integrating Since the material has been assumed strongly p-type and since drift has been assumed to dominate, the result is

$$\frac{d}{dx}(\phi - \phi_o) = \frac{\Delta n}{p_o} \frac{\mu_n}{\mu_p} \frac{1}{e} \frac{dE_G}{dx} \tag{C3}$$

$$V_{oc} = \frac{\mu_n}{\mu_p} \int_{t(1-h\nu/E_{Go})}^{t} \frac{\Delta n}{p_o} \frac{1}{e} \frac{dE_G}{dx} \, dx \tag{C4}$$

and since p_o is constant, insertion of the value found for Δn in equation C2 leads to

$$V_{oc} = \frac{g_o(h\nu)\tau}{p_o} \frac{\mu_n}{\mu_p} \frac{\Delta E_G}{e} \frac{t}{L_{dr}} (1 - e^{-\frac{L_{dr}}{t} \frac{h\nu}{\Delta E_G}}) \tag{C5}$$

which can be converted to the result in equation 5.2 simply by realizing that

$$\frac{L_{dr}}{t} = \frac{\tau d}{\tau}.$$

The behavior of this function is sketched in Fig. 5.7 and is discussed in section 5.4.

Equation C4 can also be used to explain the origin of the idea discussed

in section 5.2 that under certain conditions, the spectral response $V_{oc}/g_o(h\nu)$ should depend on the doping variation in the graded-gap region. The behavior shown in Fig. 5.7 is based on the assumption that p_o is a constant. This makes it possible to take p_o outside the integral in equation C4. However, if p_o were a function of x, this would not be possible. Now, if Δn were a narrow pulse which existed over only a small portion of the graded-gap region, the integrand would be non-zero over only a small distance near x_ν, and the quantity which would enter into equation C5 would be $p_o(x_\nu)$.

Figure C1 shows that Δn does approach a pulse with width much less than t for small enough values of τ. It was thought, therefore, that the monochromatic light of photon energy $h\nu$ might in effect be "sampling" $p_o(x_\nu)$. However, the evidence discussed in section 5.2 is against this explanation.